Large scale computations of 3-manifolds invariants

Owen Rouillé

UNIVERSITÉ CÔTE D'AZUR

ÉCOLE DOCTORALE
SCIENCES ET TECHNOLOGIES DE L'INFORMATION ET DE LA COMMUNICATION

THÈSE DE DOCTORAT

Calculs à grande échelle d'invariants de 3-variétés

Owen ROUILLÉ

Centre Inria d'Université Côte d'Azur

Présentée en vue de l'obtention du grade de docteur en Informatique **d'**Université Côte d'Azur

Dirigée par : Jean-Daniel BOISSONNAT, Directeur de recherche émérite, Centre Inria d'Université Côte d'Azur
Co-encadrée par : Clément MARIA, Chargé de recherche, Centre Inria d'Université Côte d'Azur
Soutenue le : 5 septembre 2022

Devant le jury, composé de :
Indira CHATTERJI, Professeure, Université Côte d'Azur
Fabrice ROUILLIER, Directeur de recherche, Centre Inria de Paris
Benjamin BURTON, Professeur, Université du Queensland
Dominique ATTALI, Directrice de recherche, Grenoble images parole signal automatique
Arnaud DE MESMAY, Chargé de recherche, Laboratoire d'Informatique Gaspard Monge
Michael KERBER, Professeur, Université technique de Graz
Antonin GUILLOUX, Maître de conférences, Institut de Mathématiques de Jussieu-Paris Rive Gauche

CALCULS À GRANDE ÉCHELLE D'INVARIANTS DE 3-VARIÉTÉS

Large scale computations of 3-manifold invariants

Owen ROUILLÉ

Jury :

Président du jury

Indira CHATTERJI, Professeure, Université Côte d'Azur

Rapporteurs

Fabrice ROUILLIER, Directeur de recherche, Centre Inria de Paris
Benjamin BURTON, Professeur, Université du Queensland

Examinateurs

Dominique ATTALI, Directrice de recherche, Grenoble images parole signal automatique
Arnaud DE MESMAY, Chargé de recherche, Laboratoire d'Informatique Gaspard Monge
Michael KERBER, Professeur, Université technique de Graz

Directeur de thèse

Jean-Daniel BOISSONNAT, Directeur de recherche émérite, Centre Inria d'Université Côte d'Azur

Co-encadrant de thèse

Clément MARIA, Chargé de recherche, Centre Inria d'Université Côte d'Azur

Membres invités

Antonin GUILLOUX, Maître de conférences, Institut de Mathématiques de Jussieu-Paris Rive Gauche

Université Côte d'Azur

Owen ROUILLÉ

Calculs à grande échelle d'invariants de 3-variétés

xiv+100 p.

Ce document a été préparé avec LaTeX2e et la classe `these-ISSS` version v. 2.10.

Impression : these.tex – 4/12/2022 – 23:22

Révision pour la classe : these-ISSS.cls,v 2.10 2020/06/24 14:16:37 mpelleau

Au bureau Y303.

Calculs à grande échelle d'invariants de 3-variétés

Résumé

La topologie est l'étude des objets à déformation près, sans couper ni coller : l'illustration la plus répandue est sans doute la transformation d'une tasse en donut. Parmi tous les sujets d'études en topologie, les variétés présentent un intérêt particulier : elles sont la généralisation en toutes dimensions des surfaces et permettent de représenter naturellement de nombreux objets.

Cette thèse se concentre sur la topologie en basses dimensions, et plus précisément à l'étude des 3-variétés. Celles-ci ont un statut privilégié pour les informaticiens : alors que les problèmes ont tendance à être simples en dimension 2 et impossibles en dimension 4, à l'instar du problème de l'homéomorphisme, les problèmes tendent à être difficiles mais possibles avec les 3-variétés. De plus, les 3-variétés sont triangulables et donc manipulables par des ordinateurs.

Les 3-variétés peuvent également être utilisées pour étudier les nœuds. Les nœuds peuvent être vus comme des courbes fermées et nouées, ils sont utilisés en modélisation et en physique quantique. Par le théorème de Gordon-Luecke, le complément d'un nœud est une 3-variété qui contient toutes les informations à propos de celui-ci. Avec les 3-variétés, l'étude des nœuds a connu de nombreux avancements incluant notamment le théorème de classification de Thurston qui les classes en trois familles : les nœuds toriques, satellites et hyperboliques.

Différencier des couples de variétés, ou de nœuds, est un problème difficile et central en topologie. Pour les diagrammes de nœuds, une projection d'un nœud dans le plan, il est possible d'essayer de le modifier pour le transformer en un autre, mais ces approches sont connues pour être très difficiles. Une approche plus réaliste est d'utiliser des caractéristiques topologiques : les *invariants*. Ce sont des objets mathématiques qui encodent une partie de l'information topologique d'un autre objet, ils ne dépendent donc pas de la représentation de la variété ou du diagramme du nœud, et ils sont l'objet d'intenses recherches en mathématiques.

Si calculer directement un invariant est, en général, plus simple que de résoudre le problème de l'homéomorphisme, leur calcul n'est pas toujours simple, d'où des besoins en terme de logiciels et d'implémentations. C'est d'autant plus vrai aujourd'hui qu'avec l'augmentation des puissances de calcul, de grands recensements de variétés et de nœuds sont disponibles, nécessitants analyse et extension. Les besoins de la communauté en matière de logiciels sont bien illustrés par la popularité des bibliothèques comme `SnapPy` et `Regina`.

Cette thèse est dédiée à deux invariants : le volume hyperbolique et les invariants de Turaev-Viro. Dans les deux cas des contributions sont proposées en terme d'algorithmes, de logiciels et d'analyses.

Pour le volume hyperbolique, nous proposons une approche basée sur des théorèmes de Casson et Rivin pour calculer des structures hyperboliques complètes (CHS). Étant donnée une triangulation, nous utilisons de l'optimisation convexe sur son polytope des structures angulaires ; ce qui mène soit à une CHS, soit à une configuration bloquante que nous simplifions avant de continuer. En plus de ces résultats nous proposons une hybridation entre notre méthode et celle de `SnapPy` qui est plus rapide que l'état de l'art.

Pour les invariants de Turaev-Viro, qui sont indexés par un entier r, nous proposons une méthode pour déterminer, étant donnée une collection de triangulations, sur laquelle les algorithmes de calculs seront le plus efficaces. Nous ajoutons également de l'arithmétique multi-précision à `Regina` dans le but de pouvoir calculer l'invariant, même pour de grandes valeurs de r, ce qui permet de vérifier expérimentalement une conjecture du volume basée sur les invariants de Turaev-Viro.

Mots-clés : Nœud, 3-variétés, invariants, structures hyperboliques, topologie algorithmique, implémentation.

Large scale computations of 3-manifold invariants

Abstract

Topology is the study of shapes modulo deformations, without cutting or gluing: the famous example of this is the mug that can be morphed into a doughnut. Among all the objects studied by topologists, manifolds are of particular interest: they are generalizations of surfaces to higher dimensions that are studied by many mathematicians, and they allow to represent many shapes in a rather natural way.

This thesis is focused on low dimensional topology, and more precisely on the study of 3-manifolds. 3-manifolds have a peculiar status for computer scientists: while problems tend to be polynomial on 2-manifolds and undecidable on 4-manifolds, see for instance the homeomorphism problem, problems tend to be doable but difficult on 3-manifolds. Furthermore, all 3-manifolds admit a triangulation and thus can be manipulated by computers.

3-manifolds are also an effective way to study knots. Knots can be seen as knotted closed curves in the space, they are used as modeling tools and are linked to quantum physics. The Gordon-Luecke theorem states that the complement of a knot in $\mathcal{S}^3$ is a 3-manifold that contains all the information about the knot. Using 3-manifolds, the study of knots leaped forward with Thurston's classification theorem: a knot is either torus, if its complement contains a non-trivial annulus whose boundary lies on the knot, satellite, if its complement contains an essential torus, and hyperbolic otherwise.

Distinguishing pairs of manifolds, and pairs of knots in particular, is a complex and central problem in topology. For knot diagrams, a projection of the knot in a plane, one could try to modify one into another, but these kind of approaches are infamously expensive. A more realistic approach is to use topological characteristics: the *invariants*. These invariants are mathematical objects that encode some of the topological information of the manifold, thus they do not depend on the representation of an object, such as the triangulation for a manifold or the diagram for a knot, and they are subject to intensive study.

While computing invariants is, in general, simpler than solving directly the homeomorphism problem, their computations are often non trivial, which calls for efficient algorithms and implementations. This is particularly true today as, with the increasing computation power, very large censuses of knots and manifolds are available, requiring extensions and analysis. The needs of the community in terms of software is demonstrated by the popularity and ubiquity of libraries like `SnapPy` and `Regina`.

This thesis is dedicated to two invariants: the hyperbolic volume and the invariants of Turaev-Viro. In both cases we propose contributions in term of algorithm, software, and analysis.

For the hyperbolic volume, we propose an approach based on theorems of Casson and Rivin to compute complete hyperbolic structures (CHS). Given a triangulation, we use convex optimization on its polytope of angle structures; this either leads to a CHS, or to a blocking configuration we resolve in order to proceed further. In addition to this algorithm and the analysis of its results, we propose an hybridization with `SnapPy`'s method that outperforms the state-of-the art.

For the Turaev-Viro invariants, which are indexed by an integer r, we propose a preprocessing method based on polytope theory to select the triangulation on which existing algorithms will perform the best. We then introduce multiprecision arithmetics to `Regina` in order to perform large r computations of the invariant and verify a volume conjecture based on the Turaev-Viro invariants.

Keywords: knots, 3-manifolds, invariants, hyperbolic structures, Computational topology, implementation.

Acknowledgements

Ma thèse est terminée. C'est une date importante dans mes études qui sanctionne l'intégralité d'un parcours qui ne s'est pas déroulé en autarcie. Comme le veut l'usage, je voudrais remercier ceux qui y ont contribué. Comme ne le veut pas l'usage, je ne donnerai pas de noms pour n'omettre personne, à chacun de se reconnaître.

Je remercie tout d'abord les membres du jury, notamment ceux qui ont accepté malgré quelques inquiétudes thématiques. En particulier, je voudrais remercier les rapporteurs, pour leurs précieux commentaires et leur relecture.

Ensuite, viennent naturellement mes encadrants. Initialement pour m'avoir fait confiance et de m'avoir proposé de travailler avec eux, mais surtout pour m'avoir formé et soutenu pendant ces années.

Merci aux amis du boulot. Ceux qui m'ont accueilli quand j'ai commencé mon stage de master, et que j'ai retrouvé plus tard au hasard d'un retour au pays ou que je ne retrouverai pas par la volonté d'en changer. Ceux qui ont été doctorants avec moi dans cette équipe et dans celle d'à côté. La co-bureau forcée. Les nouveaux jeunes et le nouveau vieux, qui sont finalement arrivés bien tard.

Un remerciement particulier aux collègues non-scientifiques, que j'ai toujours plaisir a revoir et qui ont été nécessaire au bon déroulement de ma thèse.

Il en va de même pour les chercheurs que j'ai pu rencontrer, sur place ou à divers événements, pour les échanges, leurs conseils et la passion qu'il ont su me transmettre.

Une pensée aussi pour ceux que j'ai croisés hors de l'univers de la thèse, notamment au sport ou chez le dentiste.

De la reconnaissance à ceux que j'ai rencontrés plus tôt dans mon parcours scolaire, amis comme enseignants, à qui je dois beaucoup.

Enfin je, termine en remerciant ma famille pour leur soutien durant toutes ces années et par la formule consacrée : "ça, c'est fait."

Table of contents

CHAPTER 1

Introduction

1.1 Low dimensional topology

Topology is the study of shapes modulo deformations by continuous transformations, that is deformations without cutting or gluing. The classical example of this is the morphing of a mug into a doughnut. Another way of grasping this concept is to consider objects and to ignore the distances within them, *i.e.* the geometry. For instance, there is only one circle for topologists.

While topology is more general, the scope of this manuscript is restricted to 3-manifolds. A n-manifold is a space that locally looks like $\mathbb{R}^n$ for a given dimension n, and n-manifolds can be understood as a generalization of surfaces, which are 2-manifolds. The study of 3-manifolds belongs to low dimensional topology, a subdomain that offers many interesting approaches from purely mathematical to computational points of views. To put it simply, 2-manifolds are classified and computational problems in dimension 2 tend to be solvable in polynomial time. In dimension 4, some manifolds do not even admit triangulations and many problems are undecidable, like the homeomorphism problem. Dimension 3 is of particular interest to computer scientists where questions may be difficult but are still answerable. Another point to highlight the specificity of low dimensional topology can be seen with the Poincaré conjecture, which was solved for all dimensions but the third in 1982, before being finally completed in 2003.

All 3-manifolds admit generalized triangulations [65]. In this context, triangulations are combinatorial objects composed of simplices and gluing relations. The gluing relation of a triangulation states, for each face of each simplex, if and to which other face it is identified, an unidentified face will be part of the boundary of the manifold. These triangulations are used to encode the topology of the manifolds and differ from other classical instances, like Delaunay triangulation or simplicial complexes, in that they do not carry geometric information and simplices can be glued to themselves. The absence of geometric information can be understood with the triangulation of a disk with one triangle and no gluing: these two objects are the same from a topological point of view as the triangle can be turned into a disk by rounding its edges. The enabling of self identification will come in handy to describe complicated manifolds with few simplices: as an example it is possible to triangulate a torus with only two triangles.

The existence of triangulations for manifolds makes their study and the computation of topological properties easier with computers, leading to the success of computational topology. Many questions can be stated in term of combinatorial problems with detailed complexity analysis, and they can be answered with programs that permit to avoid difficult computations by hand. Computational topology is crucial to make topology practical for other communities.

1.1.1 About knots

Low dimensional topology is well known for including the study of knots. A knot is an embedding of the circle $\mathcal{S}^1$ into $\mathcal{S}^3$, it can be seen as the knotting of a piece of string before gluing its ends together. Two embeddings represent the same knot if one can be turned into the other with an ambient isotopy, a continuous deformation of the space that preserves the entanglements, but these ambient isotopies are too difficult to compute in practice. Knots arise in several applied domains such as DNA study [3] and the building of a topological quantum computer [34]. The latter point is worth highlighting as quantum computing will play an important part in tomorrow's computer science, and that several invariants, like the Turaev-Viro family, are interesting in this domain.

Given two diagrams of knots, *i.e.* the projections of knots on a plane, verifying whether the underlying knots are the same is a classical problem. An approach is to try to turn one into the other. But this task can be very difficult: starting from an arbitrary diagram of the unknot, an unknotted circle that was "shuffled", turning it into a circle may require complexifying the diagram and performing a large number of elementary modifications. In fact, an upper bound on this number is $(236c)^{11}$ [52] where c is the number of crossings of the initial diagram.

Another way of working with knots is to use their complements: take a knot in $\mathcal{S}^3$ and drill out a tubular neighborhood of it from $\mathcal{S}^3$. The resulting space, the complement of the knot, is a 3-manifold and its topology is unique for every knot [63]. Thus, recognizing a knot boils down to recognizing a 3-manifold, which opens a whole family of tools such as normal surface theory.

There are three families of knots: torus, satellite and hyperbolic [82]. A torus knot is a knot that can be drawn on an unknotted torus in $\mathbb{R}^3$ and a satellite knot is a non torus knot which can be drawn inside a knotted torus (while not being contained in a ball inside said torus). Thurston proved that the complement of any other knot admits a complete hyperbolic metric. This classification is a very powerful result and the families can be characterized using normal surface theory. Normal surface theory studies the surfaces that can be embedded in a triangulated 3-manifold in a simple way with algebraic tools. Such surfaces can be enumerated: thus, given a knot complement, it is possible to look for an annulus whose boundary lies on the knot, if such annulus exists, then the knot can be drawn on a torus (see 2). It is also possible to look for a torus that would contain a satellite knot.

In the remaining case, the knot is hyperbolic. This last family is the subject of active mathematical research, which motivates the introduction of efficient algorithmic tools to study their geometric properties, and most notably their hyperbolic volume. The hyperbolic volume of a hyperbolic knot is a *topological invariant* which is powerful at distinguishing between non-equivalent knots. It is non-trivial to compute, and at the heart of several deep conjectures in topology [69]. Although a lot of work remains to be done on this topic, a notable result is a method that finds a canonical triangulation for hyperbolic knot complement, while this methods is not guaranteed to succeed, it gives a complete invariant for hyperbolic knots [87].

1.2 Properties of manifolds

The construction of a canonical triangulation for a hyperbolic knot complement requires the computation of a complete hyperbolic metric on this 3-manifold. A metric is a notion of distance, on top of a topology; it fixes the shape of the objects we consider and allows for the computation of volumes and geodesics. On knot complements, if hyperbolic metrics exist, they are unique [66, 74]. They are combinatorially represented by *complete hyperbolic structures* (CHS) and in order

to compute them, one tries to assign hyperbolic shapes to the tetrahedra. If these *shapes* verify a set of non-linear constraints called the *gluing equations*, they form a CHS and encode the complete hyperbolic metric of the space. Information on the manifold can then be computed from the CHS, like its canonical form, for the homeomorphism problem, or the hyperbolic volume, a quantity central in many theorems and conjectures.

1.2.1 The notion of invariant

Unfortunately, computing a CHS is difficult and not all 3-manifolds are hyperbolic knot complements. Topology relies on a more general concept to compare objects: the invariants. A *topological invariant* is a quantity that does not change over all possible representations of an object, *e.g.* two triangulations of the same manifold. A straightforward example of invariant is the number of connected components: let us consider an object constituted of the union of two disjoint balls and another constituted of one ball, it is not possible to turn the former into the latter without gluing the two balls or cutting the lone one.

A key to build new invariants is to make sure they are preserved under non-topological modifications of the objects we are considering. Given a triangulated 3-manifold, combinatorial modifications of the triangulation that do not modify the topology of the underlying manifold are well studied [77] and can be decomposed into a sequence of elementary modifications, called Pachner moves. Discovering and being able to compute invariants is a way to learn more about the objects we study or even to build bridges between seemingly unrelated domains of mathematics.

1.2.2 The example of Turaev-Viro

The quantum invariants of Turaev-ViroTuraev-Viro [84] are a family of real-valued quantities $(TV_r)_r$ indexed by an integer r. Given a triangulation of a 3-manifold, the invariant is defined as a sum of a large number of weights which depends on the combinatorics of the triangulation.

These invariants are very efficient at distinguishing different manifolds [58, 61], unfortunately they are extremely hard to compute in general. Their computation is *#P-hard* [18, 46], which corresponds to counting problems. For instance, counting the number of variable assignments that will satisfy a given general boolean formula is #P-hard, while only finding one is NP-hard and considered very difficult (in fact, it is the most textbook example of difficult problem in computer sciences).

They are also studied for their properties. They are linked to the *Topological Quantum Field Theory* [4] and are notably at the heart of Chen and Yang's *volume conjecture* [19, 26], the 3-manifold counterpart of the famous *volume conjecture* for knots [45, 68]. This conjecture links the *simplicial volume* of a 3-manifold to the asymptotic behavior of the sequence $(TV_r)_r$. We can note that for hyperbolic manifolds, the hyperbolic volume is proportional to the simplicial volume.

1.3 Importance of experimental work

Beside obvious pedagogical interests, intuition is crucial in mathematics: it allows one to understand complex phenomena, propose conjectures and prove results. By providing computations, visualization, large amount of data and corresponding analysis, computer science can be a great boost to it. This was highlighted by a recent cooperation between data scientists, who detected an interesting pattern, and mathematicians, who deduced a theorem [24]. Detecting new structure

among invariants could lead to new theories resembling the one of Thurston–Jørgensen [9] describing the set of possible hyperbolic volumes over all 3-manifolds. With certified computations and assisted proofs, computers actively take part in the advancement of mathematics. Low dimensional topology is a domain where the link between mathematics and computers shines due to the fact that 3-manifold can be efficiently handled by computers and by the fact that the enumeration of knots has been looked into for more than a century.

Indeed, one of the oldest problems in knot theory is the tabulation of knots. It started with a series of publications of Tait in 1877. At the time, Lord Kelvin and him believed chemical properties of elements were due to the entanglement between the atoms, motivating Tait's and several others' work [1]. This tabulation consisted in the enumeration of all the knots, represented by their diagrams, for each crossing number and similar census were started for manifolds. The tabulation continues today with the help of computers and the enumeration of all knots that admit a diagram with up to 19 crossings [16], which sum up to 350 million knots. This task cannot be realistically done by hand, and low dimensional topology calls for powerful libraries which can help manipulate manifolds. Two notable examples are `SnapPy` and `Regina`.

The computation of such censuses takes time and there are many problems in low dimensional topology that have terrible theoretical complexity, or even for which no algorithm is guaranteed to succeed. For these reasons, heuristics are very important for the domain. As an example, since the existence of CHS is not guaranteed, there is no algorithm to compute them. Instead, the state-of-the-art method is the one implemented in `SnapPy`: given an input knot, construct a triangulation of the knot complement and simplify it; in most cases, it will admit a CHS. But if the triangulation does not admit a CHS, the software offers the possibility to randomly modify and simplify the triangulation before trying again until a CHS is found. While this may not look satisfactory, in the majority of cases, this works very well, and for other cases, new heuristics may be required.

Reinforcing this idea, data sets can be very large in low dimensional topology: we mentioned the 350 million knots with up to 19 crossings, but the growth of the number of distinct knots with given crossing number is at least exponential [31]; and the same is true for the number of 3-manifolds with given size of minimal triangulation (that is the smallest number of tetrahedra over all the triangulations of the manifold).

With this amount of data, the difficult cases may multiply: Table 1.1, borrowed from Chapter 6, indicates, for knots with crossing numbers ranging from 12 to 17, the success of `SnapPy`'s method. In particular it gives the fraction of knots for which a CHS is not found on the first try, and the largest expected number of re-triangulations in the data set. Both these quantities increase with the crossing number. Given the fact that computing CHS requires solving a system of non-linear equations whose size tend to increase with the crossing number, large number of re-triangulations is to avoid.

1.4 Contributions

The contributions presented in this manuscript concerns the computation of two objects linked to the hyperbolic volume: the Turaev-Viro invariants and the complete hyperbolic structures.

1.4.1 The computation of Turaev-Viro invariants and volume conjecture

We compute TV_r for large values of r on large sets of triangulated 3-manifolds. This computation being extremely challenging, we focus our attention to small triangulations of closed 3-

	Alternating						Non-Alternating					
#crossings	12	13	14	15	16	17	12	13	14	15	16	17
% Failure on first try	0.9	1.6	2.4	3.3	4.4	5.7	0.8	0.7	1.2	1.7	2.4	3.3
Expected nb of retriang.	2.9	3.9	6.2	7.1	9.5	15.9	2.0	3.1	6.1	11.8	9.7	13.5

Table 1.1 – On all $\sim$ 9.7 millions prime knots with crossing numbers ranging from 12 to 17, alternating and non-alternating, we indicate (*% Failure on first try*) the percentage of knot complements (after triangulation and simplification) on which `SnapPy` fails to compute a CHS on first try. We also indicate (*Highest expected nb of retriang.*) the highest, over all knots, expected number of random re-triangulations necessary for `SnapPy` to succeed finding a CHS.

manifolds ($n \leq 9$ tetrahedra), and the main dependence in complexity is in r, which contrasts with the usual computation where r is small. Under this model, we study experimentally the existing algorithms—backtrack enumeration and fixed parameter tractable algorithm—and conclude that the backtracking algorithm is more appropriate for large r computations of TV_r in practice. We then resort to optimizing computation with the backtracking method. To do so, we introduce techniques and easily computable parameters to estimate the complexity of the computation of TV_r, for all r, on a triangulation T, using the backtracking algorithm. This in turn permits efficient preprocessing of the triangulation —cherry-picking the best triangulation for computation—, and the fine tuning of arithmetic precision for correct multi-precision computation. These optimizations are validated by various experimental studies. Finally, using these optimizations, we compute Turaev-Viro invariants on large sets of low complexity 3-manifolds, and for large r values. These computations on the first manifolds of low complexity allow us to provide further experimental evidence to the volume conjecture for closed 3-manifolds (graph manifolds and hyperbolic manifolds), and study the speed of convergence of the sequence $(TV_r)_r$.

This work resulted in a multi-precision class in `Regina` which is under review for integration, along with the data of the experiments which we plan to put online. This data helps visualizing and quantifying the behavior of Turaev-Viro invariants, future works include the analysis of this new data, for instance by measuring the impact of various manifold parameters on the invariants or to detect structures in the sequences or within families of manifolds.

1.4.2 New approach on the computation of CHS

We introduce a new heuristic based algorithm to improve on the essentially random approach of `SnapPy`. The method is inspired by Casson and Rivin's reformulation of the gluing equations [35, 82]: the gluing equations are split into a linear part and a non-linear part, and the resolution reduces to a convex optimization problem on a polytope domain. If the triangulation does not admit a complete structure, the optimization problem will converge on the boundary of the polytope and we exploit this information to modify combinatorially the triangulation while reusing the partially computed geometry. We experimentally illustrate the interest of the approach and propose a hybrid method with `SnapPy`, that outperforms the state-of-the-art.

This work resulted in the implementation of a method which we plan on submitting for integration into `SnapPy`. Our method's results, whether alone, compared to `SnapPy` or hybridized with `SnapPy`, constitutes interesting data to be analyzed. They rise are many questions, among other things, on *Pachner graphs* and on the effect of the optimization on the shapes of the tetrahedra.

1.5 Composition of the manuscript

This manuscript is dedicated to computational problems in low dimensional topology, and centered on two contributions. Chapters 2 and 3 are background and context for both contributions and Chapter 5 is only for the second.

Chapter 2 constitutes a presentation of low dimensional topology, highlighting its link with computer sciences. We present the manifolds, the triangulations that encode them and combinatorial modifications of triangulations. We also present the classification of 3-manifolds and of knots. Chapter 3 follows by presenting censuses and libraries to work on 3-manifolds. Then Chapter 4 consists in the first contribution [56] of this manuscript: the computation of Turaev-Viro invariants. This includes the presentation of these invariants and methods to compute it, followed by our contribution.

Chapter 5 gives the necessary background on hyperbolic geometry. It is followed by the construction of Thurston's gluing equations: the necessary and sufficient conditions to, on the one hand, have a hyperbolic structure on a 3-manifold, and on the other hand to complete this structure. Chapter 6 consists in the second contribution [57] of this manuscript: the computation of complete hyperbolic structures. An alternative condition to the gluing equations is presented before the contribution.

This manuscript is based on the following articles:

— [56] Clément Maria and Owen Rouillé. Computation of Large Asymptotics of 3-Manifold Quantum Invariants. In ALENEX 2021 - SIAM Symposium on Algorithm Engineering and Experiments, Alexandria / Virtual, United States, January 2021. URL : https://hal.archives-ouvertes.fr/hal-03133238, doi:10.1137/1.9781611976472.15.

— [57] Clément Maria and Owen Rouillé. Computing complete hyperbolic structures on cusped 3-manifolds. In ESA 2022 - European Symposium on Algorithms. URL : https://arxiv.org/abs/2112.06360.

CHAPTER 2

Topology of 3-manifolds

This manuscript concerns 3-manifolds and this chapter introduces them. Section 2.1 is dedicated to their definition, their handling and their representation by computers with triangulations. Section 2.2 introduces normal surfaces, a classical tool of the domain, and uses it to present the classification of 3-manifolds. Section 2.3 constitutes an introduction to knots.

It borrows many results and notions from [39, 61, 72, 75, 77, 82].

2.1 Representation of 3-manifolds

Manifolds are encoded using triangulations. This section gives basic definitions and results that will be useful in the rest of the manuscript.

2.1.1 The notion of manifolds

Manifolds are a generalization of surfaces to any dimensions, they are present in many domains of mathematics and a detailed presentation can be found in [27] for the Riemannian case. A major difference between manifolds and a generic topological space is that manifolds locally behave like $\mathbb{R}^n$, for some fixed n, the dimension of the manifold. For instance the sign "+" is not a manifold as the intersection in the middle is not a one dimensional line like the rest. This notion of "locally behaves like" can be formalized using maps: a neighborhood of every point of a manifold admits a map, that is an application between $\mathbb{R}^n$ and the neighborhood that locally parameterizes the manifold. All these parameterizations must be coherent and together they form an atlas. To sum things up we have:

Definition 2.1.1 (Manifold)**.** A C^k manifold of dimension n is a set M and a family of injective mappings $\phi_i : U_i \subset M \to \mathbb{R}^n$ of open sets U_i of M into $\mathbb{R}^n$ such that:

— $\cup_i U_i = M$;

— for any (i, j) with $U_i \cup U_j = W \neq \emptyset$, the transition map $\phi_j \circ \phi_i^{-1}$ is a C^k mapping from the open set $\phi_i(W)$ to the open set $\phi_j(W)$.

The set $(U_i, \phi_i)_i$ is an atlas composed of charts (U_i, ϕ_i). This definition allows to define several families of manifolds depending on characteristics imposed on the transition maps. If they are just homeomorphisms (C^0), then we have the category of topological manifolds TOP, if they are piecewise linear, then we have the category of piecewise linear manifolds PL, and if they are differential (C^1), we have the category of differential manifolds DIFF. In the literature, many theorems are stated differently depending on the family of manifolds considered. For 3-manifolds, we have TOP=PL=Diff.

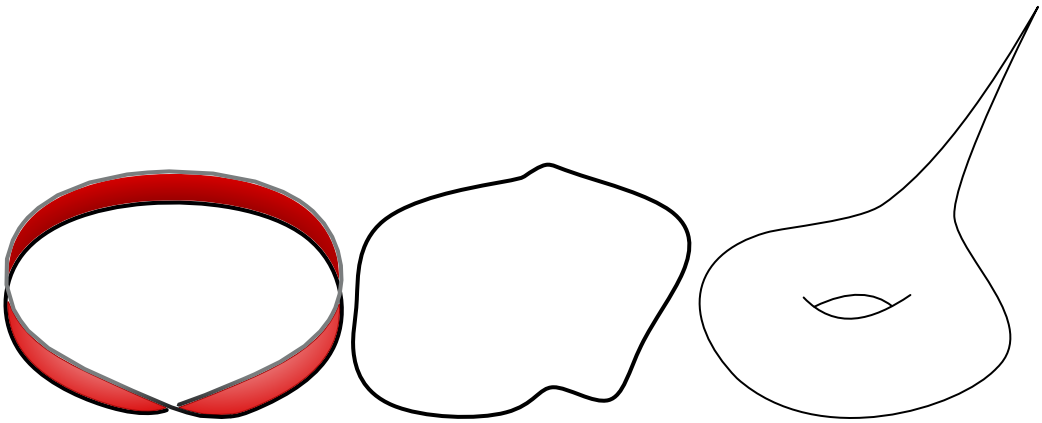

Figure 2.1 – Example of manifolds. Left: the Möbius strip, a compact non-orientable 2-manifold consisting of a twisted band with a single boundary. Middle: the one dimensional sphere S^1, also known as the circle, a closed 1-manifold. Right: the punctured torus, an open 2-manifold. This is a classical torus from which a single point has been removed, creating a cusp.

Examples of manifolds are given in Figure 2.1. Manifolds can have many other characteristics which are classic notions in topology. For instance, in this manuscript, we restrict ourselves to *orientable* and *connected* manifolds, *e.g.*, we exclude Möbius strips in Figure 2.1 (left). They can also be open, closed or compact, see Figure 2.1 for instances. In this manuscript, closed is reserved for compact manifolds with no boundaries, unless precised otherwise.

2.1.2 Generalized triangulations

The definition with maps is not easy to handle for computers. To counter this problem, we use generalized triangulations:

Definition 2.1.2 (Generalized triangulation)**.** A generalized n-triangulation T of an n-manifold M is a collection of abstract n-simplices together with gluing maps identifying their facets in pairs, such that the underlying topological space is homeomorphic to M.

From now on, we simply refer to these as triangulations and consider only 2 and 3-dimensional ones. The gluing maps identify faces of same degree, *e.g.*vertices and vertices, and edges and edges. In drawings, these maps will be represented by merging the simplices they identify or by using arrows to highlight identified simplices, see for instance Figure 2.2. We also define the *link* of a vertex v: it is the boundary of a regular neighborhood of v.

The use of triangulations is justified by Theorem 2.1.1, note that not all 4-manifolds admit triangulations.

Theorem 2.1.1 (Moise [65])**.** *All 3-manifolds admit a triangulation.*

Remark 2.1.1 – The triangulations we defined are more general than the simplicial complexes as they allow self-identifications (Figure 2.2). They are very compact ways of representing manifolds, for instance there are 13,400 topologically distinct, *prime*, closed oriented 3-manifold that can be encoded with at most 11 tetrahedra.

However, they are not more expressive as it is possible to turn a generalized triangulation into a simplicial complex using two barycentric subdivision on each tetrahedron.

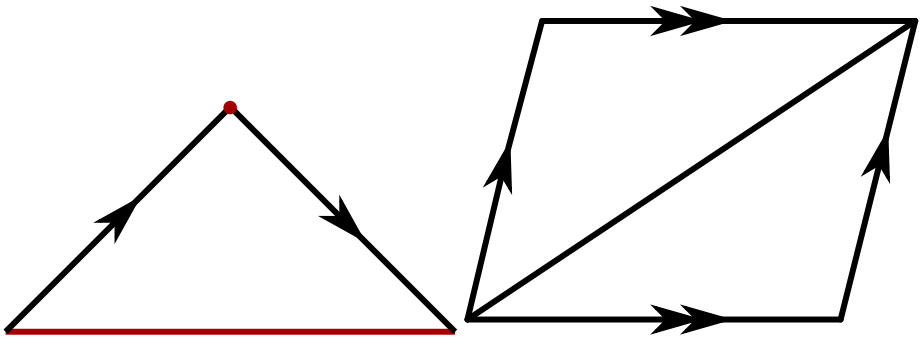

Figure 2.2 – Left: triangulation of a Möbius strip (the boundary is in red). Right: triangulation of a torus.

Points whose links are spheres are said to be *material* or *compact*, however when realizing the gluing defined by a such triangulations, it is possible to obtain *singular points* whose links are not spheres. Using re-triangulations, it is possible to turn these points into vertices. These vertices are then called *ideal*, and the underlying space is a pseudo-manifold. In this case we remove these vertices from the realization of the triangulation to obtain non-compact manifolds.

For instance, identifying an edge to itself in reverse, the neighborhood of the middle point of the edge is then bounded by a projective plane. However, this construction is not allowed as this would mean the underlying manifold is not orientable.

An important case of ideal vertex is when its link is a torus. This case will be the focus of Section 2.3.

2.1.3 Modifying triangulations with local moves

There are many different triangulations encoding the same manifold. A natural problem is the study of the space of triangulations of a given manifold. This space is the *Pachner graph* of the manifold, it is a graph whose vertices are linked by an edge if they differ by an elementary modification called a *bistellar move* or *Pachner move*. These moves can be done in triangulations of any dimension n, exchanging a k-simplex for a $n-k$ simplex, however we restrict ourselves to dimension 3 to the move that exchange three tetrahedra around an edge for two tetrahedra around a triangle *et vise versa* see Figure 2.3.

The Pachner graph has been extensively studied, for instance, given a fixed number of vertices, the graph of any 3-manifold is connected except for triangulations admitting only one tetrahedron [13, 77]. This study was extended to *geometric Pachner moves*, a variant in which the triangulation is no longer abstract and the moves are not authorized if the new simplices are not valid from a geometric point of view, see for instance Figure 2.4 (left). Among the results for geometric Pachner moves, there is the connectedness of the hypercube of dimension 4 [73] and the non-connectedness of the complements of the 8-knot [23].

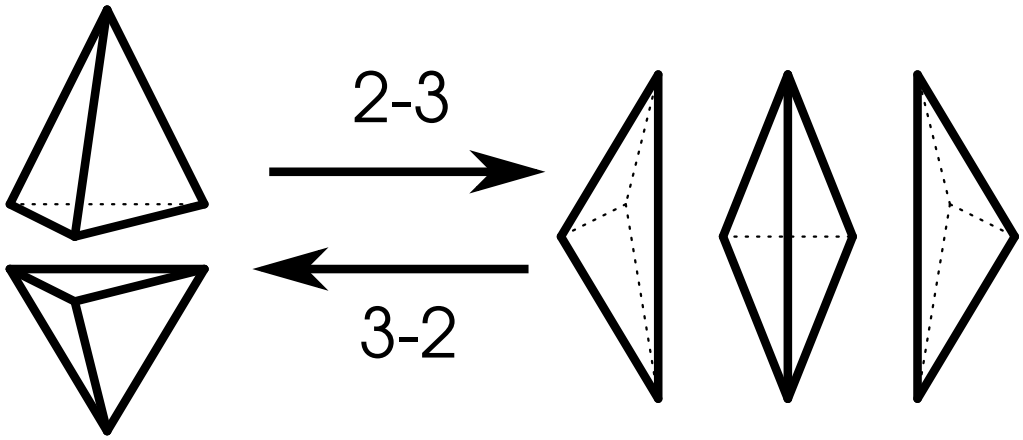

Figure 2.3 – Illustration of the Pachner moves 2-3 and 3-2 which exchange an edge for a triangle (or a triangle for an edge respectively).

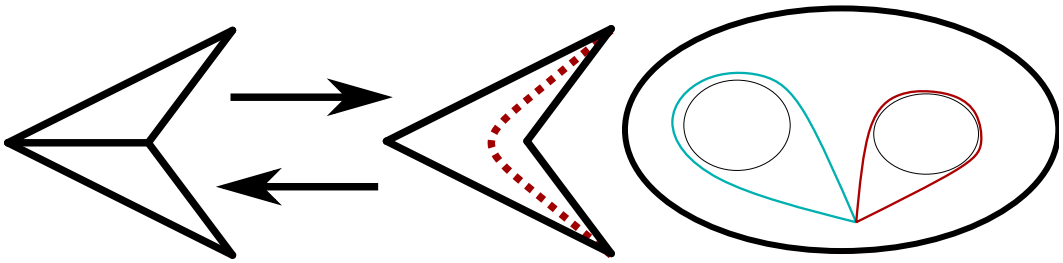

Figure 2.4 – Left: 2-dimensional triangulation in which an edge flip (a 2-2 move) is not valid for geometric reasons: the red dashed edge cannot be constructed. Right: twice punctured disk with loops going around each hole. For this space $\pi_1(X)$ is the free group on two elements, the red loop and the light blue one, and $H_1(X)$ isomorphic to $\mathbb{Z}^2$.

2.1.4 The notion of invariant

Given two triangulations, figuring out if they represent the same manifold is known as the *homeomorphism problem*, while it is known [50, 61, 83], this problem remains very difficult in practice. A reasonable approach is to consider the following notion:

Definition 2.1.3 (Invariant)**.** Let f be a function, if, for any two *objects* A and B, if A and B are *similar* implies $f(A) = f(B)$, then f is an invariant.

The notion of invariant being quite general, the notions of "objects" and "similar" are purposely vague. For instance, A and B can be any objects encoding manifolds, like triangulations, with being similar meaning being homeomorphic. They can also be knots from Section 2.3 with being similar meaning being *ambient isotopic*.

There exist many different examples of invariants: they are topological features and can take many forms. Simple examples of this are the number of connected components or the orientability. For knots there is the colorability, and several different polynomials like Jones' [44] and Alexander's [2]. Chapter 4 is dedicated to the Turaev-Viro invariant for closed 3-manifolds.

Two important examples of invariants for a topological space X we use in this manuscript are represented in Figure 2.4 (right):

— the *fundamental group*, it is the group of the equivalence classes under homotopy (continuous deformation) of the loops contained in the space. It is denoted by $\pi_1(X)$.

— the *first homology group*, it is more difficult to define, but it can be seen as the abelianization [*] of $\pi_1(X)$. It is denoted by $H_1(X)$.

2.2 Normal surfaces and manifold classification

We now define one of the most classical tools in the study of 3-manifolds: the *normal surfaces*. Introduced by Kneser in 1929 [48], their interest is both theoretical, as they can be used to categorize and describe manifolds, and practical [37], as it is possible to develop algorithms to look for and process triangulations based on them.

2.2.1 Normal surfaces: a combinatorial tool

The idea behind normal surfaces is to look at the family of surfaces that can be embedded in a given manifold, a surface S is said *properly embedded* in a manifold M if $S \cap \partial M = \partial S$ and S is not tangent to ∂M.

Definition 2.2.1 (Normal surface)**.** A normal surface in a triangulation is a properly embedded surface that meets each tetrahedron in a (possibly empty) disjoint union of *normal discs*.

A normal disk is a surface properly embedded in a tetrahedron, not intersecting the vertices, that belongs to one of two categories (see Figure 2.5):

— *triangles*: they correspond to the link of a vertex.

— *quadrilaterals*: they are surfaces with connected boundary that separate two opposite edges.

∗. This is the Hurewicz theorem, not a definition.

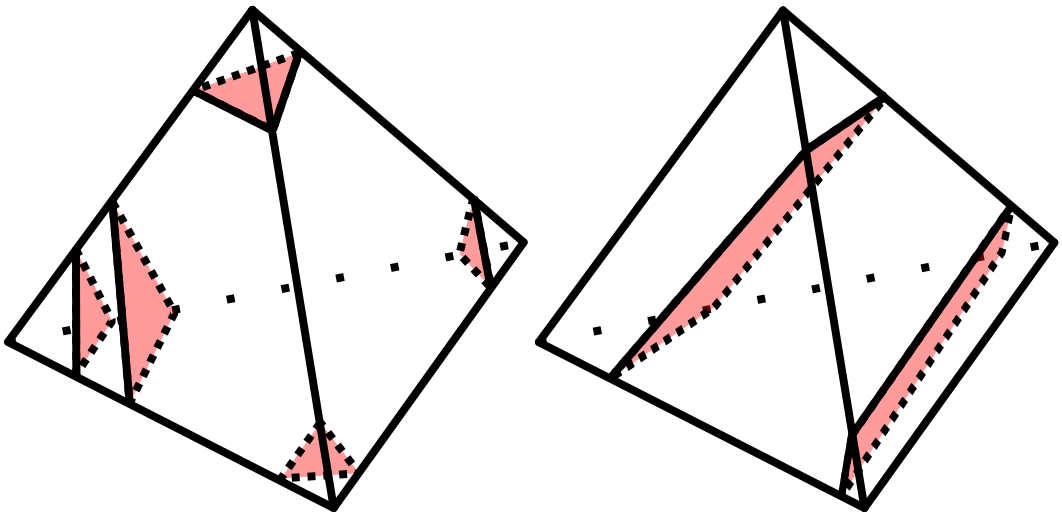

Figure 2.5 – Two kinds of normal disks. Left: the four possible triangles (one of them is doubled) are not mutually exclusive. Right: two parallel quadrilaterals.

Inside a tetrahedron, there can be any number of triangles and quadrilaterals, but quadrilaterals separating two different pairs of edges are mutually exclusive because they must intersect. Then, the restriction of a normal surface to a tetrahedron can be encoded by a vector of $\mathbb{N}^n$ $(t_1, t_2, t_3, t_4, q_1, q_2, q_3)$ where each t_i encodes the number of triangles of each type, and the q_i then same for the quadrilaterals. Thus, normal surfaces can be encoded by elements of $\mathbb{N}^{7n}$ where n is the number of tetrahedra of the triangulation.

Not all points in this space correspond to normal surfaces. They must verify a linear system of *matching equations*. These ensure the surfaces can be glued coherently inside the triangles joining the tetrahedra of the triangulation. With the mutual exclusivity of quadrilaterals, we have that the normal surfaces describe integer points of a set of cones.

The structure of these cones can then be studied leading to famous results like the recognition of the unknot, which is in NP [38], and computing the JSJ decomposition, presented in the next section, of a manifold [61].

Not all properly embedded surfaces are normal, however, given a properly embedded surface S, there is a procedure turning it into a normal surface in a finite sequence of *elementary transformations*. These transformations include removing an empty sphere and cutting the surface along a disk D (with $\partial D \subset S \cup \partial M$) (and identifying the boundary of the disk in the two components to points). A detailed presentation can be found in [60].

Not all properly embedded normal surfaces are interesting, and to characterize manifolds using normal surfaces in the next section, we need to formalize this notion of interesting surface. As an example, the link of a compact vertex is a normal sphere, but this does not bring any information about the manifold.

Surfaces that carry information will be called *essential*, this notion depends on the nature of the considered surface on we need a couple of definitions. A properly embedded surface S in M is:

— *boundary parallel* if it is isotopic to a surface contained in ∂M, with the isotopy fixing ∂S;
— *incompressible* if there is no disk D with $D \cap S = \partial D$ such that ∂D does not bound a disk in S;
— *boundary incompressible* if there is no disk D with $\partial D = \sigma \cup \mu$, $\sigma \subset S$ and $\mu \subset \partial M$, such that there is no disk $D' \subset S$ with $\partial D' = \sigma \cup \sigma'$ and $\sigma' \subset \partial S$.

Then we have:

— a sphere is essential if it does not bound a 3-ball, a manifold with no essential sphere is irreducible;
— a disk is essential if it is not boundary parallel, a manifold with no essential disk is boundary irreducible;
— a torus is essential if it is incompressible and not boundary parallel, a manifold with no essential torus is atoroidal;
— an annulus is essential if it is incompressible, boundary incompressible, and not boundary parallel, a manifold with no essential annulus is anannular.

Crushing is an operation closely linked to normal surfaces, it was introduced in [42] and a comprehensive presentation can be found in [15]. It is a procedure that eliminates normal spheres and disks from a triangulation by identifying said surfaces to points and crushing the components that bear no topology. This procedure allows to simplify triangulations, which is crucial in a domain where many algorithms have exponential complexity in the size of the triangulations.

This tool is used throughout this manuscript as a preprocessing: it is possible to assume all triangulations have *only ideal vertices* or, for closed manifolds, *only one compact vertex*.

2.2.2 Manifold classification

Being able to decompose 3-manifolds is very important to understand and classify them. To do so, we look at essential surfaces and cut the manifold along these.

Cutting along spheres. We define a basic operation to glue two manifolds:

Definition 2.2.2 (Connected sum)**.** Let M_1 and M_2 be two oriented connected 3-manifolds. Removing a 3-ball from each manifolds and then gluing the two resulting spheres via an orientation-reversing homeomorphism results in a new 3-manifold denoted $M_1 \# M_2$.

Note that the surface between the two manifolds is an essential sphere if neither of M_1 and M_2 is a 3-spheres.

Definition 2.2.3 (Prime 3-manifold)**.** A prime 3-manifold is a manifold that cannot be expressed as the connected sum of two 3-manifolds differing from the 3-sphere S^3.

Irreducible 3-manifolds are prime, the only orientable prime manifold that is not irreducible is $S^1 \times S^2$.

Theorem 2.2.1 (Milnor [47, 64]). *Every compact oriented 3-manifold M with (possibly empty) boundary decomposes uniquely into a list of prime manifolds $M = \#_i M_i$. This list is unique up to permutation and insertion of 3-spheres.*

Cutting along disks. Similarly [60], we have the following theorem by cutting along essential disks:

Theorem 2.2.2 (Boundary decomposition). *Every compact oriented irreducible 3-manifold M is obtained by adding 1-handles to a finite list of connected irreducible and boundary irreducible 3-manifolds. This list is unique up to permutation and insertion of balls.*

Cutting along tori. This last step of the decomposition is due to Jaco, Shalen and Johannson. It consists in cutting the remaining of the manifold along essential tori. A cutting of M along essential tori is a *torus decomposition* if the pieces obtained are torus (semi-)bundles, Seifert manifolds of simple manifolds. More details about definitions, theorems and explanations can be found in [60].

Theorem 2.2.3 (JSJ decomposition [43]). *Let M be an orientable irreducible, boundary irreducible, compact 3-manifold with a (possibly empty) boundary consisting of tori. A minimal torus decomposition for M exists and is unique.*

The minimality property is with respect to the inclusion. For instance, cutting a manifold along n parallel tori will result in $n-1$ torus bundles, but the decomposition will not be minimal.

2.2.2.1 Geometrization of 3-manifolds

The JSJ decomposition cuts manifolds into elementary pieces. The classification goes on with Thurston's conjecture (1982) proved by Perelman (2003), a nice presentation is in [10]. The decomposition considered by Thurston has a subtle difference with the JSJ: certain tori are not cut as it would lead to pieces that would not admit finite volume geometry.

Theorem 2.2.4 (Geometrization theorem). *Every oriented prime closed 3-manifold can be cut along tori, so that the interior of each of the resulting manifolds admits one of the eight geometries of Thurston with finite volume.*

Putting a geometry on a manifold is the topic of Chapter 5, but the definition will be slightly different for reasons exposed there. Here, to admit a geometry means to be diffeomorphic to the quotient of some Riemannian manifold X by a discrete subgroup of $\mathrm{Isom}(X)$, the group of isometries of X, acting freely on X. While the definition of a geometry is more general, we stick to the case where X is one of the eight geometries of the conjecture.

There are the spherical $\mathbf{S}^3$, Euclidean $\mathbf{E}^3$ and hyperbolic $\mathbf{H}^3$ geometries, the three Riemannian geometries of constant curvatures; there are the product geometries $\mathbf{S}^2 \times \mathbf{E}^1$ and $\mathbf{H}^2 \times \mathbf{E}^1$; the twisted product geometries Nil and $SL(\tilde{2}, \mathbb{R})$; and Sol. In all cases except for $\mathbb{H}^3$ and Sol, the underlying manifold is Seifert fibered, manifolds admitting a Sol geometry, are well understood too. This leaves the hyperbolic geometry which is actively worked on today.

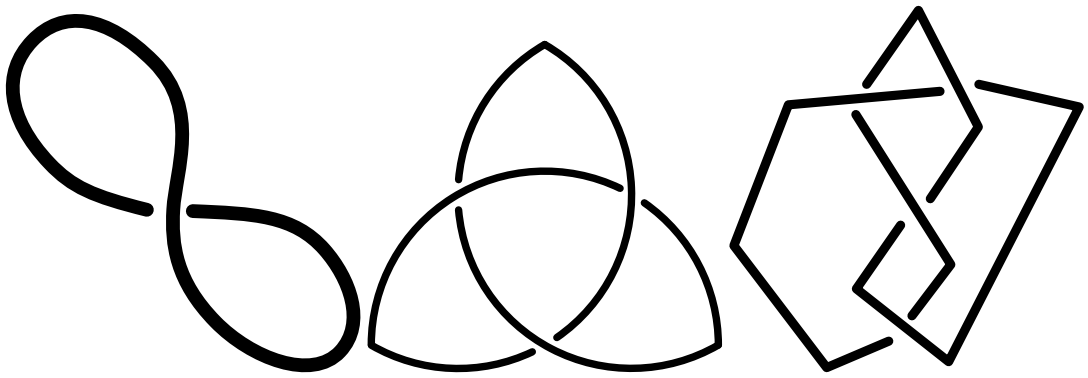

Figure 2.6 – Examples of knot diagrams. From left to right: an unknot with a twist, a trefoil knot and an 8 knot.

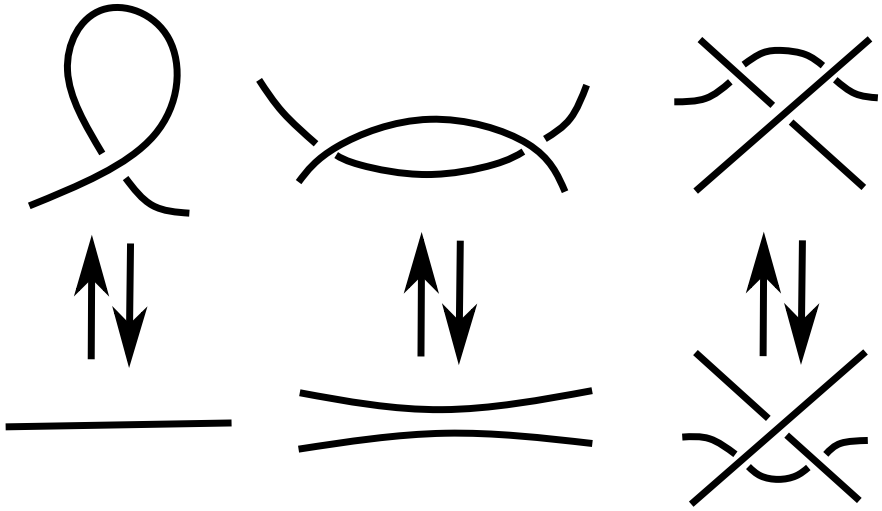

Figure 2.7 – List of Reidemeister moves.

2.3 A special case: knot and link complements

In this section we investigate specific family of 3-manifolds: the knot complements. A *knot* is an embedding of S^1 into S^3, *e.g.*, see Figure 2.6, they are useful modeling tools and have been studied for more than a century [1].

Two knots are considered identical if they are linked by an *ambient isotopy*, that is a continuous deformation of the space turning one into the other. These isotopies are difficult to represent and compute and we use other methods to compare knots.

A way of representing knots is to project them on a plane, creating *knot diagrams*. This projection must send the knot in general position, *i.e.*, strands of the knot only overlap at a finite number of distinct points, and only two strands per point, then its *crossing number* is the number of overlap points. This method is the most popular as it is visual (in fact, the vast majority of representations of knot on paper is with diagrams) and creates bridges with graph theory and combinatorics. For diagrams, equivalence is defined with *Reidemeister moves*, elementary moves presented in Figure 2.7.

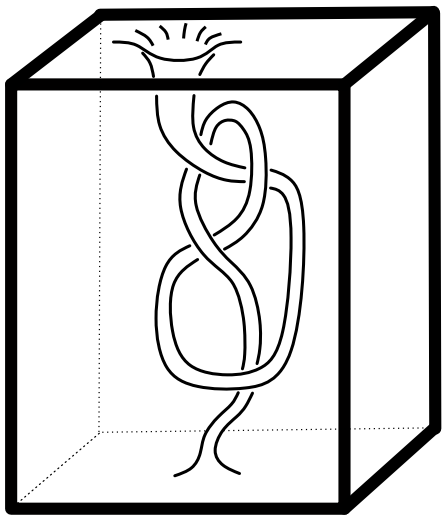

Figure 2.8 – Box representing the complement of the 8 knot in S^3.

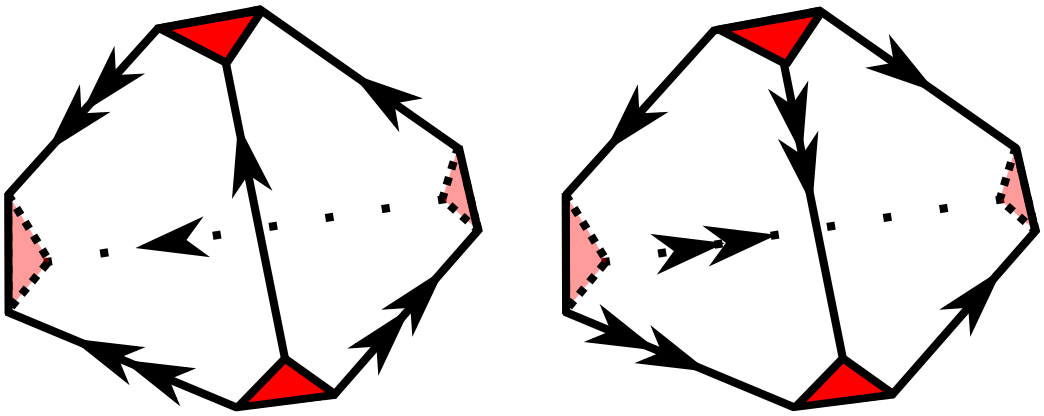

Figure 2.9 – Ideal triangulation of the 8 knot, the red surface is the link of the ideal vertex, *i.e.*, a torus.

Despite their popularity, solving the isotopy problem with diagrams is infamously difficult. For instance, given two diagrams of a knot and n the sum of their crossing numbers, an upper bound on the number of Reidemeister moves to go from one to the other is $\exp^{c^n}(n)$, where $c = 10^{10^6}$ and $\exp^a(b)$ is the a^{th} iteration of the function $\exp$ [21].

Another approach is to use the complements of the knots in S^3, for a knot K this is noted $S^3 \setminus K$, see Figure 2.8. This a a topological space that contains all the information about the knot:

Theorem 2.3.1 (Gordon–Luecke [63])**.** *If two knots have homeomorphic complements by an orientation-preserving homeomorphism, then the knots are equivalent.*

Starting from a knot diagram, computing a triangulation of such a space is polynomial in the crossing number of the diagram. Very briefly, an example of strategy is to insert tetrahedra at each crossing, plus one polyhedron above and one bellow the diagram, in order to have the

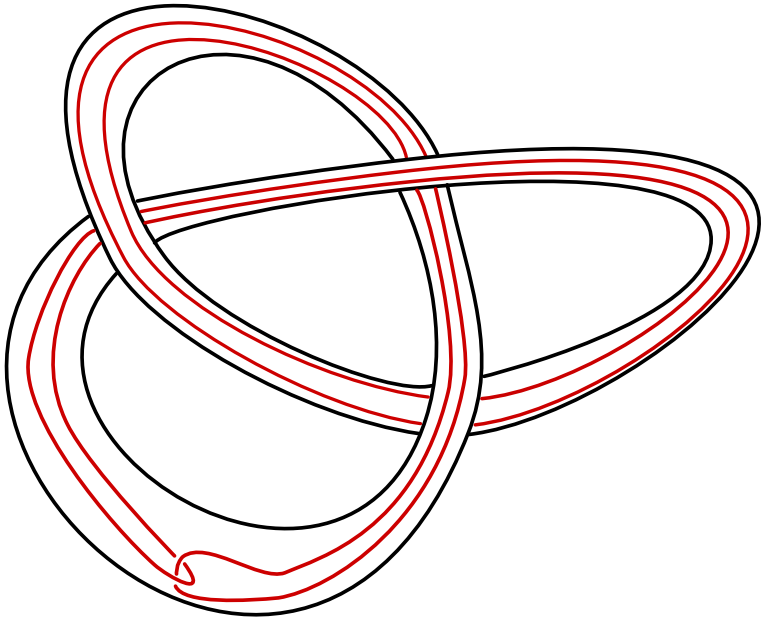

Figure 2.10 – Satellite knot in red, whose companion is the trefoil knot (in black).

knot represented on the edges of the triangulation. Then it is possible to "drill out" a tubular neighborhood of the knot from the triangulation. In details, explanations can be found in [75].

A triangulation of a knot complement can have two forms: either it is compact with a torus boundary, the boundary of the neighborhood of the knot, or it is an ideal triangulation, with one vertex whose neighborhood is a torus. The latter is obtained from the former by identifying the boundary of the triangulation to a single point, and the former from the latter by removing from the manifold an open neighborhood of the ideal vertex. An example of knot triangulation is presented in Figure 2.9, it is an ideal triangulation of the complement of the 8-knot, the vertices of the tetrahedra have been removed and the red area corresponds to a tubular neighborhood of the knot.

Thurston proved that knots are grouped in three mutually exclusive families: the satellite knots, the torus knots and the hyperbolic knots.

Definition 2.3.1 (Satellite knot)**.** A knot is satellite if its complement contains an essential torus.

The essential torus is itself a knotted torus, it is called the companion of the knot, see Figure 2.10 for a knot whose companion is the trefoil knot. This family includes *composite* knots, that is knots that can be obtained by taking two non-trivial knots, cutting them at a point, and merging the ends obtained into making a single knot. Knots that are not composite are said *prime*.

Definition 2.3.2 (Torus knot)**.** A knot is torus if it is the unknot or if it is not satellite and its complement contains an essential annulus.

These knots can be drawn on a torus, cutting the torus along the drawing of the knot produces the essential annulus. This family includes the unknot and the trefoil knot, see Figure 2.11.

Definition 2.3.3 (Hyperbolic knot)**.** A knot is hyperbolic if its complement is anannulus and atoroidal.

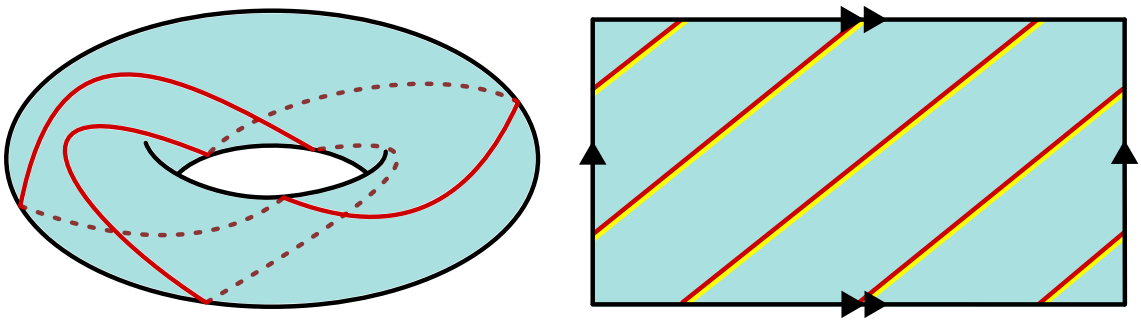

Figure 2.11 – Drawing of the trefoil knot (in red) on a torus, the annulus in the light blue surface. The knot is also known as the (2,3)-torus knot, as the knot goes two times around the torus while doing three turns around its cavity. On the Left is the draing of the torus and on the right the torus is cut open. On the right drawing, one boundary of the annulus is in red and the other is in yellow.

This family is the focus of Chapter 6. The complement of these knots admits a complete hyperbolic metric.

CHAPTER 3

Low dimensional topology and software

From representation to censuses, computers greatly help the study of 3-manifolds. As stated in Chapter 2, all 3-manifolds admit a triangulation greatly helping in their representation. The theory of normal surfaces constitutes a fundamental tool for their study, and once again, these can be handled efficiently by computers and thus the decomposition of a 3-manifold can be computed. Even the homeomorphism problem is (at least in theory) computable.

However, algorithms working on 3-manifolds tend to be complex and slow, at least in theory. This calls for global efforts to produce and maintain libraries to assist topologists in their tasks. Heuristics and alternative methods are also very important in this domain, as some families of triangulations can be more difficult to handle than others for some algorithms, and if such a family is the one important in a given problem, rooting for super exponential algorithms may not be a viable solution. This need for well developed libraries is further highlighted by the success of proof assistants like Lean [67] and Coq [6], which could become an asset in a close future.

This brief chapter presents some of the available resources, libraries and data sets, that we use and refer to in this manuscript.

3.1 Two major libraries

There exists a large quantity of code available online, a sample can be found on Dunfield's webpage [*]. The code on this page ranges from archives not designed to be read (see for instance Cusp and Geo by Casson [†]) to very popular standards known by a lot a people, and even outside the community. In this section, we present two major libraries: `SnapPy` and `Regina`.

3.1.1 SnapPy

`SnapPy` [22] is a Python library dedicated to the study of hyperbolic 3-manifolds mainly developed by Marc Culler, Nathan Dunfield, and Matthias Goerner, with outside contributions.

`SnapPy` is based on *SnapPea*, a C kernel created by Weeks during his PhD in the 80s. This kernel was known for its capability to compute complete hyperbolic structures and canonical triangulations of hyperbolic manifolds [87], even if both of those algorithms do not output a solution all the time. A particularity of SnapPea is that the sources contain comments that are mathematical proofs concerning the functions.

∗. https://nmd.web.illinois.edu//computop/

†. https://nmd.web.illinois.edu//computop/software/casson.tar.gz

On top of this kernel, a graphical interface and many modules where added, including certification with sage for instance. Its popularity can be explained by the fact it is simple to use and efficient at what is does. It is most likely the most well known library in low dimensional topology.

In Chapter 5, we dive into the computation of complete hyperbolic structures and use `SnapPy` as a baseline.

3.1.2 Regina

`Regina` [17] is a C++ library, with python and graphical interfaces, dedicated to the study of normal surfaces and 3-manifolds and mainly developed by Benjamin A. Burton, Ryan Budney, William Pettersson.

`Regina` is very efficient and well documented, among its most notable features are the enumeration of normal surfaces, the crushing and the computation of angle structures. A nice summary can be found in [14].

In Chapter 4, we use `Regina`'s implementations of the computation of Turaev-Viro invariants.

3.2 Data sets

In addition to libraries, it can be useful to have data sets to perform experiments, and make and test hypotheses. A recent example is a collaboration where a conjecture was made using AI before being proven mathematically [24]. There exist several data sets available, either only containing manifolds, like the one by Hodgson and Weeks [40], or with invariants computed, like KnotAtlas [5]. `SnapPy` and `Regina` are shipped with data sets to run experiments on, and a good source for censuses is the website of `Regina` ‡. In this manuscript, all our data come from this website.

Building these censuses is not a trivial matter, as it requires to check data for doubles, and this check is essentially the homeomorphism problem. Furthermore, the quantity of data to check is very large: the number of different prime knots increases at least exponentially with the crossing number [31]. The same goes for manifolds, with the difference that, instead of the crossing numbers, we look at the number of tetrahedra in the smallest triangulation.

Knots have been attracting the curiosity of mathematicians since Gauss, the history of their tabulation goes on today.

3.2.1 About knot censuses

The origin of knot theory dates back to the mid XIX$^{\text{th}}$ century, when ether was still a thing. With his theory of *vortex atoms* [81], Lord Kelvin believed that atoms were knotted vortices in ether whose chemical properties depended on the topological properties of these vortices. This led to a collaboration between Kirkman, Tait [78, 79, 80], and Little [53, 54, 55] which led to an enumeration of non-alternating knots with at most 10 crossings and alternating knots with at most 11 crossings. The next landmark occured in 1970, many years after the collapse of the vortex atoms theory with Conway's enumeration of alternating knots with eleven crossings [20]. At the time, he stated that the use of computers was redundant to compute his census, but they would be useful to compute algebraic knot invariants.

‡. https://regina-normal.github.io/data.html

Year	1890	1970	1983	1998	2020
#crossings	10	11	13	16	19
Total knots	249	801	12965	1.7×10^6	3.5×10^8
Total alternating	196	563	6729	4.9×10^5	5.2×10^7
Total non-alternating	53	238	6236	1.2×10^6	3.0×10^8

Table 3.1 – Evolution of the size of knot censuses through time.

Until this point censuses were built by hand, consisting of daunting work with several errors. In 1983, Dowker and Thistlethwaite [28] gave an algorithm and extended the census to 13 crossings; and to 16 crossings in 1998 with Hoste [41] with the software *KnotScape*. The last addition to this census was done recently by Burton [16] with the help of `Regina`. This last addition brings the census to knots with at most 19 crossings, for a total of about 350 million knots (see Table 3.1). For these last contributions, the method was based on diagram enumeration: list all planar graphs (which is reasonably easy) and then rid of diagrams representing identical knots (which is difficult).

Remark 3.2.1 – On the census from [16], out of more than 350 million knots only less than 400 are not hyperbolic. This would lead to the idea that most of the knot are hyperbolic, but this would go against several well established conjectures [85].

CHAPTER 4

Computation of Large Asymptotics of 3-Manifold Quantum Invariants

A main objective of low-dimensional topology is to study and classify 3-manifolds up to homeomorphisms. To do so, topologists have designed a variety of *topological invariants*, *i.e.*, properties allowing to distinguish between non-homeomorphic manifolds.

A remarkable family of topological invariants are the quantum invariants of Turaev-Viro [84]. They consist of an infinite family of real-valued quantities $(TV_r)_r$, indexed by an integer $r \geq 3$, defined on a triangulation of a manifold. Each invariant TV_r is made of an exponentially large sum of weights associated to combinatorial data attached to the triangulation.

These invariants have played a key role in computational topology. On the one hand, their combinatorial nature has allowed for the design of algorithms and the study of their computational complexity. Defined as a sum over combinatorial states, they can be computed with a simple backtracking algorithm of exponential complexity. They also admit a fixed parameter tractable algorithm, relying on dynamic programming and parameterized by the tree-width of the dual graph of the triangulation [18]. Algorithms can be further improved by pruning the search space for enumeration [58]. These algorithms are implemented in `Regina` and *Manifold Recogniser* [61, 62], and permit efficient computation of invariants TV_r for small values of r in practice. These invariants remain however extremely hard to compute in general: their computation belongs to the complexity class #P-hard [18, 46], which includes any algorithm that rely on the enumeration of exponentially large sets. Most notably, computing TV_r for large values of r, is a theoretical and practical challenge, even on small input triangulations.

On the other hand, these topological invariants are remarkably efficient to distinguish between non-equivalent manifolds in practice [58, 61]. As a consequence, their efficient implementations have played a fundamental role in the composition of census databases of 3-manifolds (by work of Burton, Matveev, Martelli, Petronio), which are analogous to the well-known dictionaries of knots [12, 61].

Turaev-Viro invariants are also central in mathematics. They are notably at the heart of Chen and Yang's *volume conjecture* [19, 26], the 3-manifold counterpart of the famous *volume conjecture* for knots [45, 68]. Chen and Yang's conjecture states that the asymptotic behavior of the sequence $(TV_r)_{r\geq 3}$ for a fixed manifold M is connected to the *simplicial volume* of M, a quan-

tity of distinctively different nature. The volume conjectures in low dimensional topology have attracted a lot of effort from the topology community. They have been partially proved on restricted families of manifolds and knots [19, 25], and verified experimentally on few spaces with very specific structures [19]; they remain some of the major open conjectures in low dimensional topology.

Contributions. In this chapter, we take a different turn on the computation of Turaev-Viro invariants, and compute large r values of TV_r on large sets of triangulated 3-manifolds. This computation being extremely challenging, we focus our attention to small triangulations of closed 3-manifolds ($n \leq 9$ tetrahedra), and the main dependence in complexity is in r, which contrasts with the usual computation where r is small. Under this model, we study experimentally the existing algorithms—backtrack enumeration and fixed parameter tractable algorithm—and conclude that the backtracking algorithm is more appropriate for large r computations of TV_r in practice (Section 4.2). We then resort to optimizing computation with the backtracking method. To do so, we introduce techniques and easily computable parameters to estimate the complexity of the computation of TV_r, for all r, on a triangulation T, using the backtracking algorithm (Section 4.3). This in turn permits efficient preprocessing of the triangulation—cherry-picking the best triangulation for computation (Section 4.4 and 4.5)—, and the fine tuning of arithmetic precision for correct multi-precision computation (Section 4.6). These optimizations are validated by various experimental studies.

Finally, using these optimizations, we compute Turaev-Viro invariants on large sets of low complexity 3-manifolds, and for large r values. These computations on the first manifolds of low complexity allow us to provide further experimental evidences to the volume conjecture for closed 3-manifolds (graph manifolds and hyperbolic manifolds), and study the speed of convergence of the sequence $(TV_r)_r$ (Section 4.7).

4.1 Background

Manifolds and triangulations. Unless mentioned otherwise, we consider in this chapter closed oriented 3-manifolds, *i.e.*, compact oriented manifolds locally homeomorphic to $\mathbb{R}^3$, represented by *generalized triangulations*.

We denote by v, e, f, and n the number of vertices, edges, triangles, and tetrahedra of a triangulation T, after gluings of the tetrahedra. The number of tetrahedra n of T is the *size* of the triangulation. By standard topological arguments, involving Euler characteristic and Poincaré duality, a triangulation of a closed 3-manifold satisfies:

$$e = n + v \tag{4.1}$$

We refer the reader to Chapter 2 for more details.

Turaev-Viro invariants. Turaev-Viro type invariants [84] of a triangulation T are defined as exponentially large sums of weights associated to *admissible colorings* of the edges of T.

Let T be a generalized triangulation of a closed 3-manifold M, let $r \geq 3$ be an integer, and let $I = \{0, 1/2, 1, 3/2, \ldots, (r-2)/2\}$ be the set of the first $r-1$ positive half-integers.

#tetra.	1	2	3	4	5	6	7	8
#Mani.	3	7	7	14	31	74	175	436
$\#H_1 = 0$	2	3	3	8	15	33	78	193

Table 4.1 – Number of topologically distinct, prime, closed, orientable 3-manifolds ("#Mani.") with a minimal triangulation of size n, $1 \leq n \leq 8$, ("#tetra.") and those among them with trivial first homology group $H_1(M, \mathbb{Z}/2\mathbb{Z}) = 0$ ("$\#H_1 = 0$").

Let E be the set of edges of T. A *coloring* of T is defined to be a map $\theta : E \to I$ from the edges of T to I. A coloring θ is *admissible* if, for each triangle of T, the three edges e_1, e_2, and e_3 bounding the triangle satisfy the following constraints:

$$\text{parity condition: } \theta(e_1) + \theta(e_2) + \theta(e_3) \in \mathbb{Z}; \tag{4.2}$$

$$\begin{aligned}&\text{triangle inequalities: } \theta(e_1) \leq \theta(e_2) + \theta(e_3),\\ &\theta(e_2) \leq \theta(e_1) + \theta(e_3), \text{ and } \theta(e_3) \leq \theta(e_1) + \theta(e_2);\end{aligned} \tag{4.3}$$

$$\text{upper bound: } \theta(e_1) + \theta(e_2) + \theta(e_3) \leq r - 2. \tag{4.4}$$

The set of admissible colorings of T is denoted by $\mathrm{Adm}(T, r)$.

Note that in generalized triangulations, a triangle may be defined by less than three different edges, in which case the constraints need to be slightly adapted. This is a simple technicality we do not mention in the following.

Given an admissible coloring θ of T, a *weight* $|x|_\theta$ of a face (vertex, edge, triangle, or tetrahedron) of T is a complex number that depends exclusively on the colorings $\theta(e)$ of the edges e incident to x.

Given an integer r and a weight system, the Turaev-Viro invariant $TV_r(T)$ associated to a triangulation is defined by:

$$\sum_{\theta \in \mathrm{Adm}(T,r)} \prod_{x \text{ face of } T} |x|_\theta. \tag{4.5}$$

In the definition of their invariant, Turaev and Viro describe sufficient conditions for the weight system to construct a topological invariant with the above formula, *i.e.*, $TV(T) = TV(T')$ for any two triangulations T and T' of the same manifold M. They also describe a specific weight system associated to the Lie algebra $\mathrm{sl}_2(\mathbb{C})$, and depending of an extra parameter $q \in \{1, 2\}$, leading to interesting topological invariants. We refer to [84] for exact definitions of these ; we use them in our computations for $q = 2$, which corresponds to the Chen-Yang volume conjecture verified in Section 4.7.

Note that this chapter focuses on the efficient enumeration of the set of admissible colorings $\mathrm{Adm}(T, r)$ of a triangulation, and is consequently mostly generalizable to any weight system.

Computation, data, and their representation. The computation of Turaev-Viro invariants belongs to the complexity class #P-hard, which makes them extremely challenging to compute for large triangulations or large values r. The state-of-the-art algorithms working for any $r \geq 3$ all have worst case complexity of the form $r^{\Theta(n)}$, for n tetrahedra triangulations (more details in Section 4.2).

In this chapter, we study the computation and values of invariants TV_r for large values of r (up to 100). This bonds our computations to *small* triangulations (mostly less than 6 tetrahedra, and up to 9 tetrahedra for the most challenging experiments) in order to be feasible. Note however that generalized triangulations can represent a vast variety of distinct topologies with very few tetrahedra. Table 4.1 summarizes the number of distinct, prime, oriented, closed 3-manifolds admitting a triangulation of minimal size n, for $n \leq 8$. In consequence, the experiments in this chapter concern tens of topologically distinct topologies, with no topological restriction other than admitting a small triangulation. In comparison, the volume conjecture for closed manifolds, verified experimentally in Section 4.7 as application of our work, has only been verified experimentally on a few triangulations of closed 3-manifolds [19] that admit the very specific topological property of being constructible by surgeries along two simple knots (K_{4_1} and K_{5_2}), which allows for faster computation. The methods in this chapter improve computation of TV_r for any triangulated 3-manifold.

In order to present statistics over censuses of triangulations, box and whisker plots are used. For all of them, the line inside the box represents the median of the sample and the box the first and last quartile. The whiskers cover the rest of the sample until 1.5 times the size of the box, every point outside this reach is added to the graph.

All programs are in `C++`, compiled with `gcc 9.3.1`, and run on a Linux machine with 2.40GHz processors and 128GB RAM.

4.2 Backtracking vs Parameterized Algorithms

Existing algorithms for Turaev-Viro invariants. In this section, we compare the performance of existing methods to compute TV_r for large r. We start by reviewing algorithms for Turaev-Viro invariants.

#tetra.	1	2	3	4	5	6	7	8
#Mani.	3	7	7	14	31	74	175	436
%faster	100	100	100	79	52	34	19	9

Table 4.2 – For fix number of tetrahedra $n \leq 8$ ("#tetra."), % of triangulations in the census for which the backtracking algorithm is faster than the FPT algorithm, when computing TV_r at $r = 11$ with single precision arithmetic.

Let T be a triangulation of a 3-manifold, and $r \geq 3$ be an integer. There is a straightforward backtracking algorithm to enumerate all admissible colorings $\mathrm{Adm}(T, r)$ of order r, and compute $TV_r(T)$. Let v be the number of vertices and n the number of tetrahedra in T. Consequently, T admits $n+v$ edges (Eq.(4.1)). Order the edges $e_1, \ldots, e_{n+v}$ of T. There are $(r-1)$ possible colors for an edge, consequently the backtracking algorithm consists of traversing a regular $(r-1)$-tree of depth $n+v+1$, where nodes at depth i, $1 \leq i \leq n+v$, correspond to the edge e_i, and

any of the $r-1$ downward facing arcs at such node corresponds to the assignment of a color $\{0, 1/2, \ldots, (r-2)/2\}$ to e_i in some coloring. In consequence, leaves of the tree are in bijection with colorings. The algorithm consists of traversing this tree in a depth-first fashion, stopping when any of the admissibility constraint (4.2), (4.3), or (4.4) is violated. If a leaf is reached, it corresponds to an admissible coloring θ, and we keep track of the sum $\sum_{\theta \in \mathrm{Adm}(T,r)} |T|_\theta$. Ordering the edges appropriately [18], this algorithm runs in worst case $O((r-1)^{n+v})$ operations (machine and arithmetic), storing a constant amount of data (pointers and weights *). However, in practice, only a small portion of the tree is explored, as admissibility constraints are violated early on ; see Section 4.4 for an experimental analysis.

The fixed-parameter tractable (FPT) algorithm introduced in [18] uses a standard dynamic approach to compile the sum (4.5) defining $TV_r(T)$, run on a combinatorial decomposition of the triangulation T. When k is a parameter measuring the *sparsity* of the triangulation †, with $1 \leq k \leq n-1$, it runs in $O(n \cdot (r-1)^{6(k+1)} k^2 \log(r))$ operations (machine and arithmetic) when $6(k+1) \leq n+v$, or $O(n \cdot (r-1)^{n+v}(n+v)^2 \log(r))$ operations otherwise. However, this algorithm has worst case exponential memory, and requires to store $O((r-1)^{6(k+1)})$ arithmetic values.

As predicted by the complexity analysis of these algorithms, the FPT algorithm shows better performance than the backtracking algorithm on most input triangulations with $n \leq 20$ tetrahedra, for very small values of r ($r \leq 7$) [18]. We study in the following the case of interest for this chapter, i.e., smaller triangulations $n \leq 9$ and larger values of r, and draw different conclusions.

Performance of algorithms for large r. Figure 4.1 presents the performance of the backtracking and parameterized algorithms on a 5-tetrahedra, treewidth 4 triangulation of a 3-manifold, with different arithmetic precision. The triangulation is the worst case possible for the parameterized method, and was selected to highlight the interest of the backtracking on some triangulations. In this analysis, we focus on the single precision backtracking ("Backtracking") and parameterized ("Parameterized") algorithms. The computation are run with the `C++` library `Regina` [17] with no original modifications. The backtracking algorithm clearly performs orders of magnitude better than the parameterized algorithm, and the difference of performance to compute TV_r increases with larger values of r.

In fact, even if the parameterized algorithm performs better than the backtracking algorithm in *larger* triangulations, as observed in [18], it is not the case for small triangulation. Table 4.2 pictures the fraction of triangulations of the census for which the backtracking algorithm performs better for the computation of TV_r, with $r = 11$. For triangulations with at most 5 tetrahedra, the backtracking algorithm performs better in the majority of cases, and still remains a better option in a substantial fraction of triangulations with up to 8 tetrahedra.

This interpretation is twofold. First, the exponent $6(k+1)$ in the complexity of the parameterized algorithm, $k \geq 1$, is likely to be larger than the exponent $(n+v)$ in the complexity of the backtracking algorithm, when n is small. Second, the backtracking algorithm explores a very small portion of the search tree when enumerating colorings.

Additionally, a main difficulty of the parameterized algorithm is its memory consumption. Indeed, Figure 4.1 stops at $r = 73$ because it is the last order r before which the parameterized algorithm requires more than the 128GB of memory available in the machine, with single precision

∗. Note that depending on the arithmetic precision required, weights may be stored on large numbers of bits.

†. More precisely, k is the *treewidth* of the dual graph of T [18].

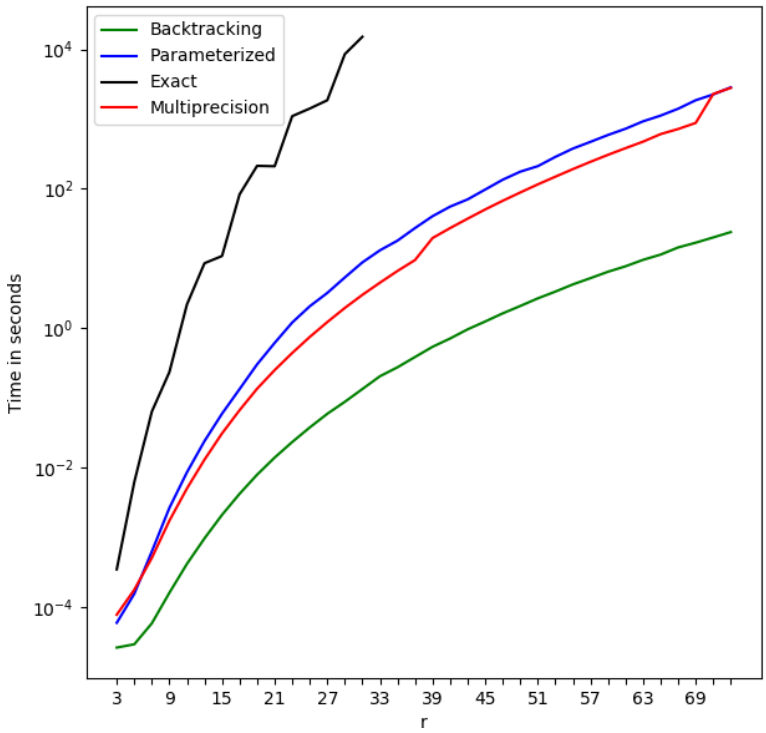

Figure 4.1 – Time performance for computing TV_r, $3 \leq r \leq 73$, on a 5-tetrahedra, treewidth 4 minimal triangulation of the manifold $\mathtt{SFS}[\mathtt{S}^2 : (2,1)(3,1)(5,-4)]$, using the backtracking algorithm with single precision arithmetics ("Backtracking"), with multi-precision arithmetics ("Multiprecision"), and with exact arithmetic in a cyclotomic field ("Exact"), and the FPT algorithm with single precision arithmetic ("Parameterized"). Note that having a very large treewidth, this example is very punishing for the later method.

numbers (*i.e.*, not taking into account the substantial space required by high precision arithmetic, which is necessary to get a correct result, due to the nature of the computation). Recall that the FPT algorithm has exponential memory complexity, which makes it rapidly intractable for larger triangulations and larger values of r. In comparison, the backtrack search uses a space linear in the size of the input times the size of the numbers used in the computations.

In conclusion, the backtracking algorithm is a better choice for computing large r asymptotics of the Turaev-Viro invariants on small triangulations. In the following sections, we describe optimizations to and implementation of the backtracking algorithm.

4.3 Ehrhart theory for counting admissible colorings

In this section, we introduce Ehrhart theory and use it to estimate the number of valid colorings for a subset of the manifold census.

4.3.1 Ehrhart theory and counting lattice points in polytopes

We introduce Ehrhart theory [29] on counting lattice points in polytopes.

Definition 4.3.1. A *polytope* P is a bounded subset of $\mathbb{R}^d$ defined as the set of solutions of a system of linear inequalities:

$$P = \{x | Ax \leq b\}, \text{with } A \in \mathbb{R}^{m \times d},\ b \in \mathbb{R}^m.$$

The polytope P is *rational* if $A \in \mathbb{Q}^{m \times d}$ and $b \in \mathbb{Q}^m$.

The *dilatation* of a polytope P by a factor $k \in \mathbb{N}$, denoted by kP, is the polytope obtained by multiplying b by k:

$$kP = \{x | Ax \leq kb\}.$$

It is equivalent to multiplying the coordinates of the vertices of P by k.

Ehrhart theorem states that the number of lattice points, *i.e.*, points with integer coordinates, in the dilatation kP of a rational polytope P, admits a closed form as a quasi-polynomial. Specifically,

Theorem 4.3.1 (Ehrhart [29])**.** *Let P be a rational polytope of dimension d. There exists a finite family of periodic functions $(e_i \colon \mathbb{N} \to \mathbb{R})_{i=0\ldots\deg}$ such that for all $k \in \mathbb{N}$:*

$$\#(kP \cap \mathbb{Z}^d) = \sum_{i=0}^{\deg} k^i \cdot e_i(k).$$

Where $\deg \in \mathbb{N}$.

Let us denote $L(P,k) = \sum_{i=0\ldots\deg} k^i \cdot e_i(k)$. We refer to this function as Ehrhart's polynomial. *It admits several remarkable properties:*

- *the period of the coefficients $e_i(\cdot)$ is the smallest integer k such that kP is a polytope with integer coordinates vertices;*
- *the degree* $\deg$ *of $L(P,\cdot)$ is equal to the dimension d of the polytope P;*
- *the leading coefficient $e_d(\cdot)$ of $L(P,\cdot)$ is a constant function, whose value is equal to the d-dimensional volume of the polytope P.*

The quasi-polynomial $L(P,\cdot)$ of a rational polytope P can be computed in time exponential in the embedding dimension:

Theorem 4.3.2 (Barvinok [7, 8])**.** *Let Δ be a d-dimensional simplex with integer coordinates vertices. Then $L(\Delta,\cdot)$ can be computed in time $(d \cdot |\Delta|^{O(d)})$ where $|\Delta|$ is the number of bits needed to encode Δ. This result can be extended to rational polytopes.*

4.3.2 Application to Turaev-Viro invariants

In this section, we adapt the definition of admissible colorings for Turaev-Viro invariants to Ehrhart theory's settings, and describe criteria for triangulations of a manifold M to admit a minimal number of colorings.

It was observed [58] that for a 3-manifold M with trivial homology group $H_1(M, \mathbb{Z}/2\mathbb{Z})$, all admissible colorings $\mathrm{Adm}(T,r)$ of any 1-vertex triangulation T of M and of any order $r \geq 3$ can only admit integer colors in $\{0, 1, 2, \ldots, \lfloor \frac{r-2}{2} \rfloor\}$. As a consequence, for such triangulations, the backtracking algorithm needs only explore a tree of much smaller size $O(\lfloor \frac{r}{2} \rfloor^{n+v})$. Additionally, the parity constraints (4.2) for admissibility, which is the only non-linear constraint, is always

satisfied with integer colors and can be omitted. In the following analysis, we exploit this fact to estimate the number of colorings in a triangulation, without enumerating them all, using Ehrhart theory.

As a consequence, we focus our attention to 3-manifolds M with trivial homology group $H_1(M, \mathbb{Z}/2\mathbb{Z})$ for the following theoretical analysis. Note that among the first smallest minimal triangulations of prime closed 3-manifolds, nearly half have trivial $\mathbb{Z}/2\mathbb{Z}$ homology; see Table 4.1. We also assume triangulations to be 1-vertex ; this is not a strong assumption as triangulations can be preprocessed efficiently to reduce the number of vertices to 1 (see Section 4.4).

Analysis and experiments. The following theoretical analysis follows the case $H_1 = 0$ and 1-vertex triangulation, to compute an accurate estimator of the number of admissible colorings. In the more general cases (manifolds with non-trivial homology, more than 1 vertex), the following analysis still provides a *lower bound* on the number of admissible colorings of a triangulation, and is still of interest. In consequence, in *all* following experiments—except Figure 4.4 that concerns the *exact* approximation of the number of admissible colorings and Figure 4.5 that concerns performances of the backtracking algorithm under this hypothesis—the full census of manifolds is used, regardless of their homology.

Consider now the admissibility constraints (4.3) and (4.4), *i.e.*, the constraints defining the admissible colorings minus the parity constraint. They are linear and consequently define a polytope. More specifically, let us consider the following:

Definition 4.3.2. Let T be a triangulation, with v vertices, f triangles, n tetrahedra, and $n + v$ edges. Consider the following $2(n + v) + 4f$ inequalities:

— for every edge, $-\theta(e) \leq 0$, and $\theta(e) \leq 1/2$,

— for every triangle with edges e_1, e_2, e_3, $\theta(e_1) - \theta(e_2) - \theta(e_3) \leq 0$, $\theta(e_2) - \theta(e_1) - \theta(e_3) \leq 0$, $\theta(e_3) - \theta(e_1) - \theta(e_2) \leq 0$, and $\theta(e_1) + \theta(e_2) + \theta(e_3) \leq 1$.

Let A be the $(2(n+v)+4f, n+v)$-matrix with $\{-1, 0, 1\}$ coefficients, and b the $(n+v)$-vector with $\{0, 1/2, 1\}$ coefficients, defining the rational polytope $P_T = \{x | Ax \leq b\}$ corresponding to this set of equations. We call P_T the *admissibility polytope* associated to T.

Lemma 4.3.3. *Let $r \geq 3$ be an integer, T a 1-vertex triangulation, with $n+1$ edges, of a manifold M with trivial $H_1(M, \mathbb{Z}/2\mathbb{Z})$, and P_T the associated admissibility polytope. Then the admissible colorings of* $\mathrm{Adm}(T, r)$ *are in bijection with the lattice points* $((r-2)P_T \cap \mathbb{Z}^{n+v})$.

proof.

Let x be an integer coordinate vector such that $x \in (r-2)P_T$, *i.e.*, $Ax \leq b$ as defined in Definition 4.3.2. Interpreting the i^{th} coordinate x_i of x as an integer color $\theta(e_i)$ for the i^{th} edge e_i of T, we note that, by definition of $(r-2)P_T$, all colors $\theta(e_i)$ are positive integers smaller than $(r-2)/2$, and the coloration θ satisfies admissibility constraints (4.2), (4.3), and (4.4). It consequently defines an admissible coloring. Because $H_1(M, \mathbb{Z}/2\mathbb{Z})$ is trivial and T is 1-vertex, all admissibility colorings appear as such integral vector (see discussion in Section 4.3.2).

□

Consequently, by Theorem 4.3.1, the number of admissible colorings in $\mathrm{Adm}(T, r)$ is equal to $L(P_T, r-2)$. We call the quasi-polynomial $L(P_T, \cdot)$ the *Ehrhart polynomial* of the triangulation T.

4.4 Triangulations with fewer colorings and estimation of running times

Choosing the triangulation that admits the smallest number of colorings among a given set of triangulations boils down to computing the Ehrhart polynomials of the triangulations and choosing the one with the minimal value at the desired dilatation. Computing these polynomials is however expensive, and we only consider their asymptotic values, *i.e.*, their degrees and leading coefficients.

4.4.1 Degree of Ehrhart polynomial.

For a triangulation T, the degree of $L(P_T, \cdot)$ is equal to the dimension of the polytope P_T (Theorem 4.3.1).

Lemma 4.4.1. *Let T be a triangulation and P_T the associated polytope. Then the dimension of P_T equals the number of edges in T.*

proof.

Vector $(\frac{1}{4}, \frac{1}{4}, \ldots, \frac{1}{4})$ does not saturate any of the constraint defining P_T, and consequently lies in the interior of P_T. Hence P_T is full dimensional. The dimension of the embedding space being the number of edges, this is also the dimension of P_T.

□

As a consequence of Lemma 4.4.1, finding a triangulation with smallest asymptotic number of admissible colorings starts with finding a triangulation with smallest number of edges. In a closed triangulation, the number of edges is equal to $n + v$, the number of tetrahedra plus the number of vertices (Equation 4.1), which can be controlled:

Theorem 4.4.2 (Jaco and Rubinstein [42])**.** *Aside from a small set of exceptions, a triangulation T of a prime, closed, orientable 3-manifold M, with n tetrahedra and v vertices, can be turned in polynomial time into a 1-vertex triangulation T' of M, with $n' \leq n$ tetrahedra.*

Notably, if M can be triangulated with a minimal number n_0 of tetrahedra, M admit such minimal triangulation with 1-vertex.

As a consequence, for a fixed prime, closed, orientable 3-manifold M, the number of admissible colorings $\mathrm{Adm}(T, r)$ for any triangulation T of M grows at least as fast as $r \mapsto ((\frac{r}{c})^{n_0+1})$, where n_0 is the size of a minimal triangulation for M and c is a constant. This is asymptotically optimal. We study the constant c, in connection with Ehrhart theory, in the next section.

4.4.2 Leading coefficient of Ehrhart polynomial.

The leading coefficient of $L(P_T, \cdot)$ is constant and equal to the volume of the polytope P_T (Theorem 4.3.1). Computing the volume of a polytope is #P-hard. However, there exist approximation schemes that are polynomial in the dimension of the polytope. For instance, [30] gives an ϵ-approximation of the volume of a d-dimensional polytope defined by m hyperplanes in time $O(\epsilon^{-2} m d^3 \log(d))$ (other terms depending on the geometry of the polytope are hidden).

We study experimentally the values of the volumes of polytopes associated to minimal triangulations of closed, prime, oriented 3-manifolds from the census.

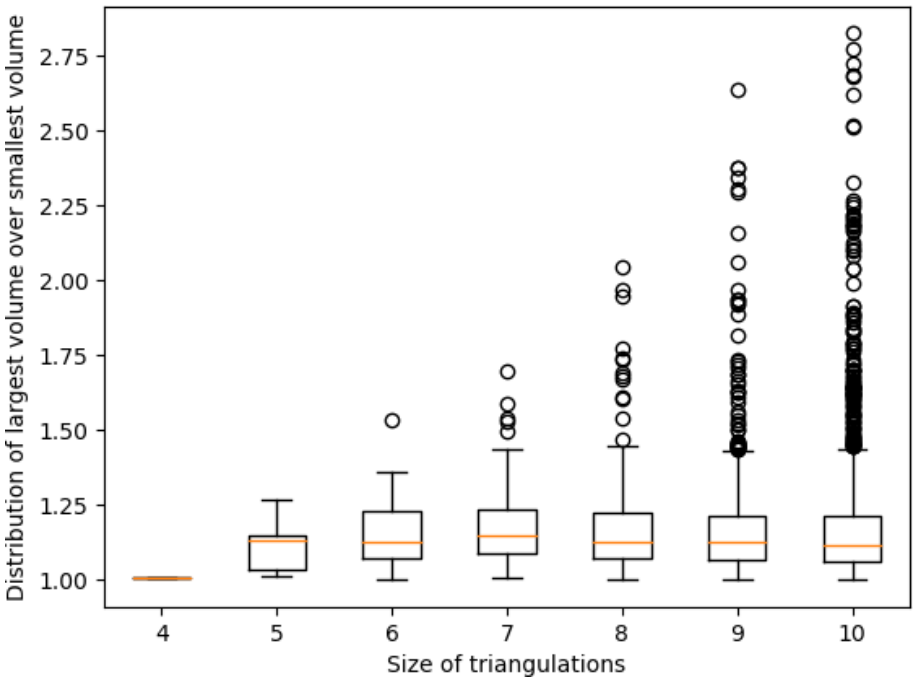

Figure 4.2 – Distribution of the ratio of the largest volume over the smaller volume (Equation 4.6) of polytopes associated to minimal triangulations, for all prime closed oriented 3-manifold admitting minimal triangulations of size 4 to 10.

Volumes of minimal triangulations of a same manifold. Figure 4.2 presents the distribution, over all prime closed orientable 3-manifolds M admitting minimal triangulations of up to 10 tetrahedra, of the ratio of the largest volume over the smallest volume of any polytope P_T associated to a minimal triangulation of M, *i.e.*,

$$\frac{\max\{\mathrm{vol}P_T | T \text{ minimal triangulation of } M\}}{\min\{\mathrm{vol}P_T | T \text{ minimal triangulation of } M\}} \tag{4.6}$$

Volumes for triangulations of up to 8 tetrahedra are exact, computed with Normaliz [11], and volumes for 9- and 10-tetrahedra triangulations are approximated within 5% with the approximation library VolEsti [30, 32].

The ratio of a majority of manifolds is close to 1. However, more outliers appear with larger triangulations, which is explained by the fact that manifolds tend to have an increasing number of distinct minimal triangulations for a growing number of tetrahedra. Consequently, on certain manifolds of up to 10 tetrahedra, choosing the appropriate minimal triangulation leads to a gain of a factor close to 3 when minimizing the asymptotic number of admissible colorings. Note that manifolds with less than 4 tetrahedra are omitted because they are few with several minimal triangulations.

In the following, we call a minimal 1-vertex triangulation T, with smallest volume $\mathrm{vol}P_T$ over all such triangulations of a manifold M, the *optimal triangulation* for M. In the following experiments, we use optimal triangulations of manifolds.

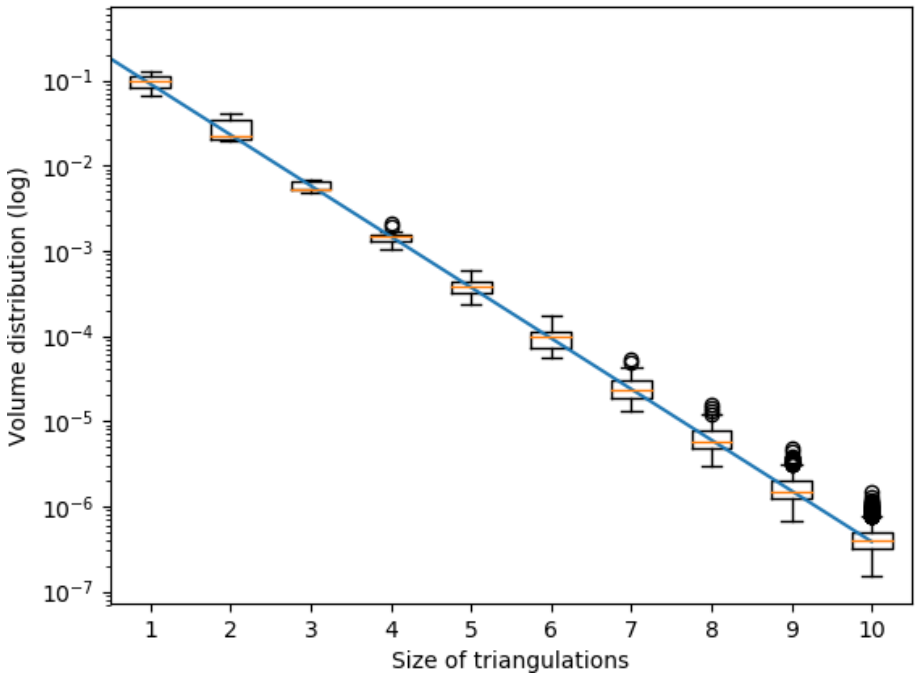

Figure 4.3 – Distribution of the volumes of optimal triangulations for all manifolds of the census, up to 10 tetrahedra. Medians are interpolated (r-value $= -0.9999$) by a straight line of slope -0.598 in log scale.

Polytope volumes of increasingly large minimal triangulations. Figure 4.3 presents the distribution of the volumes of polytopes P_T for optimal triangulations of manifolds in the census, ranging from 1 to 10 tetrahedra. We observe a clear exponential decay of the volumes of the polytopes for optimal triangulations of larger sizes.

By interpolating the medians, and using Ehrhart theory, we deduce that in average, an optimal triangulation T, with $n+1$ edges, admits experimentally $\Theta(\left[\frac{r-2}{3.97}\right]^{n+1})$ admissible colorings in $\mathrm{Adm}(T,r)$. This is a (practical) improvement by an exponential factor over the expected $O(\left[\frac{r}{2}\right]^{n+1})$ admissible colorings predicted by the theory for 3-manifolds with trivial homology, and $O([r-1]^{n+1})$ in the general case.

4.4.3 Accuracy of the parameter

For an optimal triangulation P_T with $n+1$ edges, we study the accuracy of the parameter $\mathrm{vol}P_T \cdot (r-2)^{n+1}$ (*i.e.*, the leading term of the Ehrhart polynomial counting $\mathrm{Adm}(T,r)$) to estimate the number of admissible colorings of T, and the running time of the backtracking algorithm.

Estimating the number of admissible colorings. Figure 4.4 presents the ratio:

$$\max\left\{\frac{\mathrm{vol}P_T\cdot(r-2)^{n+1}}{\#\mathrm{Adm}(T,r)}, \frac{\#\mathrm{Adm}(T,r)}{\mathrm{vol}P_T\cdot(r-2)^{n+1}}\right\} \geq 1, \tag{4.7}$$

for optimal triangulations with n tetrahedra, $1 \leq n \leq 6$, of the manifolds in the census with trivial homology H_1. Curves give the worst values of the ratio (4.7) over optimal triangulations of

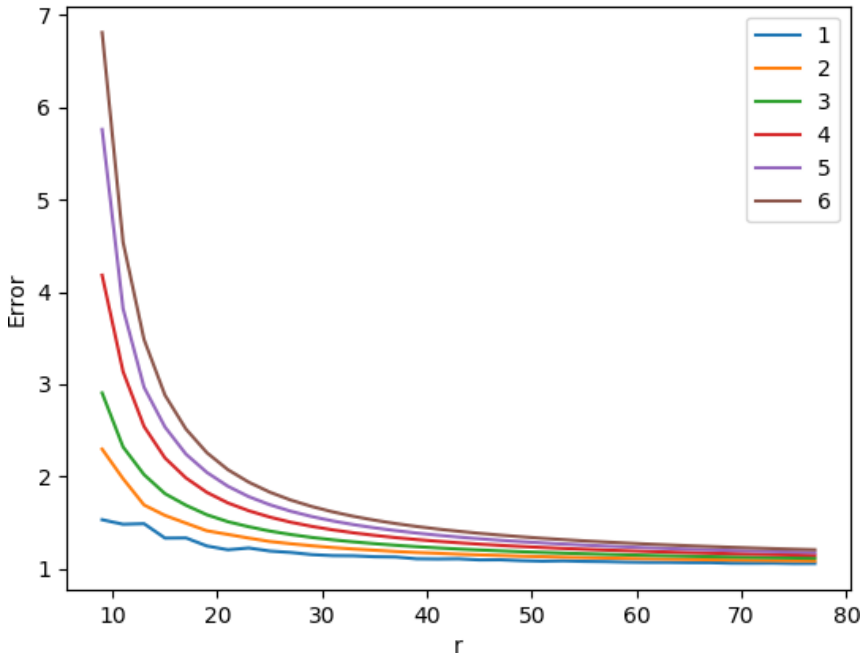

Figure 4.4 – Maximal value of ratio (Equation (4.7) between the estimator and number of admissible colorings for optimal triangulations with trivial H_1 of the census, from 1 to 6 tetrahedra, for increasing r.

the same size. As we are considering a first order approximation of the Ehrhart polynomials, we observe an expected error of order $O(r^{-1})$, and the quantity $\mathrm{vol}P_T \cdot (r-2)^{n+1}$ appears to be an accurate estimator of the size of $\mathrm{Adm}(T,r)$ for moderate values of r and above.

Estimating the combinatorial complexity of the backtracking algorithm. Figure 4.5 presents the ratio between the size of the search tree traversed by the backtracking algorithm, and the number of admissible colorings:

$$\frac{\text{size backtracking search}}{\#\mathrm{Adm}(T,r)} \geq 1, \tag{4.8}$$

for optimal triangulations T of the census of 5-tetrahedra triangulations with trivial homology H_1. The size of the backtracking search is an estimate of the number of combinatorial operations the backtracking algorithm for $TV_r(T)$ performs. For moderate values of r and above, we observe that the backtracking search is output-sensitive in the size of $\mathrm{Adm}(T,r)$, and there is no triangulation of size 5 that traverses a search tree larger that $4 \cdot \mathrm{Adm}(T,r)$ for $r \geq 39$.

In conclusion to this section, given a (1-vertex) triangulation T of a closed 3-manifold, we can compute efficiently the leading term $\mathrm{vol}P_T \cdot (r-2)^{n+1}$ of the Ehrhart polynomial, and estimate accurately both the number of admissible colorings in $\mathrm{Adm}(T,r)$ and the expected running time of the backtracking algorithm to compute Turaev-Viro invariants on T. We deduce a preprocessing strategy.

It is worthwhile, when computing large r asymptotics of Turaev-Viro invariants of a manifold M, to find an optimal (or close-to-optimal) triangulation of M minimizing the leading of the

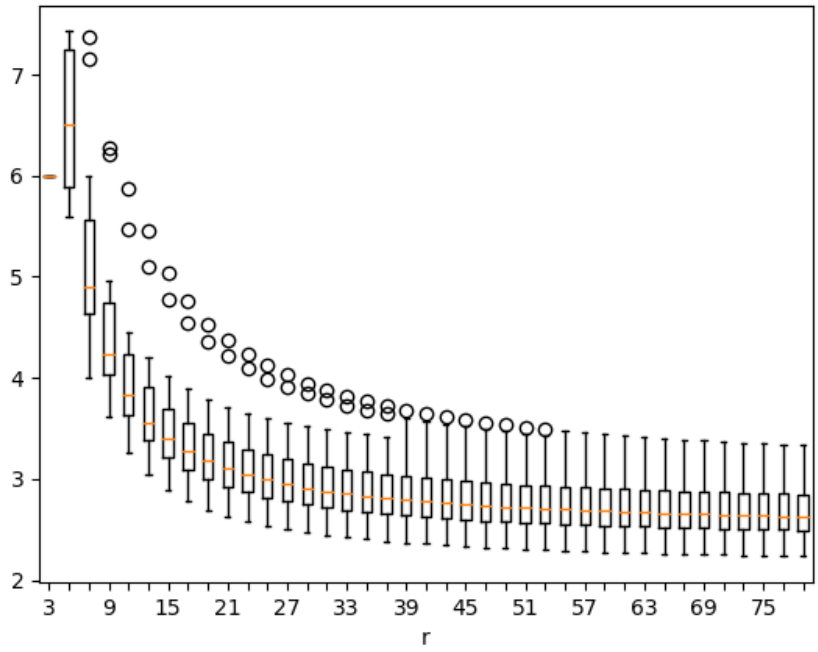

Figure 4.5 – Distribution, against r, of the number of tree nodes explored by the backtracking divided by the number of valid colorings for all manifolds with trivial homology H_1 and smallest triangulation of size 5.

corresponding Ehrhart polynomial. When preprocessing an input triangulation, we consequently reduce it (in polynomial time) into a 1-vertex triangulation (Theorem 4.4.2), and search for a minimal such one. The later step is a theoretically hard procedure, however proceeding to random combinatorial modifications of the triangulation, preserving its underlying topology, such as Pachner moves, is efficient in practice for reducing the size of triangulations [14]. Additionally, keeping track of the minimal triangulations encountered, we record the volume of their associated polytopes P_T, and keep the minimal triangulation of smallest polytope volume. Note that computing Ehrhart polynomials is very expensive and can be a major bottleneck. In practice, approached methods works well [30] to compute (part of) the polynomial.

In the following, we use census triangulations that are already minimal, and we select the optimal such triangulation.

4.5 Admissible colorings of manifolds with non-trivial first homology group

In this section, we propose a result similar to Lemma 4.3.3 for manifolds with non-trivial $H_1(T, \mathbb{Z}/2\mathbb{Z})$.

Let M be a prime, closed, oriented 3-manifold. Let T be a 1-vertex triangulation of M. Let E be the set of edges of T. Let $\tilde{E}$ be the vector space generated by E over the field $\mathbb{Z}/2\mathbb{Z}$.

Definition 4.5.1 (Parity function, associated cycle)**.** Given a coloring θ of the edges of T, the associated *parity function* is a linear form ℓ over $\tilde{E}$ such that for any $e \in E$, $\ell(e) = 1$ if and only

if $\theta(e) \equiv 1/2 \mod 1$. A parity function is *admissible* if it is associated to an admissible coloring. There can be several colorings associated to a parity function, by default we pick the one with values in $\{0, 0.5\}$.

Given a parity function ℓ, let its *associated cycle* be the cycle

$$c_\ell := \sum_{e \in E, \ell(e)=1} e,$$

with $\mathbb{Z}/2\mathbb{Z}$ coefficients.

The following lemma is very similar to a result that can be found in [58]. Its proof is included as it is more straight forward, since it boils down to one argument.

Lemma 4.5.1. *Given a 1-vertex triangulation T of a prime, closed, oriented 3-manifold, $H_1(T, \mathbb{Z}/2\mathbb{Z})$ and the set of admissible parity functions of T equipped with a structure of $\mathbb{Z}_2$ vector space are isomorphic.*

Furthermore, for each element $[c] \in H_1(T, \mathbb{Z}/2\mathbb{Z})$ there exists a unique parity function such that its associated cycle belongs to the homology $[c]$.

proof.

Let ℓ be a parity function over E, the edges of T. In order to exist, the only constraint it should verify is its admissibility.

The number of admissible parity functions is the number of linear forms ℓ over $\tilde{E}$ such that for all (x, y, z) colors corresponding to edges of a triangle in T, $l(x + y + z) = 0$. This statement means that the kernel of ℓ must contain the subspace of $\tilde{E}$ generated by the sums of edges that define triangles in T. Let K be this subspace, the set of admissible parity functions is the space $(E/K)^*$ dual of (E/K).

$H_1(T, \mathbb{Z}/2\mathbb{Z})$ is defined as $\mathbf{Z}_1(T, \mathbb{Z}/2\mathbb{Z})/\mathbf{B}_1(T, \mathbb{Z}/2\mathbb{Z})$, the quotient of the space of 1-cycles by the space of boundaries of collection of triangles. On the one hand, as T has only one vertex, any collection of edges is a cycle and $\mathbf{Z}_1(T, \mathbb{Z}/2\mathbb{Z})$ is equal to $\tilde{E}$. On the other hand, $\mathbf{B}_1(T, \mathbb{Z}/2\mathbb{Z})$ is the space generated by the sums of edges that define triangles in T, thus $\mathbf{B}_1(T, \mathbb{Z}/2\mathbb{Z}) = K$.

Since the spaces considered are of finite dimension, $(E/K)^*$ and $H_1(T, \mathbb{Z}/2\mathbb{Z})$ are isomorphic.

□

Lemma 4.5.1 gives the set of all possible parities given a triangulation. In order to characterize all possible colorings, ignoring the upper-bound constraint for now, we use the following lemma:

Lemma 4.5.2. *Let T be a triangulation and $r \geq 3$, we consider the admissible colorings of T.*

For all θ integer colorings and θ' coloring associated to an admissible parity functions of T (hence with values in $\{0, 0.5\}$).

- *If θ is admissible, then $\theta + \theta'$ is also admissible up to the bounding conditions.*
- *If $\theta + \theta'$ is admissible, then θ is admissible up to the bounding conditions except for $O(r^n)$ values of $\theta + \theta'$.*

proof.

Let x, y and z be the edges of some triangle t.

The first point is straightforward:

— since the parity function is admissible, the parity condition is satisfied;

— since θ is admissible, the triangle inequalities remain valid as either they are not modified or θ' adds to the greater side at least 0.5 and adds at most 0.5 to the two shorter sides of the inequalities.

For the second point let us assume $\theta + \theta'$ is admissible. Since θ' is admissible, θ satisfies the parity condition. If the triangle inequalities are strict for $\theta + \theta'$, then, with a similar argument as for the first point, by removing θ' the inequalities are still satisfied.

Let us assume at least one of the inequalities is not strict, that is, without loss of generality, $\theta(x) = \theta(y) + \theta(z) + 1$ and θ' adds 0.5 to $\theta(y)$ and $\theta(z)$. Then, at least for this triangle and it is the only way to have this, $\theta + \theta'$ is admissible while θ is not.

This is only possible if θ' adds 0.5 to $\theta(y)$ and $\theta(z)$, and all these "problematic" points are on the hyperplane $\theta(x) = \theta(y) + \theta(z) + 1$. Since there is a constant number of triangles (the triangulation is fixed) on which θ' can do this pattern and a constant number of parity functions, there are at most $O(r^n)$ such colorings. The result follows.

□

We can now have an estimation of the number of admissible colorings for triangulations of manifolds with non-trivial first homology group:

Lemma 4.5.3. *Let T be a 1-vertex triangulation with $n+1$ edges of a manifold M:*

$$\#(\mathrm{Adm}(T, r)) = \Theta_{r\to\infty}(|H_1(T, \mathbb{Z}/2\mathbb{Z})|\#(rP_T \cap \mathbb{Z}^{n+1})).$$

proof.

Since by Lemma 4.5.2, the number of non-integer admissible colorings that is not the sum of an integer admissible coloring and a admissible parity function ($O(r^n)$) is negligible compared to the number of integer colorings ($O(r^{n+1})$), they are ignored in this proof.

Let $r \geq 7$ be an odd integer. It was shown in the proof of Lemma 4.3.3 how each coloring with integer values of $\#(\mathrm{Adm}(T, r))$ corresponds to a point in $\#((r-2)P_T \cap \mathbb{Z}^{n+1})$. This can be extended to any element of $\#(\mathrm{Adm}(T, r))$ corresponding to a point in $\#((r-2)P_T \cap (1/2 \times \mathbb{Z})^{n+1})$.

From Lemma 4.5.1, for each admissible parity function, there exists a unique associated cycle, and for each such cycle interpreted as a collection of edges, there exists a unique corresponding vector $v' \in \{0, 1/2\}^{n+1}$ such that for $v \in \mathbb{Z}^{n+1}$, the admissibility of the coloring associated to $v + v'$ depends only on the linear constraints. Thus, $\#(\mathrm{Adm}(T, r))$ is bounded from above by $\#(|H_1(T, \mathbb{Z}/2\mathbb{Z})|(r-2)P_T \cap \times\mathbb{Z}^{n+1})$.

Let P' be the polytope defined by the inequalities $\theta(e_i) - \theta(e_j) - \theta(e_k) \leq -1$ and $\theta(e_i) + \theta(e_j) + \theta(e_k) \leq (r-3)$ for all e_i, e_j and e_k defining a triangle in T and $\theta(e_i) \in [1, (r-4)/2]$. Clearly, $\#(\mathrm{Adm}(T, r))$ is bounded from bellow by $\#(|H_1(T, \mathbb{Z}/2\mathbb{Z})|P' \cap \times\mathbb{Z}^{n+1})$. Furthermore, after translating P' along the vector $(-1)^{n+1}$, it becomes defined by the inequalities $\theta(e_i) - \theta(e_j) - \theta(e_k) \leq 0$ and $\theta(e_i) + \theta(e_j) + \theta(e_k) \leq (r-6)$ for all e_i, e_j and e_k defining a triangle in T and $\theta(e_i) \in [0, (r-6)/2]$. The polytope is equal to $(r-6)P_T$. As the translation is done by an integer vector, $\#(\mathrm{Adm}(T, r))$ is bounded from bellow by $\#(|H_1(T, \mathbb{Z}/2\mathbb{Z})|(r-6)P_T \cap \times\mathbb{Z}^{n+1})$.

By Ehrhart's theory, for large r and by setting k the volume of P_T times $|H_1(T, \mathbb{Z}/2\mathbb{Z})|$,

$$\#(\mathrm{Adm}(T, r)) \in [k(r-6)^{n+1} + O_{r\to\infty}(r)^n, k(r-2)^{n+1} + O_{r\to\infty}(r)^n].$$

Finally $(r-2)^{n+1} - (r-6)^{n+1} = O_{r\to\infty}(r)^n$ means the actual value of $\#(\mathrm{Adm}(T, r))$ cannot be too far away fro the estimate.

□

In conclusion to this section, using P_T provides a good estimate for the number of admissible colorings, no matter the first homology group of the manifold. This work can be extended with a more complete analysis of the second case of Lemma 4.5.2 to provide a better backtracking algorithm. For instance by being able to list all non-integer colorings around a given integer coloring.

4.6 Multi-precision arithmetics

The enumeration of the colorings and the complexity of the computation of their weights imply a large number of arithmetic operations during the computation of Turaev-Viro invariants. In this section we discuss this aspect of the computation.

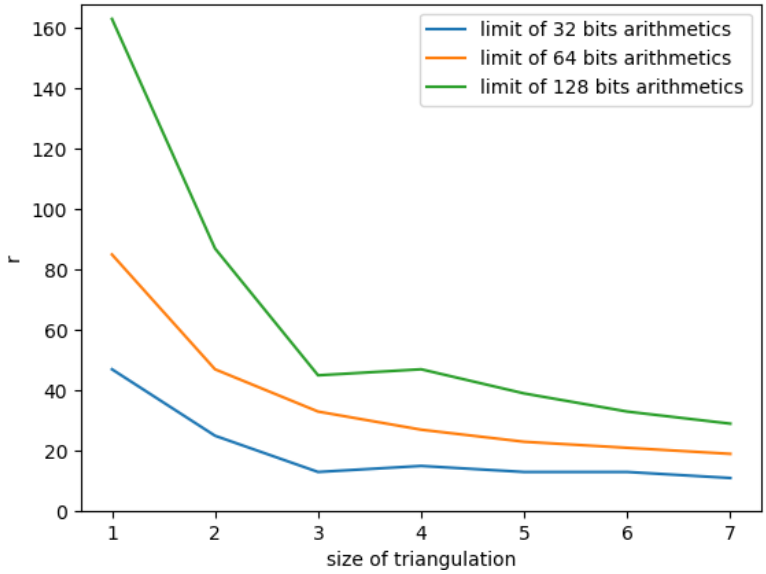

Figure 4.6 – Maximal value of the order r for different triangulation sizes such that the error on the multi-precision computation of TV_r is smaller than 5% on at least half of the census, for 32, 64 and 128 bits.

The weights for Turaev-Viro invariants [84] are complex numbers, and the Turaev-Viro invariant $TV_r(T)$ of an n-tetrahedra triangulation is made of an exponential large ($r^{O(n)}$) sum of products of $O(n)$ weights. As a consequence, arithmetic errors may accumulate. We implement multi-precision arithmetic using the `MPFR` library [33], within the backtracking algorithm of `Regina` [17].

Figure 4.6 illustrates the importance of high-precision arithmetics for computing Turaev-Viro invariants. For a given arithmetic precision, the curve in Figure 4.6 illustrates the maximal value of r for which the output of the backtrack algorithm is *correct* on more than half of the census. We define *correctness* by a relative error of less than 5%. We note that for single precision 64-bits arithmetic, the computation is already incorrect for values of $r \geq 33$ on more than half the triangulations larger than 3 tetrahedra.

Remark 4.6.1 – We did not use any oracle with the correct value to obtain an error margin of 5%. We did each computation two times, one with a given number of bits, and one with twice that number. If both values agree, we considered them to be correct, otherwise we star again with twice the number of bits. This approach assumes a low chance of collisions, *i.e.*, two identical wrong values. This can be done as there is a regularity in the precision when the parameter increases: the values of the decimals of the invariants slowly become wrong and the difference between a calculation and the same one with twice the number of bits can easily be observed. For (much) larger manifolds, in case of a doubt, three of four times the number of bits can be taken. The starting number of bites was fixed at 64, and since we did many computations for the same manifold, we could remember the number of bits required at each step.

Note that the estimator of the number of admissible colorings from Section 4.3 can be used to estimate the number of arithmetic operations to be performed by the backtracking algorithm, and in turn set the necessary precision of arithmetic numbers to compute a provably correct approximation of TV_r. However, bounds are pessimistic, and we use the following practical approach.

For each order r, we compute each invariant at least twice: with a given number of bits and with twice that number. If the relative difference between the two quantities is larger than a given threshold, we start again with twice the number of bits for the two values until the gap is small enough. For the following order, keep the numbers of bits that were sufficient at the previous order r. We begin the computation of the invariants of order $r = 3$ using 128 and 256 bits.

Note that the Turaev-Viro invariant can be equal to zero, in that case the relative difference between our two computations may be large. We used a threshold bellow which the invariant is considered equal to zero.

We validated this approach by testing it for some small triangulations and for small orders on larger triangulations and comparing the results to the same computation with a a larger number of bits. The use of multi-precision has a large impact on computation times. Figure 4.1 shows the difference between the backtracking algorithm with single precision arithmetic (leading to erroneous values of TV_r already for small r), the backtracking algorithm using exact encoding of polynomials, and the multi-precision arithmetic we implemented. Both exact and multi-precision arithmetic lead to correct computation of TV_r. We however observe that the multi-precision approach is about 4 orders of magnitude faster in practice.

Remark 4.6.2 – The multi-precision curve of Figure 4.1 presents two jumps, one for $r = 39$ and one for $r = 71$. They correspond to the doubling of arithmetic precision following the strategy described above.

Integration to `Regina`. Our use of `MPFR` resulted in an interface for `Regina` that is currently under review for integration. The methods available in `Regina` to compute the Turaev-Viro invariants are templated and all of them will be able to use multi-precision arithmetic, which is non negligible as it offers flexibility between the speed of the floats and the precision of exact computations.

4.7 Asymptotics of the sequence of Turaev-Viro invariants

In this section, we verify experimentally and extend, based on our observations, Chen and Yang's volume conjecture [19], and its extension by Detcherry, Kalfagianni, and Yang [26], for

closed 3-manifolds. The conjecture asserts that the growth rate of the Turaev-Viro invariants of a manifold M is governed by the *simplicial volume* of M. Note that there are several other volume conjectures for manifolds (non-compact, with boundary, etc), but we state only the case of closed manifolds.

4.7.1 Volume conjecture for 3-manifolds

The *simplicial volume* of a (compact oriented) manifold M, denoted by $||M||$, is a topological invariant introduced by Gromov [36] as a norm on singular homology. Two very important families of manifolds appear in our experiments, *graph manifolds* and *hyperbolic* manifolds.

All closed orientable irreducible 3-manifolds that admit triangulations with at most 8 tetrahedra are *graph manifolds* [61], and they all have simplicial volume 0.

There exist closed hyperbolic 3-manifolds, *i.e.*, manifolds admitting a (unique) complete hyperbolic geometry, that can be triangulated with 9 tetrahedra. For an hyperbolic 3-manifolds M, the simplicial volume $||M||$ is strictly positive, and is equal to the hyperbolic volume of M times a universal constant $1/v_3$. In that sense, the simplicial volume is a generalization of the hyperbolic volume to all compact 3-manifolds.

By work of Jaco-Shalen-Johannson, and the Thurston-Hamilton-Perelman geometrization theorem (see [61, Section 2.4]), graph manifolds and hyperbolic manifolds form the building blocks of any 3-manifold.

A motivation of this work is the following extension of the following conjecture by Chen, Yang [19] (for hyperbolic manifolds), and Detcherry, Kalfagianni, Yang [26] (for general manifolds):

Conjecture 4.9 (C-Y [19], D-K-Y [26])**.** For a closed oriented hyperbolic 3-manifold M, let $TV_r(M)$, $r \geq 3$, be its Turaev-Viro invariants (at $\mathrm{sl}_2(\mathbb{C})$ with $q = 2$) and let $||M||$ be its simplicial volume. Then, for r running over all odd integers,

$$\lim_{r\to+\infty} \frac{2\pi}{r} \log(TV_r(M)) = v_3||M||. \tag{4.10}$$

Additionally, for any closed oriented (not necessarily hyperbolic) 3-manifold M, and r running over all odd integers,

$$\limsup_{r\to+\infty} \frac{2\pi}{r} \log(TV_r(M)) = v_3||M||. \tag{4.11}$$

This volume conjecture has attracted attention from the topology community. Notably, Equation (4.10) has been proved for closed hyperbolic manifolds obtained by integral Dehn surgery along the figure eight knot [71]. Additionally, any closed 3-manifold M with $||M|| = 0$ satisfies Equation (4.11) [25]. Further, a convergence estimate has been proved for *Seifert fibered spaces* (a subclass of graph manifolds), where $\frac{2\pi}{r} \log(TV_r(M)) \in O(\log r/r)$.

In the following, we apply the optimized computation of Turaev-Viro invariants described in earlier sections in order to verify experimentally the behavior of the sequences $(\frac{2\pi}{r} \log(TV_r(M)))_r$ on the census of closed 3-manifolds for large r. Our experimental study below allows us to refine the volume conjecture:

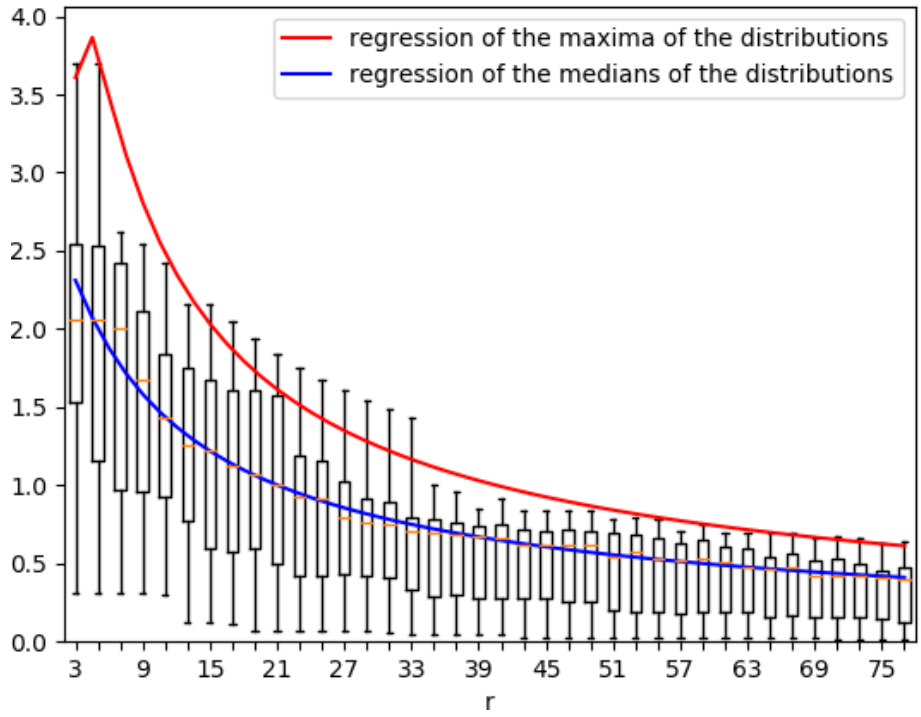

Figure 4.7 – Distribution of $(S_r(M))_r$ for all manifolds with minimal triangulation of size 5 in the census. The maxima and medians of the distributions are interpolated with fitting Model 1.

Conjecture 4.12. Let M be any closed oriented (not necessarily hyperbolic) 3-manifold, $TV_r(M)$ and $||M||$ as above. Then, the set of odd integers r such that $TV_r(M) \neq 0$ (denoted R^*_M) is infinite. Additionally, when r runs over R^*_M, we have,

$$\liminf_{r\to+\infty} \frac{2\pi}{r} \log(TV_r(M)) = v_3||M||.$$

This last conjecture completes the above volume conjectures, and both of them fully characterize the asymptotics behavior of the Turaev-Viro sequence of invariants, for any closed 3-manifolds.

Additionally, for a fixed 3-manifold M, we observe, on all manifolds studied, a rate of convergence of the sequence $\frac{2\pi}{r}\log(TV_r(M))$ towards its limit $v_3||M||$, of order $\widetilde{O}(\frac{1}{r})$, where $\widetilde{O}$ hides a poly-log factor in r.

Measuring the speed of convergence. Let M be a manifold for which all Turaev-Viro invariants have been computed until some index $r_{\max}$. Consider the quantity:

$$S_r(M) = \max_{r\leq k\leq r_{\max}} \left(\left| \frac{2\pi}{k} \log(TV_k(M)) - v_3||M|| \right| \right).$$

This quantity decreases when r grows, and allows us to study the convergence of the sequence $\frac{2\pi}{r}\log(TV_r(M))$. We study two sets of manifolds.

4.7.2 Graph manifolds with up to 7 tetrahedra

In this section we are considering all manifolds with minimal triangulations with at most 6 tetrahedra, and some triangulations with 7 tetrahedra. As per the discussion above, they all have

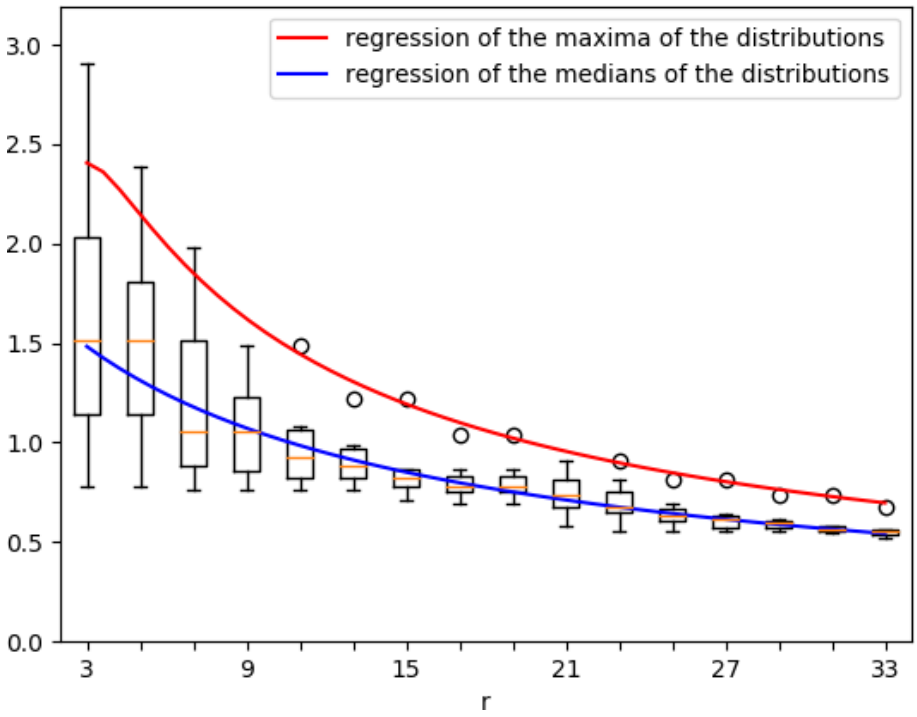

Figure 4.8 – Graph of $(S_r(M))_r$ for non-Seifert fibered graph manifolds with 7-tetrahedra triangulations. They are obtained by gluing two Seifert fibered spaces along their boundaries. The maxima and medians of the distributions are interpolated with fitting Model 1.

simplicial volume 0. Several manifolds from the census have recurring values of r for which their Turaev-Viro invariant equals 0 (and the term $\log TV_r$ is undefined). For all manifolds M, we only consider orders $r \in R_M^*$ for which $TV_r(M) \neq 0$ in the experiments. No sequence appear to become uniformly trivial.

Figure 4.7 presents, for every closed 3-manifolds whose minimal triangulation admits 5 tetrahedra, the distribution of the quantity $S_r(M)$ for an $r_{\max} = 77$. Appendix A (Figures A.1a, A.1b, A.1c, A.1d, A.1f) introduces similar plots for the other minimal triangulations with ≤ 6 tetrahedra. All sequences appear to converge towards 0. We interpolate the maximal and median values of S_r over the census with a fitting model:

$$x \mapsto \frac{a \log(x+b)}{x+b}. \tag{1}$$

All manifolds in the census with less than 6 tetrahedra are Seifert fibered spaces, and the $O(\log r/r)$ behavior is proved for the $\limsup$ of the sequence [25] for such spaces. Figure 4.7 emphasizes that the $\liminf$ of the sequence, for all values for which $TV_r \neq 0$, also converges towards the quantity $v_3||M|| = 0$, with experimental convergence $O(\log r/r)$.

We draw similar conclusions when extending our analysis to the first seven 7-tetrahedra triangulations of graph manifolds (volume simplicial 0), that are not Seifert fibered ; see Figure 4.8.

These experiments motivate the new conjecture 4.12, describing fully the convergence of the sequence of Turaev-Viro invariants for all graph manifolds.

Additionally, when comparing similar plots for minimal triangulations of ≤ 6 tetrahedra (see Appendix A), we notice that the fitting curves, describing the convergence of the sequence, are almost independent of the number of tetrahedra of the triangulations. This suggests the existence of a *slowly growing function* f, in the minimal number of tetrahedra, such that for any graph manifold M that can be triangulated with n tetrahedra, if $TV_r(M) \neq 0$ then:

$$\left|\frac{2\pi}{r}\log(TV_r(M))\right| \leq f(n) \cdot \frac{\log r}{r}$$

4.7.3 Hyperbolic manifolds with 9 tetrahedra

We verify experimentally Conjecture 4.9 for the four 9-tetrahedra closed hyperbolic 3-manifolds. For 9-tetrahedra triangulations, the computation are much more challenging, and we compute the Turaev-Viro invariants up to $r_{\max} = 39$. Figure 4.9 presents the sequence $2\pi/r \log TV_r(M)$ of Conjecture 4.9 for the Weeks manifold, and we observe its convergence towards $v_3||M|| = 0.9427\ldots$ (the *hyperbolic volume* of the manifold). The sequence is interpolated with the following fitting model:

$$x \mapsto \frac{a}{x+b} + c. \tag{2}$$

We observe a similar converging behavior for the other three hyperbolic manifolds with a nine tetrahedra triangulation (see Figures A.2b, A.2c and A.2d in Appendix A).

We assume that we could not observe the potential $\log x$ factors, as in Model 1, due to lack of data points. However, the 9-tetrahedra closed hyperbolic 3-manifold show the convergence behavior predicted by the volume conjecture, and the convergence of the sequence is experimentally in $\widetilde{O}\left(\frac{1}{r}\right)$, where $\widetilde{O}$ hide poly-log factors in r.

Conclusion

The Turaev-Viro invariants constitute an important family of topological invariants for three manifolds. Their combinatorial nature led to several algorithms for their computations and they are efficient to distinguish different manifolds. The recent volume conjecture of Chen and Yang stressed the importance of studying $(TV_r)_{r\geq 3}$ for large r, which is hard in practice.

In this chapter, we aimed at computing (TV_r) for large r. To that extend, we looked at two algorithms: a FPT algorithm, theoretically faster but memory consuming, and a backtracking one, with negligible memory cost and good performances on small triangulations.

The contributions of this chapter are twofold. First, we establish a easily computable estimator of the complexity of a triangulation with respect to the backtracking algorithm. This is based on the estimation of the number of integer points inside a polytope and done using Ehrhart polynomial. It leads to a preprocessing that minimize the size of the search tree for the backtracking algorithm. Enriched with the use of multi-precision arithmetics, this approach has allowed the computation of sequences of Turaev-Viro invariants for manifolds with small triangulations. In turn, these experiments have made possible the elaboration of new conjectures extending the seminal one of Chen and Yang.

While we pursue our computations with increasingly large triangulations, the asymptotic behaviors becomes harder to observe. Future work in this direction will require a finer understand-

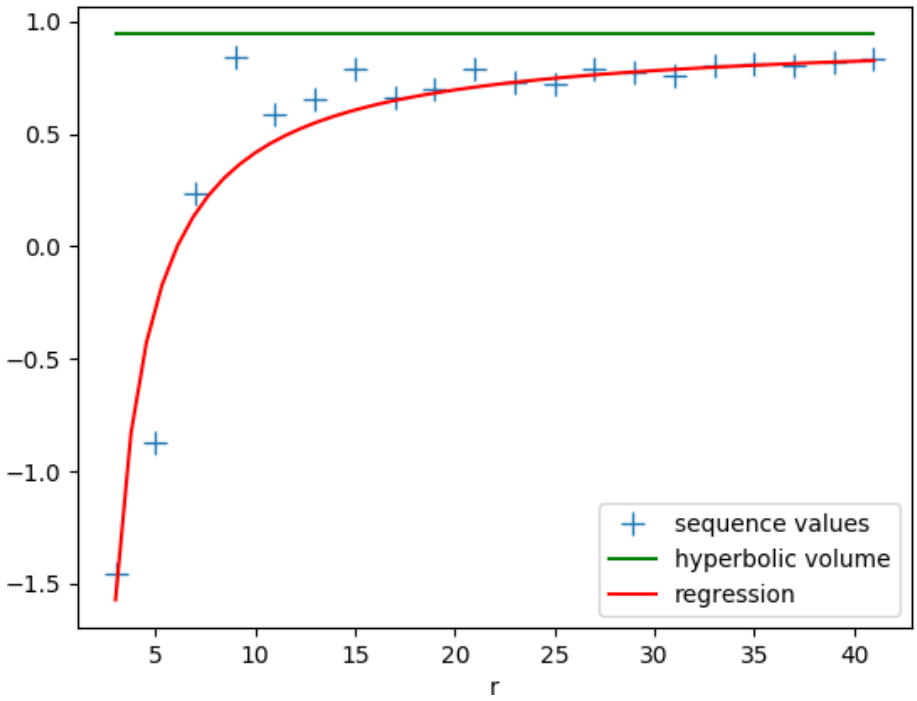

Figure 4.9 – Graph of the sequence of Conjecture 4.9 for the Weeks manifold. The expected limit of the sequence is shown in green. The regression with Model 2 is shown in red.

ing of the complexity of computing Turaev-Viro invariants, in particular in relation of topological properties of the manifold studied ; see for example [59].

CHAPTER 5

Building hyperbolic manifolds

This manuscript is centered on topological questions. *A priori* geometrical tools are no use to build topological invariants, *e.g.*, the size of the triangles of a triangulation is not a topological invariant. This can be seen on the 2-dimensional torus: if a flat torus is cut into a triangulation, scaling all the pieces by some constant will result in a new torus, scaled from the previous one, with different area for instance. However, Theorem 5.0.1 states that this is not the case for the hyperbolic geometry.

Theorem 5.0.1 (Mostow–Prasad Rigidity [66, 74])**.** *Let M and N be complete finite-volume hyperbolic manifolds of dimension larger than three, then any isomorphism $f : \pi_1(M) \to \pi_1(N)$ is realized by a unique isometry.*

Applying Theorem 5.0.1 to twice the same 3-manifold M gives that the hyperbolic metric is unique up to isometry. The hyperbolic geometry, under the hypothesis of the theorem, is said rigid: it is entirely determined by the topology. Hence any quantity related to this geometry, such as the *hyperbolic volume*, is a topological invariant.

The results of this chapter concern hyperbolic manifolds with torus boundaries, which includes hyperbolic knots complements. These complements fall within the scope of Theorem 5.0.1 and in combination with Theorem 2.3.1, we have that the hyperbolic geometry is able to distinguish between any two knots.

This chapter provides an introduction to hyperbolic geometry, along with the construction of a hyperbolic geometry from a triangulation. It is inspired from, and more details can be found in, [9, 75, 82].

Section 5.1 gives a summary of the minimal takeaway of this section. Section 5.2 gives ways of representing the hyperbolic space and Section 5.3 defines some basic geometry we need. Section 5.4 defines hyperbolic structures and gives conditions on what is required to have one. Finally Section 5.5 characterizes the complete hyperbolic structures and gives equations to solve to construct one.

Sections 5.1, 5.2 and 5.3 provide the necessary prerequisites for Chapter 6.

Sections 5.4 and 5.5 are more mathematical and constitute an explanation on the gluing equations. The important message is summed up in Section 5.1. They can be skipped during a first reading, they are included for completeness.

5.1 Main ideas

From this section, it is important to grasp the notion of hyperbolic ideal tetrahedra (Definition 5.3.3): they are the convex hull of vertices on the boundary of the hyperbolic space, and the problem will be to assign them a shape (a complex number z called edge parameter, see Definition 5.3.5) so our manifold defined by a topology will have a geometry. Then we construct 2-dimensional triangulations on surfaces around the cusps (Remark 5.3.3 and Figure 5.2 (right)) described by the shapes of the tetrahedra. The main result of this section (Theorems 5.5.1 and 5.5.3) is a set of conditions on the shape parameters stated in terms of normal curves (Definition 5.5.4) leading to a hyperbolic manifold, and then to a complete hyperbolic manifold:

Theorem 5.1.1 (Thurston [82])**.** *A hyperbolic 3-manifold M admitting an ideal triangulation T admits a hyperbolic structure if and only if for any closed normal curve σ going around an edge e of T, the edge equation is verified:*

$$\sum_{z_i \in \sigma} \log(z_i) = 2i\pi.$$

Furthermore, M admits a complete hyperbolic structure if and only if for any cusp C of M and any normal curve $\sigma \in \pi_1(C)$, the completeness equation is verified:

$$\sum_{z_i \in \sigma} \varepsilon_i \log(z_i) = 0.$$

where $\varepsilon_i \in \{-1, +1\}$ depends on the position of the tetrahedra with respect to σ.

The edge equation can be illustrated by Figure 5.4: we want the tetrahedra to glue up coherently around edges. The completeness equation can be illustrated by Figure 5.5: the tori on the cusps must be Euclidean.

5.2 Hyperbolic models

A hyperbolic space $\mathbb{H}^n$ does not behave like the usual Euclidean space $\mathbb{R}^n$. In particular the *parallel postulate* does not hold: given a line L and a point P not on L, there are at least two different lines passing by P and contained in the same plane as L that do not intersect L. Thus, representing $\mathbb{H}^n$ is not trivial and various *models* can be used to that extent. Models require compromises, like having to represent straight lines with arcs of circles instead, but can have qualities we can use at our advantage. In particular we define a conformal model; a property that will be used later in this thesis.

Definition 5.2.1 (Conformal model)**.** A conformal model of the hyperbolic space is a model for which the measure of the angles is the same as their actual values in the hyperbolic space.

This section defines two models: the Poincaré disk model, for completeness and clarity as it is one the most common model, and the Poincaré halfspace model. We detail the latter in dimensions 2 (the halfpane model) and 3. All these models are conformal, and a more detailed presentation can be found in [9].

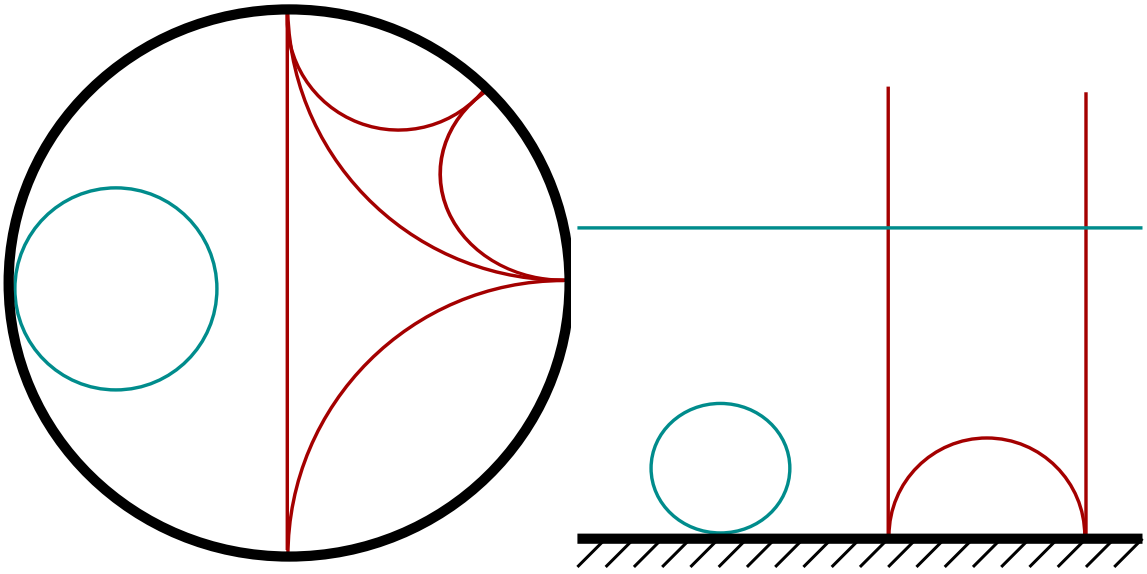

Figure 5.1 – Two models of $\mathbb{H}^2$, the boundary $\partial\mathbb{H}^2$ is in black, in red are geodesics and in light blue are horocircles. Left: Poincaré disk model. The boundary of this model is a circle. The geodesics define two triangles with vertices at infinity sharing a common edge. Right: Poincaré halfplane model. The boundary is a line plus one point at infinity, the geodesics define a triangle, with two vertices on the line and one at ∞. The line parallel to the boundary is a horocircle around ∞.

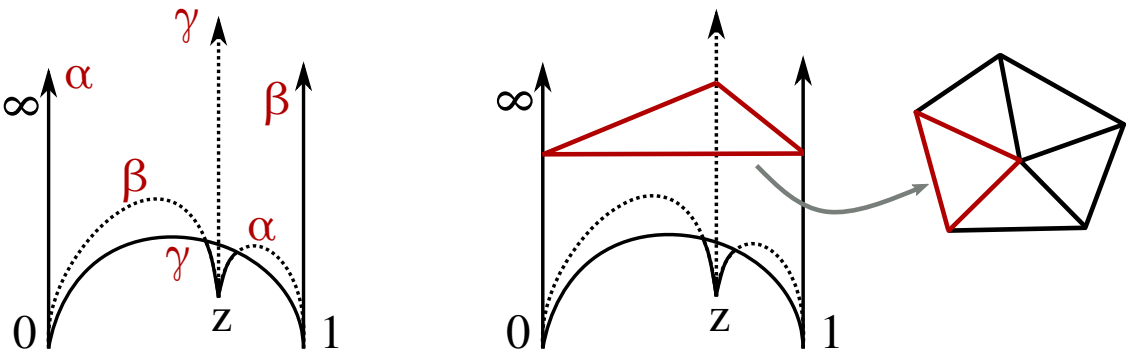

Figure 5.2 – Left: ideal tetrahedra in the Poincaré halfspace model. Its vertices are in position 0, 1, ∞ and some complex number z in $\partial\mathbb{H}^3$ identified with the complex plane C. Dihedral angles are displayed. Right: representation of the intersection between the previous tetrahedra and a horosphere around ∞, it is a Euclidean triangle. Later in this manuscript, gluings of ideal tetrahedra will be considered, this can be represented by looking at it from the point ∞ (or a cusp when talking about manifolds). In consequence, such gluings of tetrahedra become gluings of Euclidean triangles.

The Poincaré Disk. This model represents $\mathbb{H}^2$, the hyperbolic space of dimension 2, as the interior of a disc D^2. The straight lines are arc of circle orthogonal to the boundary of D^2 and this is represented in Figure 5.1.

The Poincaré halfplane. This model represents $\mathbb{H}^2$ as the upper-halfplane $\mathbb{R} \times \mathbb{R}_+^*$ where straight lines are either arcs of circles orthogonal to the line $\{(x,0)|x \in \mathbb{R}\}$ or lines of the form $\{(x,y)|y > 0\}$. Its boundary $\partial\mathbb{H}^2$ is $\{(x,0)|x \in \mathbb{R}\} \cup \infty$, where $(+\infty, 0)$, $(-\infty, 0)$ and (x, ∞) are identified with ∞. It can be obtained from the disk by sending one point of the boundary circle at the infinity while the rest is sent to the line $\{(x,0)|x \in \mathbb{R}\}$.

Poincaré halfspace. This model represents $\mathbb{H}^3$, the 3-dimensional real hyperbolic space, as the upper-halfplane $\mathbb{C} \times \mathbb{R}_+^*$. It is a natural extension of the halfplane, and we mainly use this model for our computations and representations. The boundary is composed of a complex plane and a point at infinity ∞ and when talking about points on the closure $\overline{\mathbb{H}^3}$, a complex number or ∞ refers to points on the boundary. In this model, hyperplanes are either half spheres centered on the complex plane or Euclidean planes orthogonal to the complex plane. A tetrahedron is represented in Figure 5.2.

Note that we can extend this model by taking $\mathbb{H}^{n+1} \sim \mathbb{R}^n \times \mathbb{R}_+^*$.

In this model, the derivative of the metric at a point $(u + iv, w)$ is:

$$ds^2 = \frac{du^2 + dv^2 + dw^2}{w^2}.$$

This form allows us to compute the length of curves via integration.

5.3 Elements of geometry

This section describes elementary geometrical concepts that will be used throughout the manuscript.

To describe the models above, we used "straight lines", the mathematical concept behind this is the *geodesic*. They are curves that locally minimize the distance everywhere. They define the distances between points and allow to define hyperplanes for instance. The next notion is crucial in geometry as there are often more than a single way to represent a given situation, they are transformations that allow to switch between them.

Definition 5.3.1 (Isometry)**.** An isometry is a transformation of the space that preserves the distances.

The set of orientation preserving isometries of a space forms a group. For $\mathbb{H}^2$, this group is $PSL(2,\mathbb{R})$, and for $\mathbb{H}^3$ it is $PSL(2,\mathbb{C})$, they are generated by reflections on hyperplanes. These isometries can be characterized by their restrictions to $\partial\mathbb{H}^n$:

Definition 5.3.2 (Ideal point)**.** An ideal point is a point on the boundary of the space, in our case $\partial\mathbb{H}^3$.

Theorem 5.3.1. *Orientation preserving isometries of $\mathbb{H}^3$ are uniquely determined by the image of three ideal points.*

To represent triangulations in the hyperbolic space, we use hyperbolic tetrahedra, and for our needs we consider ideal tetrahedra. In general we have:

Definition 5.3.3 ((Ideal) polytopes)**.** A hyperbolic polytope is the convex hull of a collection of distinct points in hyperbolic space, its vertices. It is said ideal if all its vertices are ideal.

The tetrahedra of Figure 5.2 are ideal. If its vertices are aligned, then a tetrahedron can be degenerated, we forbid this case for the chapter.

Remark 5.3.1 – Since an ideal triangle is defined by its three vertices on $\mathbb{H}^3$, by Theorem 5.3.1, all ideal triangles are isometric.

Definition 5.3.4 (Horosphere)**.** Given a point $p \in \partial\mathbb{H}^n$, a closed hypersurface orthogonal to all geodesics ending at p is called a horosphere centered at p.

Remark 5.3.2 – Horospheres in $\mathbb{H}^{n+1}$ are n-dimensional Euclidean planes. Combinatorially, they constitute the link of their center.

This can be seen in the halfspace model: let $p \in \partial\mathbb{H}^{n+1}$, using an isometry we can assume $p = \infty$. All geodesic ending at ∞ are straight vertical lines orthogonal to the base plane $\mathbb{R}^n \subset \partial\mathbb{H}^{n+1}$. Thus in this model, all horospheres centered at ∞ are planes on which the metric is Euclidean (scaled by the height of the plane). This remains true for all p as isometries preserve the metric.

Due to the fact that ideal vertices are at infinity, they are not part of the tetrahedron. To be able to do geometry, we now focus on the representations of ideal tetrahedra.

Definition 5.3.5 (Edge parameter)**.** Given an ideal tetrahedron, setting a first vertex at 0, a second at 1 and a third at ∞, with 0 and 1 points of $\partial\mathbb{H}^3$ seen as $\mathbb{C}$, the position of the fourth vertex in the complex plane, $z \in \mathbb{C}$, is the parameter associated to the edge 0∞. It characterizes the shape of the tetrahedron. When the orientation of the tetrahedra is not fixed, z can be picked with non-negative imaginary part.

There is an edge parameter for each edge of an ideal tetrahedron. Edge parameters of opposite edges are equal, and they can be deduced one from another: if the first one is z, then the others are $z' = \frac{1}{1-z}$ and $z'' = \frac{z-1}{z}$. As they can be deduced from each other, any one of them characterize the shape of the tetrahedron. Thus any one of them is called the *shape parameter*.

Remark 5.3.3 – Due to the nature of the ideal tetrahedra, the shape parameters are rich in information:

- We have the identity $zz'z'' = -1$.
- The argument of z is the measure of the dihedral angle between the plane defined by the vertices in $(0, 1, \infty)$ and $(0, z, \infty)$ and $arg(z) + arg(z') + arg(z'') = \pi$.
- The intersection between an ideal tetrahedron and a "sufficiently small" horosphere centered at one of its vertices is a Euclidean triangle with angles $arg(z)$, $arg(z')$, and $arg(z'')$. In Figure 5.2, $\alpha = arg(z)$, $\beta = arg(z')$ and $\gamma = arg(z'')$. Thus, gluings of ideal tetrahedra define 2-dimensional triangulations on horospheres centered at one of their vertices.
- Given a tetrahedron with edge parameter z, in the Euclidean triangle described at the previous item, the module of z is the ratio of the Euclidean lengths of the sides of the triangle (see Figure 5.2 and Equation 5.1). For instance, in Figure 5.4, this ration is equal to $|2i| = 2$.

By the previous remark, another way of encoding the shape of a hyperbolic ideal tetrahedron is to use its dihedral angles. As the edge parameters of opposite edges are equal, so are opposite dihedral angles. Furthermore, with the notations of Remark 5.3.3 and Figure 5.2, we have:

$$z = \frac{\sin(\beta)}{\sin(\gamma)} \exp^{i\alpha}. \tag{5.1}$$

5.4 From topology to geometry

The aim of this section is to assign a geometry to a cusped 3-manifold M represented by an ideal triangulation:

Definition 5.4.1 (Geometric manifold)**.** A manifold is geometric if it admits a complete metric.

The manifolds we consider in this section have cusps, *i.e.* singularities. These manifolds can be pictured as topological spaces with some points whose link are tori, since these points prevent the space from being a manifold, they are removed creating these cusps. If an open neighborhood of these points is removed, this leads to a compact manifold whose boundary consists of tori.

We begin by defining a way of putting a metric on a manifold using (G, X)-structures, the problem being that these may lead to non-complete metrics.

5.4.1 (G,X)-structures

Defining geometries over manifolds uses *group actions*, we start by giving some reminders:

Definition 5.4.2 (Group action)**.** Let G be a group with identity element e and X a set (in this manuscript we assume X non-empty). G is said to act on X if there is a binary operation $\cdot : (G \times X) \to X$, called the group action, such that for any $x \in X$:

— $e \cdot x = x$;

— for any $(g, h) \in G^2$, $g(h \cdot x) = (gh) \cdot x$.

Note that in our case G will be a group of morphisms of X, and we can write $h(x)$ instead of $h \cdot x$. Group actions can have several other properties, let x and y be any elements of X and g and h be any elements of G. The action is said *transitive* if there exists $g' \in G$ such that $x = g' \cdot y$. The group acts *freely* if $g \cdot x = h \cdot x$ implies $g = h$. The group acts *properly discontinuously* if there exists a neighborhood U of x such that for $g \neq e$, $g(U) \cap U = \emptyset$, the action can also be called discrete.

In Section 2.2.2.1, we defined a hyperbolic 3-manifold as the quotient of $\mathbb{H}^3$ by a subgroup of its isometries acting freely and properly discontinuously on $\mathbb{H}^3$. This section uses (G, X)-structures.

Definition 5.4.3 ((G, X)-structures)**.** Let X be a connected, simply connected, oriented, real analytic manifold and let G be a group of real analytic diffeomorphisms acting transitively on X. We say a manifold M has a (G, X)-structure if there exists an open covering $\{U_i\}$ of M and a set of diffeomorphisms $\{\phi_i : U_i \to \phi(U_i) \subset X\}$ such that if $U_i \cap U_j \neq \emptyset$ then $\phi_i \circ \phi_j^{-1}$ is an element of G on each connected component of $\phi_j(U_i \cap U_j)$.

$\{U_i, \phi_i\}_i$ is called an atlas, and an element (U_i, ϕ_i) is a chart. Maps of the form $\phi_i \circ \phi_j^{-1}$ are called transition maps. The analytic property will be used in Section 5.5 and can be ignored for now.

(G, X)-structures are more general than the quotient based definition: this is illustrated in Examples 5.4.1 and 5.4.2, they allow for the representation of non-complete manifolds. In the case where the manifold is not complete, the action of G will not necessarily be properly discontinuous and defining such a manifold by quotienting could lead to degeneracy.

We now give two examples of (G, X)-structures on the torus.

Example 5.4.1 – The most famous structure is the one of the flat (meaning Euclidean) 2-dimensional torus T^2.

This torus can be constructed by gluing together opposite sides of a parallelogram as in Figure 5.3. Now, this initial parallelogram can be used to tile $\mathbb{R}^2$. For simplicity, let us assume this parallelogram is the unit square ($[0, 1]^2$).

Each point $p \in T^2$ is lifted to a collection of points in $\mathbb{R}^2$, one for each copy of the square. Let U_p be the neighborhood of p constructed by taking the preimage of the disk of radius $1/4$ around each lift of p. Let ϕ_p be the map that sends U_p to one of its representative.

Defining $\{U_p, \phi_p\}$ for all $p \in T^2$, gives an atlas, now we just need to verify that we have a structure. Let us fix p and take another point $q \in U_p$ on the torus. The transition map $\phi_p \circ \phi_q^{-1}$ sends part of $\phi_q(U_q)$ to another square around $\phi_p(p)$. For any point $x \in \phi_q(U_p)$, the map sends a representative x_0 from a square to another representative x_1 in another square; for all x this is the same translation from $\phi_q(U_p)$ to $\phi_p(U_q)$. Translation being isometries of $\mathbb{R}^2$, T^2 admits an $(\mathrm{Isom}(\mathbb{R}^2), \mathbb{R}^2)$-structure.

In this case the Euclidean metric of $\mathbb{R}^2$ can be pulled back on each representative of T^2 and ultimately on T^2.

Example 5.4.2 – Another example of structures arises when, instead of tiling $\mathbb{R}^2$ with parallelograms, we use another polygon as fundamental domain for T^2.

Keeping in mind that T^2 bears, *a priori*, no notion of metric, the length of its edges when cut along its meridian and longitude does not need to be pairwise equal. For instance, let us assume that cutting T^2 produces a trapezoid. Just like in the previous example, starting with a representative of the trapezoid, we "tile" $\mathbb{R}^2$ by gluing a scaled and rotated copy of the trapezoid to each of its edges and repeating the process (see Figure 5.3).

The situation is very different from the previous case. This time we have described a $(\mathrm{Aff}(\mathbb{R}^2), \mathbb{R}^2)$-structure, Aff being the group of affine transformations of the plane (composition of scalings, translations and rotations).

This time, it will not be possible to put the metric of $\mathbb{R}^2$ on the torus as it would not be properly defined.

5.4.2 Hyperbolic structures

Carefully selecting a way of putting a structure on T^2 allowed us to pull back the metric of $\mathbb{R}^2$ in the first example and not in the second. The reason for this is the particular case of having the isometries as acting group:

Definition 5.4.4 (Hyperbolic structure)**.** An n-manifold is said to admit a hyperbolic structure if it admits a $(\mathrm{Isom}(\mathbb{H}^n), \mathbb{H}^n)$-structure. It is a called a hyperbolic manifold.

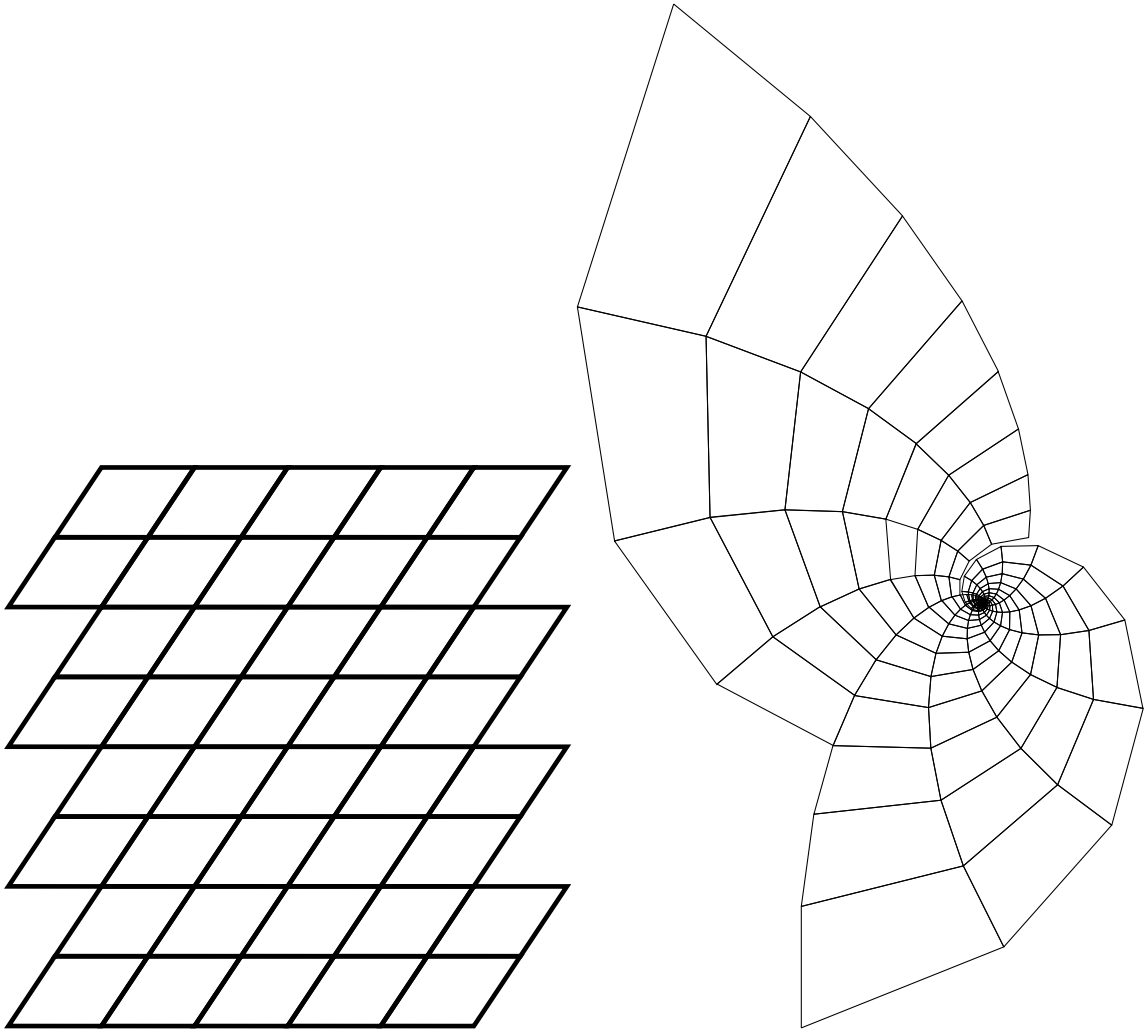

Figure 5.3 – Two developments of T^2 from two different fundamental domains obtained by replicating the torus along the edges of the fundamental domains. Right: the fundamental domain is a parallelogram and developing the torus tiles $\mathbb{R}^2$. Left: the fundamental domain is a generic parallelogram. In this case, the lift of a point of the torus is dense in $\mathbb{R}^2$. Note that developing the torus does not yield a covering of the plane, a single vertex will be omitted.

Remark 5.4.1 – For a manifold, being hyperbolic is a topological feature independent of whether a hyperbolic structure is computed.

Euclidean and spherical structures are defined in the same way, with respectively $\mathbb{R}^n$ and $\mathcal{S}^n$ for the space. The manifold is said hyperbolic because it actually admits a hyperbolic metric:

Theorem 5.4.1 (See [75])**.** *If X is a metric space, G a group of isometries acting transitively on X, and M a manifold admitting a (G, X)-structure, then M inherits a* metric*,* i.e.*, a notion of distance, from X.*

By Theorem 5.4.1, to build a geometric manifold, we need to start by a hyperbolic structure. However, using an atlas is not always the most direct and simple way to do it. In this manuscript, we are working with triangulated 3-manifolds, thus it is possible to put a structure on each tetrahedra before identifying the faces isometrically, *i.e.* with a *gluing*. We remind that by Remark 5.3.1, it is always possible to glue two tetrahedra isometrically along a common face.

Remark 5.4.2 – Putting a structure on a tetrahedron is just assigning a shape to it.

Theorem 5.4.2 (See [75])**.** *A gluing of n-dimensional hyperbolic polyhedra yields a hyperbolic n-manifold, with hyperbolic structure agreeing with that in the interior of the polyhedra, if and only if each point has a neighborhood (in the quotient topology) isometric to a ball in $\mathbb{H}^n$ with the isometry the identity in the interior of the polyhedra.*

Theorem 5.4.2 requires each point x of the manifold to lift to a (set of) point(s) in the gluing that has a neighborhood isometric to a ball in $\mathbb{H}^3$.

— When x lifts to a point $\hat{x}$ inside a tetrahedron, then it is always possible to restrict a neighborhood around $\hat{x}$ to a ball contained in the polyhedron.
— When x lifts inside a triangular face of two tetrahedra, then it lifts to two points with two half neighborhoods. These can be restricted to two half balls which are then glued isometrically, leading to a neighborhood of x isometric to a ball.
— When x lifts inside an edge shared by several tetrahedra, then the situation is similar to the previous case except that instead of two half balls, there are several pieces of balls glued together. To ensure the gluing of these pieces is a ball, the sum of the inner angles of these pieces must be equal to 2π, the case where this is not verified is illustrated in Figure 5.4. However, this condition alone is not enough as illustrated in Example 5.4.3. This problem will be formalized in Section 5.5.
— Since we are working with ideal triangulationS, x cannot be lifted to a vertex as they do not belong to the manifold.

Example 5.4.3 – Let us consider the case where four identical ideal tetrahedra are joined along an edge as illustrated in Figure 5.4. Let the shape parameter be $2i$ between a face a and b, and for each tetrahedron let us glue a face a to a face b.

These gluings can be made isometrically as all ideal triangles are similar and the sum of the angles around the central edge is 2π. However a point lifted on the central edge will not have a neighborhood isometric to a ball: it will not be well defined on the central edge.

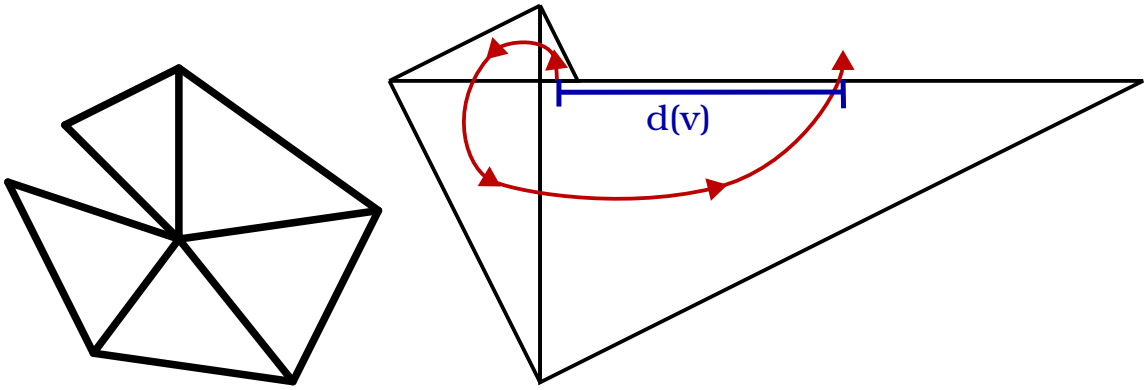

Figure 5.4 – Two types of singularities around an edge seen from the cusp. Left: the sum of the dihedral angles is smaller than π. Right: gluing of four identical tetrahedra with shape parameter $2i$. When taking a path around the edge, the gluing appears no longer coherent even if the faces are isometrically identified. In blue is the distance $d(v)$ between the first and last points.

5.5 The developing map

The beginning of this section is technical and dedicated to the construction of the developing map, which is a way of extending the atlas defining (G, X)-structures. The unfamiliar reader can see this as a way of projecting the set of paths of M onto X, giving them a notion of metric.

The singularity of Example 5.4.3 can be formulated as follows: if a gluing is coherent between pairs of tetrahedra, it may not remain coherent when considering more the whole triangulation. To formalize this, we will use paths over the gluing of tetrahedra and look at what happens to the tetrahedra when following the path: this is based on the developing map and the universal covers.

Definition 5.5.1 (Universal cover)**.** The universal cover $\tilde{M}$ of a space M is a simply connected covering space of M.

Remark 5.5.1 – The universal cover $\tilde{M}$ of M can be interpreted as the space of the paths over M that start at a given base point.

Since we defined X as a real analytic manifold and G as a group of real analytic diffeomorphisms of X, then any element of G is determined by its restriction to any open set of X. Let M be a manifold admitting a (G, X)-structure and $\{(U_i, \phi_i)\}_i$ be the associated atlas.

We want to look at the image in X of the paths over M. Let $x \in U_i$ be a point of M and $\sigma : [0, 1] \to M$ a path starting at $\sigma(0) = x$. If σ remains in U_i, then its image is well defined in X through ϕ_i. Otherwise we want to extend ϕ_i using a function $h : M \to G$ that picks a transition map when leaving U_i. Let us assume the path ends at some point $\sigma(1) \in U_j$ such that

$$\sigma([0, 0.5]) \in U_i,\ \sigma([0.5, 1]) \in U_j. \tag{5.2}$$

Let $\alpha(0.5) = y \in U_i \cap U_j$ and let $h(y) \in G$ be a transition map between U_i and U_j defined at $\phi_i(y)$. Then

$$\Phi(\sigma(t)) = \begin{cases} \phi_i(\sigma(t)) & if\ t \leq 0.5 \\ h(y)(\phi_j(\sigma(t))) & if\ t > 0.5 \end{cases}$$

extends ϕ_i for σ. However, this definition depends on the choice of $h(y)$. $h(y)$ is defined on a open neighborhood of $\phi_i(y)$, and since G is a group a real analytic diffeomorphisms, $h(y)$ is uniquely determined in this neighborhood. Thus the function h that selects the transition map is locally constant. Hence, for all paths going from U_i to U_j, h would have picked the same transition map and ϕ is well defined for any σ verifying the constraints 5.2, which is general up to re-parametrization.

The construction of Φ can be extended using the function h for every path in M, that is on $\tilde{M}$, this constitutes the *analytic continuation* of ϕ_i.

Definition 5.5.2 (Developing map)**.** Let M be a (G, X)-manifold and $\tilde{M}$ its universal cover, the map

$$D : \tilde{M} \to X$$

as defined above is called the developing map of M.

The developing map is unique up to composition with elements of G, this changes the initial map ϕ_i in the definition above. D is well defined, and is independent of the charts and the decomposition of the path used to compute it.

5.5.1 Holonomy

Let σ be a closed loop on M starting at some point x and (U_x, ϕ_x) a chart for x. ϕ_x can be analytically continued along σ into ϕ'_x, giving a new chart in a neighborhood of x, thus there is an element of G such that $\phi'_x = g_\sigma \circ \phi_x$. Let T_σ be the transformation of $\tilde{M}$ associated to σ, we have:

$$D \circ T_\sigma = g_\sigma \circ D.$$

Furthermore, since for β another closed loop of M

$$D \circ T_\sigma \circ T_\beta = g_\sigma \circ D \circ T_\beta = g_\sigma \circ g_\beta \circ D,$$

the map

$$H : \sigma \to g_\sigma$$

is a group homeomorphism.

Definition 5.5.3 (Holonomy)**.** The homeomorphism H is the holonomy of M and its image is the holonomy group of M.

Remark 5.5.2 – In Examples 5.4.1 and 5.4.2, $\mathbb{R}^2$ is the universal cover of the torus. The developing map "develops" the torus over $\mathbb{R}^2$. The holonomy corresponds to the transformations applied to a fundamental domain of a manifold when following a given path. For instance the holonomy group obtained in Example 5.4.1 is a translation group as all parallelograms are identical, and the one obtained in Example 5.4.2 is generated by the two similarities turning one edge of the trapezoid into the opposed one.

Holonomy and shape parameter When M is defined by a gluing of tetrahedra, given a (G, X)-structure, that is a shape assignment to the tetrahedra per Remark 5.4.2, the holonomy can be expressed in terms of these shape parameters. In all generality, given two triangular faces of an ideal tetrahedron, per Remark 5.3.1 there is an isometry of $\mathbb{H}^3$, depending only on the parameter of the edge between the two, turning one into the other. Thus given a closed *normal curve* in the triangulation, it is possible to compute its holonomy: it is the composition of each isometry turning each successive triangle encountered into the next one.

Remark 5.5.3 – The holonomy is well defined for surfaces: in the case of 2-triangulation, instead of turning triangles into triangles, edges are turned into edges. For instance, the computation of the holonomy can be done in the surface defined by the intersection of the 3-triangulation and a horosphere just like in Figure 5.5.

Definition 5.5.4 (Normal curve)**.** A normal curve in an n-triangulation is a curve contained only in the n-simplices (minus the $(n-1)$-skeleton of the triangulation) except for a finite number of points contained in the $(n-1)$-simplices (minus the $(n-2)$-skeleton of the triangulation), such that two successive intersections with the $(n-1)$-simplices are not contained in the same $(n-1)$-simplex.

The restriction of a curve to a n-simplex is called an arc.

In the following we will mainly consider the holonomy for normal curves included in a horosphere around a cusp.

When an ideal tetrahedron has its vertices in 0, 1 and ∞, the third one is in some position z_1. Just as some transformations of the complex plane can be expressed by a multiplication by a complex number, z_1 is the image of 1 after a multiplication by z_1. If another tetrahedron has its vertices in 0, z_1 and ∞, calling z_2 the parameter associated to its edge 0∞, its last vertex will be in position $z_1 z_2$ (Figure 5.5). Generalizing this procedure, it is possible to compute a complex number for any *normal curve* inside the triangulation: the product of the parameters of the edges around which the curve turns. Doing so, one has to be careful with the orientation of the edges, and with the fact that we do not stay around a single edge (this gives a *holonomy modulo translations*). We have the formula:

$$H(\sigma) = \prod_i z_i^{\varepsilon_i}$$

where i is the index of each edge encountered by σ, z_i the corresponding shape parameter and ε_i is 1 or -1, depending on the orientation of the edge. Figure 5.5 illustrates this formula.

Remark 5.5.4 – The value of the holonomy is informative about its effects:
— the module of the holonomy is the scaling of the distances;
— the argument of the holonomy is the rotation operated.
In the future, we may use the logarithm of the holonomy as it separates imaginary and real parts.

Example 5.5.1 – In Example 5.4.3 the complex number associated to the normal curve that goes around the central edge is $(2i)^4 = 16$. In terms of developing maps, starting at a point in a tetrahedron and turning around the central edge before measuring a distance will give a distance 16 times longer than if it were measured without doing the transformation.

We can now express the condition on the shape parameters to have a geometric structure:

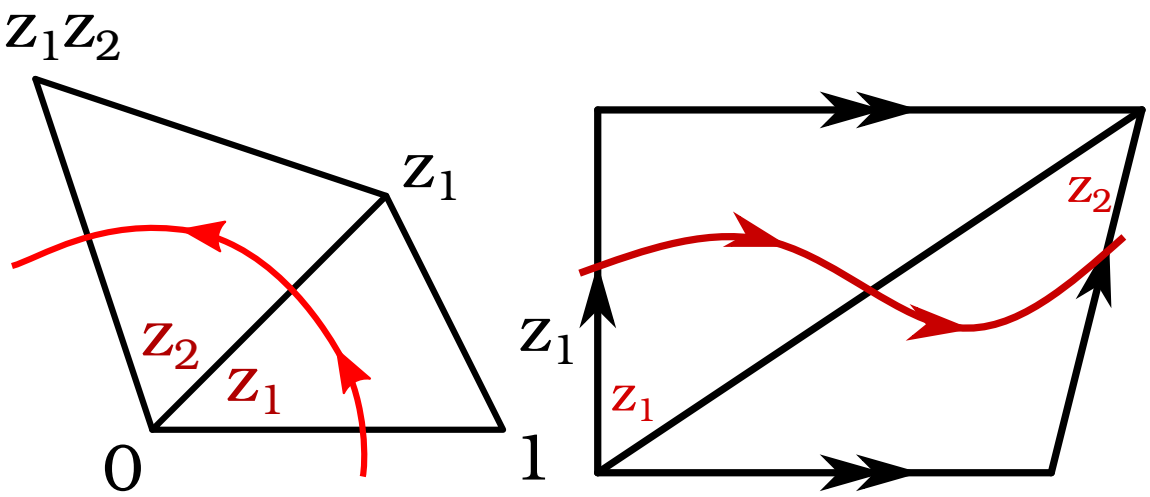

Figure 5.5 – Examples of normal curves on 2-dimensional triangulations, the edge parameters are in red. Left: two triangles with edge parameters z_1 and z_2, the holonomy of the red curve is $z_1 z_2$. Note that this curve is not closed, thus $z_1 z_2$ is actually the contribution of this piece of curve. Right: the gluing of two triangles triangulating a torus, the normal curve corresponds to a meridian of the torus. Since both edges are not on the same side of the curve, the holonomy is $\frac{z_2}{z_1}$. This complex number is a similarity that turns the left edge of the torus into the right one.

Theorem 5.5.1 (Thurston [82])**.** *An ideal triangulation of a hyperbolic manifold admits a hyperbolic structure if and only if for any closed path σ around an edge of the triangulation:*

$$\log(H(\sigma)) = i2\pi.$$

Remark 5.5.5 – In Theorem 5.5.1 and the other results of this section, we also want the imaginary part of all the tetrahedra to be positive, as negative imaginary parts would mean tetrahedra that are not oriented in the same way as the others, and null imaginary parts define degenerated (flat) tetrahedra.

5.5.2 The shape of the cusp: the completeness problem

If the previous section gave a criterion to obtain a hyperbolic manifold, it is not guaranteed to be complete. Incompleteness happens when Cauchy sequences may not converge, for hyperbolic manifolds this cannot happen on the inside of the manifold, the problem will come from the ideal points.

The main result of this section lies in Theorem 5.5.3, providing a condition similar to Theorem 5.5.1 to have a complete hyperbolic metric on a 3-manifold. This section constitutes a summary of the ideas leading to this result.

5.5.2.1 2-dimensional case

Let S be a 2-manifold defined by the gluing of ideal triangles, let v be a vertex of the triangulation. Note that since it is triangulated by ideal triangles, all the vertices are ideal and, from a

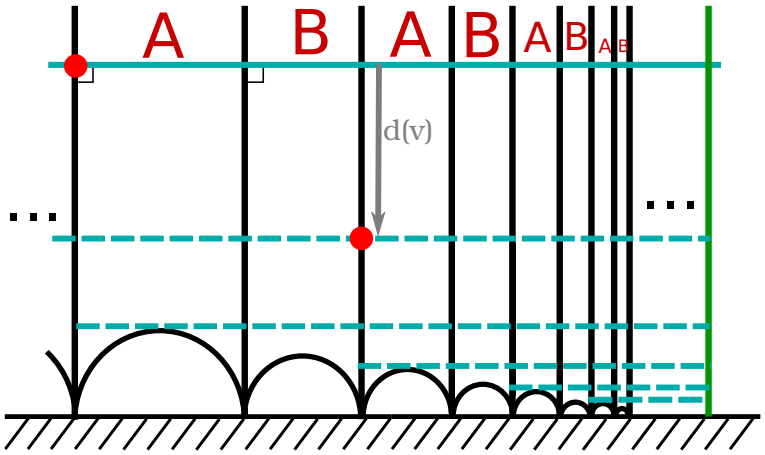

Figure 5.6 – Part of the developing image of an incomplete 2-manifold triangulated by two ideal triangles A and B glued along their edges. This is obtained by choosing the distance $d(v)$ for v the vertex at infinity and copying the triangles using this holonomy. In green is the limit of the sequence of edges of the triangles, it is a geodesic outside the manifold. In light blue is a horosphere, its image in the manifold intersects infinitely many times both triangles, each intersection being at distance $d(v)$ of each other. The two red points are identified in the 2-manifold, the dashed blue lines are identified with the horosphere in the manifold.

geometrical point of view, in a cusp. Let us consider a horocircle centered at v, and let us draw this horocircle on the triangulation of S as a sequence of arcs of circles orthogonal to the edges of the triangles in a counter-clockwise order (Figure 5.4 illustrates this, but this time it should not be interpreted as a section of a 3-dimensional triangulation but as a 2-dimensional triangulation with a cusp in the center). It is possible that this procedure does not produce a closed loop around v: assuming we started at an edge e, the initial point and the one after the procedure can be at a signed distance $d(v)$ from each other.

This quantity $d(v)$ depends only on the vertex v and on the manifold. It is an invariant that exactly corresponds to the holonomy of a normal path going around the vertex.

Remark 5.5.6 – Since we are working with manifolds admitting hyperbolic structures, the elements of the holonomy group are actually isometries and going around the cusp does not change the triangles: the distances and the developing map are changed because we go closer to the cusp. This is illustrated in Figure 5.6. This is identical to the 3-dimensional case, in Figure 5.3 (right) the size of the fundamental domain of the torus seems to change. This is because the horosphere in the developing space intersects tetrahedra that are identified in the manifold at different heights.

Theorem 5.5.2 (Thurston [82])**.** *S is complete if and only if $d(v) = 0$ for all vertices v of S.*

The idea behind the theorem is the following:

— if $d(v) = 0$ for all vertices v, then it is possible to cut § along arbitrary horocircles h_v centered at v for each v. Let $\{x_n\}_n$ be a Cauchy sequence and k a number such that for all n, $|x_n - x_0| < k$. Without loss of generality let us assume x_0 is not contained in any horodisks defined by the h_v, then for each v let h'_v be the horocircle centered at v which is at distance k from h_v in the direction of v. Cutting S along the h'_v is well defined as $d(v) = 0$, resulting in a compact manifold in which the sequence $\{x_n\}_n$ converges.

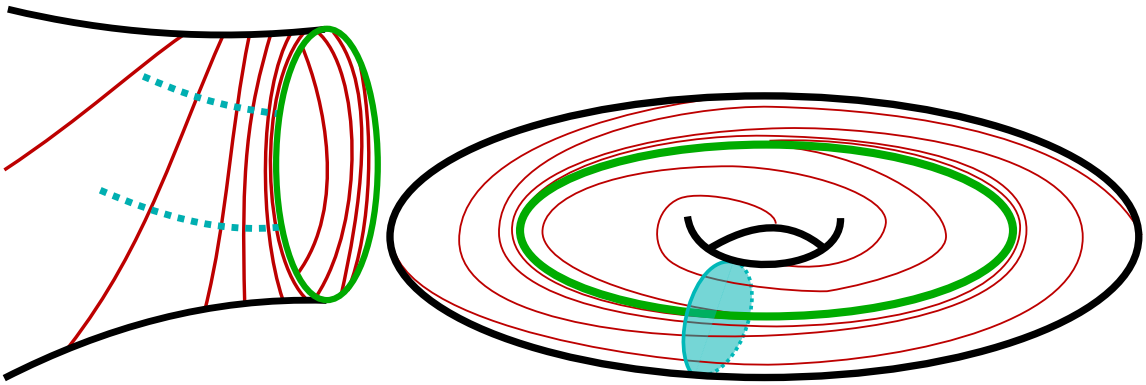

Figure 5.7 – Representations of incomplete cusps in 2 (left) and 3 (right) dimensions. In red are examples of edges of the simplices going to the cusp, in blue are horocircles, and in green are the missing geodesics making the manifold incomplete.

— if $d(v) = k < 0$ for some vertex v, let p be the normal path following an horocircle around v starting at the edge of some triangle. When doing one turn around v, the length of the arc of circle of p are reduced by a factor e^k (this is a consequence of the triangles being ideal and hyperbolic), thus the length of p is bounded as a geometric series. Let x_n be the n^{th} intersection between p and the edge of a triangle, this is a Cauchy sequence whose limit, v, is not in S, hence S not complete. The case $k > 0$ is identical.

It is possible to represent these *incomplete vertices* as the surface admits a hyperbolic structure: each horocircle around v reaches it in finite time, crossing increasingly fast the edges of the triangle. $d(v)$ is the distance, in each triangle, between two arcs of the same horocircle. All this is represented in Figure 5.7: the vertex v is turned into some geodesic of length $d(v)$, the horocircles are orthogonal to this geodesic and the triangles wrap around the geodesic.

Remark 5.5.7 – These incomplete cusps can be completed by adding the geodesic of length $d(v)$ to S.

5.5.2.2 3-dimensional case

The approach for the 3-dimensional case is similar to the previous one: given a cusp of a 3-manifold M, we will take a horosphere around the cusp and geometrize its intersection with the manifold.

Since the cusp is a point whose neighborhood is a torus that was removed, this intersection should be a 2-dimensional torus. Developing M in $\mathbb{H}^3$, and sending the cusp we study in ∞ in the halfspace model, a developing of the torus is obtained when taking the intersection of $\tilde{M}$ with a horosphere centered at ∞, *i.e.*, a Euclidean plane parallel to the complex plane.

We have two cases that correspond to Examples 5.4.1 and 5.4.2:

— If the torus admits a Euclidean structure, *i.e.*, the holonomy group of the torus is trivial, then it means the surface defined in $\tilde{M}$ by the horosphere is well defined and closed in M. This is because the intersections between the horosphere and each fundamental domain in $\tilde{M}$ is identical.

— If the torus does not admit a Euclidean structure, *i.e.*, the holonomy group of the torus is not trivial, then the surface induced on M is not closed. This is because the non-triviality

of the holonomy means that when following a closed curve of the fundamental group of the torus, its shape changes.

In the second case, the structure inherited by the torus is called a similarity structure in the literature: a $(\mathrm{Sim}(\mathbb{R}^2), \mathbb{R}^2)$-structures where $\mathrm{Sim}(\mathbb{R}^2)$ is the group of similarities of $\mathbb{R}^2$. In this case there is always a point of $\mathbb{R}^2$ not covered by the developing of the torus. The developing of the torus does not depend on the chosen horosphere, thus there will be such a point and by shifting the initial horosphere, we see that these points correspond to a geodesic in $\mathbb{H}^3$ that is not covered by $\tilde{M}$.

Just like for Theorem 5.5.2, there will not be non converging Cauchy sequences if and only if it is possible to cut M along a horosphere.

Theorem 5.5.3 (Thurston [82])**.** *Let M be a hyperbolic manifold with cusps, M is complete if and only if the holonomy of the fundamental groups of the tori in its cusps is trivial. Equivalently, if we take M as a compact manifold with torus boundaries $T_1, \dots, T_k$:*

$$\forall i \in [1, k],\ \forall \sigma \in \pi_1(T_i),\ \log(H(\sigma)) = 0.$$

Completing 3-manifolds Let C be a cusp of M and let α and β be the generators of its holonomy group. α and β are isometries that act on the missing geodesic. Let x be a point of the missing geodesic g.

— If the orbit of the action of α and β on x is dense in g, then M can be completed by a 1-point compactification. However this does not produce a manifold as the neighborhood of the point we added is a torus.

— If the orbit of the action of α and β on x is discrete in g, then M can be completed by adding a closed geodesic in the cusp.

CHAPTER 6

Localized geometric moves to compute hyperbolic structures on 3-manifolds

A main problem of knot theory is to tell whether two knots are equivalent or distinct. Equivalence between knots is defined by the existence of an isotopy of the ambient space that would turn one knot into the other, *i.e.*, a continuous deformation of the space that preserves the entanglement.

Isotopies are too difficult to compute in practice, and practitioners use *invariants* to tackle the knot equivalence problem. A *topological invariant* is a quantity assigned to a presentation of a knot, that is invariant by isotopy.

Hyperbolic knots are an important family of knots are the, they are the knots whose complements admit a *complete hyperbolic metric*. They are the subjects of active mathematical research, which motivates the introduction of efficient algorithmic tools to study their geometric properties, and most notably their *hyperbolic volume*. The hyperbolic volume of a hyperbolic knot is a topological invariant which is powerful at distinguishing between non-equivalent knots, is non-trivial to compute, and is at the heart of several deep conjectures in topology [69]. It is important to note that the hyperbolic volume being a real number, equality can be difficult to assert, and a better invariant to distinguish hyperbolic manifold is their canonical triangulation. However, the only known method to compute it does not always work and is from Weeks [87], the algorithm requires information on the geometry from which the volume can be computed easily.

If it exists, the complete hyperbolic metric on a 3-manifold is unique [66], and may be combinatorially represented by a *complete hyperbolic structure* (CHS). In order to compute geometric properties (such as the volume) of a hyperbolic knot, one triangulates the knot complement, and tries to assign hyperbolic shapes to its tetrahedra. If these *shapes* verify a set of non-linear constraints called the *gluing equations*, they form a CHS and encode the complete hyperbolic metric of the space.

A major issue with this approach is that a solution to the constraints may not exist on all triangulations of a manifold, even if, as topological object, the manifold can carry a complete hyperbolic metric. Worst, it is not known whether every hyperbolic 3-manifold admits a triangulation on which a solution as CHS exists.

In practice, given an input knot, software can construct a triangulation of the knot complement, and simplify it to have a CHS. But if this fails, the only implemented practical solution, proposed

	Alternating						Non-Alternating					
#crossings	12	13	14	15	16	17	12	13	14	15	16	17
% Failure on first try	0.9	1.6	2.4	3.3	4.4	5.7	0.8	0.7	1.2	1.7	2.4	3.3
Expected nb of retriang.	2.9	3.9	6.2	7.1	9.5	15.9	2.0	3.1	6.1	11.8	9.7	13.5

Table 6.1 – On all $\sim$ 9.7 millions prime knots with crossing numbers ranging from 12 to 17, alternating and non-alternating, we indicate (*% Failure on first try*) the percentage of knot complements (after triangulation and simplification) on which `SnapPy` fails to compute a CHS on first try. We also indicate (*Highest expected nb of retriang.*) the highest, over all knots, expected number of random re-triangulations necessary for `SnapPy` to succeed finding a CHS.

by `SnapPy`[22], is to randomly modify and simplify the triangulation before trying again until a CHS is found.

Table 6.1 provides data on the search for a CHS with `SnapPy`, on the $\sim$ 9.7 millions prime knots with crossing numbers up to 17. As observed, `SnapPy` has a high rate of success in finding a CHS after a standard triangulation and simplification of the knot complement. However, this standard construction of a triangulation fails to admit a CHS on more than 350 thousand knots in the census, and the percentage of problematic triangulations needing re-triangulations tends to increase with the crossing numbers. Additionally, we observe that some knot complements may require in expectation a high number of random re-triangulations (up to 15.9), and the number of re-triangulations may itself suffer a high variance, as illustrated in Figure 6.1.

Checking for the existence of a CHS is a costly procedure, that requires the resolution of the non-linear system of gluing equations (with e.g. Newton optimization method). Reducing the number of re-triangulations is consequently critical for performance of computations in knot theory, most notably for knots on which the state-of-the-art methods implemented in `SnapPy` require large numbers of re-triangulations, and even more so when proceeding to very large scale experiments such as the computation of the knot censuses [16], where "difficult" knots are many.

Contribution: This chapter a new heuristic based algorithm to improve on the essentially random approach of `SnapPy`. The method is inspired by Casson and Rivin's reformulation of the gluing equations [82, 35]: the gluing equations are split into a linear part and a non-linear part, and the resolution reduces to a convex optimization problem on a polytope domain. If the triangulation does not admit a complete structure, the optimization problem will converge on the boundary of the polytope and we exploit this information to modify combinatorially the triangulation while reusing the partially computed geometry. We illustrate experimentally the interest of the approach in Section 6.5 and propose a hybrid method with `SnapPy` in Section 6.5.3, that outperforms the state-of-the-art.

We introduce necessary background on triangulations and geometry in Section 6.1, and the computation of hyperbolic structures with optimization in Section 6.2. We analyze precisely the behavior of the optimization phase on triangulations not admitting a CHS in Section 6.3, and introduce a re-triangulation algorithm in Section 6.4 guided by the partially computed geometry of the optimization phase. Section 6.5is dedicated to the implementation and the results of the methods,along with the hybrid method in Section 6.5.3.

Note that, in this chapter we focus on complements of hyperbolic knots. However, the techniques introduced extend to more general hyperbolic 3-manifolds with torus boundaries [35].

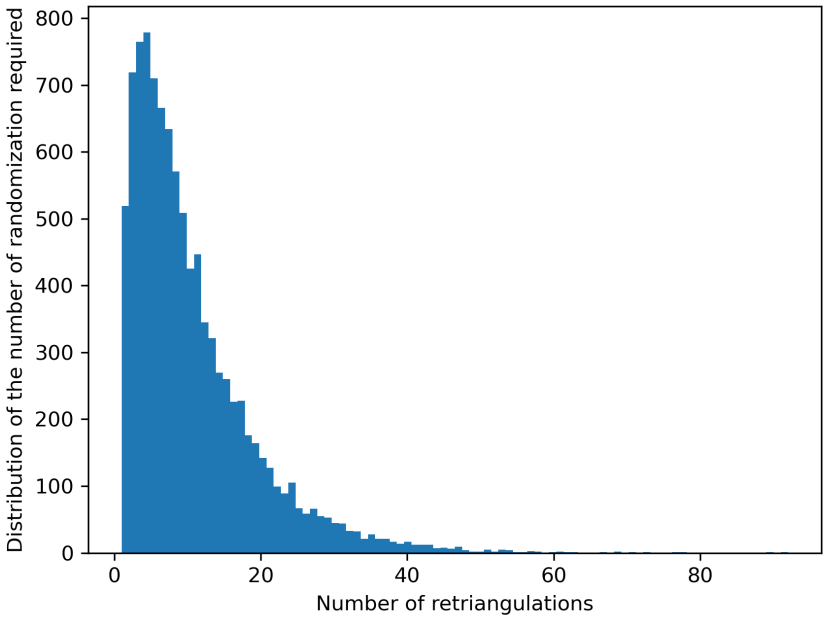

Figure 6.1 – Distribution of the number of randomizations required to find a CHS for the complement of the knot "17nh_2654001" of the census, for 10000 tries. The mean is 10.3 randomizations, and the standard deviation is 8.8. The minimum number of re-triangulations is 1, and the maximum 92

6.1 Background

The background for this chapter is detailed in Chapters 2 and 5.

In this chapter, we consider *compact manifolds with torus boundaries*, and in particular knot complements. Removing their boundary, they can be triangulated with *1-vertex ideal generalized triangulations*.

Any two ideal triangulations of the same 3-manifold can be connected by a sequence of 2-3 and 3-2 *Pachner moves* [72].

We focus on *hyperbolic knot complements*, meaning their complements admit *hyperbolic structures* which we want to compute. Computations and representations are done with the *conformal* model of *Poincaré's halfspace*, where $\mathbb{H}^3 \sim \mathbb{C} \times \mathbb{R}_+^*\}$.

We remind that the shape of an ideal hyperbolic tetrahedron can be encoded with a complex number z called a *shape parameter*, or with the values of its three dihedral angles.

The aim of this section is to compute *complete hyperbolic structures*. Necessary and sufficient conditions are stated in terms of normal curves by Thurston [82]. The result can be summarized by Theorem 5.1.1 which we remind:

Theorem 5.1.1. *[82] A hyperbolic 3-manifold M admitting an ideal triangulation T admits a hyperbolic structure if and only if for any closed normal curve σ going around an edge e of T, the edge equation is verified:*

$$\sum_{z_i \in \sigma} \log(z_i) = 2i\pi.$$

Furthermore, M admits a complete hyperbolic structure if and only if for any cusp C of M and any normal curve $\sigma \in \pi_1(C)$, the completeness equation is verified:

$$\sum_{z_i \in \sigma} \varepsilon_i \log(z_i) = 0.$$

where $\varepsilon_i \in \{-1, +1\}$ depends on the position of the tetrahedra with respect to σ.

These are non-linear equations in terms of the shape parameters. While computing a solution, when it exists is a numerical problems with existing solution, finding a triangulation of the manifold on which these equations admit a solution is a difficult problem with no known solutions.

6.2 Angle structures and hyperbolic volume

In this section, we introduce another method to compute complete hyperbolic structures on triangulations, via optimization methods. We refer the reader to [35, 82] for more details.

6.2.1 Linear equations and angle structures

Let T be a 1-vertex ideal triangulation of a knot complement M with n tetrahedra. Since opposite edges have the same dihedral angles, all possible shapes of the tetrahedra can be represented by a point in $\mathbb{R}^{3n}$. We define an *angle structure*:

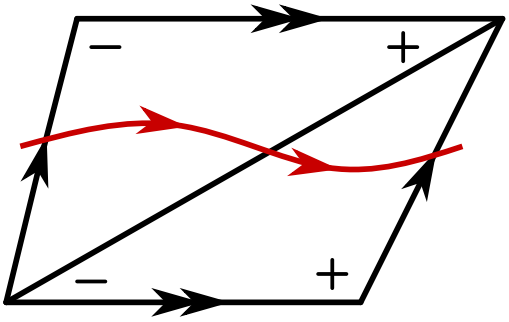

Figure 6.2 – Leading $(+)$ and trailing $(-)$ corners associated to a closed normal curve on a torus.

Definition 6.2.1 (Angle structures)**.** Given an ideal triangulation T, an *angle structure* is a value assignment to the dihedral angles of the tetrahedra of T such that opposed dihedral angles are equal (we then talk about the three dihedral angles of a tetrahedron). Furthermore, the following constraints must be verified:

1. all the angles are strictly positive;
2. the three dihedral angles (α, β, γ) of a tetrahedron sum to π;
3. the dihedral angles around each edge of T sum to 2π.

The set of angle structures on T is denoted $\mathcal{A}(T)$.

Conditions 1 and 2 ensure the angles are in $(0, \pi)$ and that the tetrahedra have the same orientation. Condition 3 is necessary for points on the interior of edges to have a neighborhood isometric to a hyperbolic ball.

Constraints 1, 2, 3 are linear, hence the set $\mathcal{A}(T)$ of angle structures of a triangulation is the relative interior of a polytope in $\mathbb{R}^{3n}$. It is of dimension $n + |\partial M|$ where $|\partial M|$ is the number of cusps of M; in the case of knot complements, there is a single cusp. This polytope satisfies:

Theorem 6.2.1. *(Casson; see [51]) Let T be an ideal triangulation of M, an orientable 3–manifold with toric cusps. If $\mathcal{A}(T) \neq \emptyset$, then M admits a complete hyperbolic metric.*

Furthermore, a generating family for the tangent space of $\mathcal{A}(T)$ can be computed in polynomial time [35], using leading-trailing deformations, which are based on closed normal curves.

Definition 6.2.2 (Leading-trailing deformations)**.** Let T' be a triangulation of a 2-dimensional torus and σ an oriented closed normal curve on T'. Let n be the number of triangles of T' and $\mathbb{R}^{3n}$ be a vector space of the values of the angles of the triangles. Given a directed arc in a triangle, the leading corner is the one opposite to the entering side of the segment, and the trailing is the one opposite to the exiting side.

Starting from $0 \in \mathbb{R}^{3n}$, and for each segment of σ, add 1 to the coordinate corresponding to the leading corner and subtract 1 to the coordinate corresponding to the trailing one. The resulting vector of $\mathbb{R}^{3n}$ is the leading-trailing deformation associated to σ.

Figure 6.2 illustrates the leading (marked $+$) and trailing (marked $-$) corners associated to normal curves. In practice, in a 1-vertex ideal triangulation of a knot complement, T' will be the triangulated torus made of the intersection between T and the link of the ideal vertex. Let us consider the set B of vectors corresponding to the leading-trailing deformations of:

— one closed normal curve around each vertex of T';

— two normal curves generating the fundamental group of T', see Figure 6.2.

Then we have:

Theorem 6.2.2 ([35]). *B spans the tangent space of $\mathcal{A}(T)$.*

6.2.2 Maximizing the hyperbolic volume

The hyperbolic volume of an ideal hyperbolic tetrahedron with dihedral angles $(\alpha, \beta, \gamma) \in (0, \pi)^3$ is given by the function vol:

$$\mathrm{vol}(\alpha, \beta, \gamma) = \mathrm{L}(\alpha) + \mathrm{L}(\beta) + \mathrm{L}(\gamma)$$

where L is the Lobachevsky function $\mathrm{L}(x) = -\int_0^x \log|2\sin t|\,\mathrm{d}t$. The volume functional can be extended to the whole polytope $\mathcal{A}(T)$ by summing the volumes of the hyperbolic tetrahedra. The following result is due independently to Casson and Rivin.

Theorem 6.2.3 (Casson, Rivin [76]). *Let T be an ideal triangulation with n tetrahedra of M, an orientable 3–manifold with boundary consisting of tori. Then a point $p \in \mathcal{A}(T) \subset \mathbb{R}^{3n}$ corresponds to a complete hyperbolic metric on the interior of M if and only if p is a critical point of the function* vol.

Additionally, the volume functional is concave on $\mathcal{A}(T)$ and the maximum can be computed via convex optimization methods.

The proof of this result is obtained by looking at the derivatives of the hyperbolic volume for points in $\mathcal{A}$ along leading-trailing deformations. These derivatives are equal to the real part of the holonomy along the leading-trailing deformations we look at [35]. Since the angle structures constrain the imaginary part of the gluing equations, we have the theorem.

Remark 6.2.1 – In the literature, the Casson program * is a reference to this maximization problem. It includes a simplification phase of the triangulation with the heuristic that fewer tetrahedra meant thicker ones, avoiding singularities in the maximization.

6.3 Behavior of the optimization

Exploiting the formalism of the previous section, one can design an algorithm [35] to find and compute a CHS by first finding a point in the polytope $\mathcal{A}(T)$, then computing a basis of the tangent space of $\mathcal{A}(T)$, and then maximizing the (concave) hyperbolic volume functional on this subspace. If $\mathcal{A}(T) \neq \emptyset$ and the procedure finds the point maximizing the volume in the inside of the polytope, then the triangulation admits a complete hyperbolic structure represented by this point. Finally, if $\mathcal{A}(T) \neq \emptyset$ but the maximum of the volume functional is on the boundary, then one needs to re-triangulate the manifold in order to search for a triangulation admitting a CHS.

∗. https://nmd.web.illinois.edu//computop/software/casson.tar.gz

In this section, we study the outcome of the hyperbolic volume maximization on the space of angle structures. The result is given by the following lemma, which also appeared independently in [70]:

Lemma 6.3.1. *Let T be an ideal triangulation of M, a non-compact orientable 3–manifold with toric cusps. Let p be the point maximizing* vol *over $\overline{\mathcal{A}(T)}$ (the topological closure of $\mathcal{A}(T)$), then at p, if a tetrahedron has an angle equal to 0, then all other angles of the tetrahedron are in $\{0, \pi\}$.*

In other words, either the maximization succeeds in $\mathcal{A}(T)$, or there is at least one tetrahedron with angles $(0, 0, \pi)$ in p. Such tetrahedron is called *flat*. It is not possible to have a tetrahedron with angles $(0, a, b)$, $(a, b) \in (0, \pi)$ in p.
proof.

Let $\vec{p} \in \mathcal{A}(T)$ be an angle structure over T. Let $\vec{w} \in \mathbb{R}^{3n}$ be a vector tangent to $\mathcal{A}(T)$, then:

$$\frac{\partial \mathrm{vol}(\vec{p})}{\partial \vec{w}} = \sum_{i=1}^{3n} -w_i \log \sin(p_i).$$

Note that because $\vec{w}$ is tangent to $\mathcal{A}(T)$, its restriction to a single tetrahedron is three elements whose sum is equal to zero. Let us assume the maximum of the volume is reached on some point $\hat{p}$. Let us assume a tetrahedron t has angles $(0, a, b)$ at $\hat{p}$, $0 < a \leq b$, let $\hat{w}$ be a vector tangent to $\mathcal{A}(T)$ pointing towards the interior of the polytope with respect to $\hat{p}$ (and thus $w_1 > 0$) and $\hat{w}_t = (w_1, w_2, w_3)$ be its restriction to t. Then:

$$\lim_{\epsilon \to 0^+} \frac{\partial \mathrm{vol}(t + \epsilon \hat{w}_t)}{\partial \hat{w}_t} = -w_2 \log \sin(a) - w_3 \log \sin(b) + \lim_{\epsilon \to 0^+} -w_1 \log \sin(\epsilon w_1) = +\infty.$$

Now, with the same notations, let us assume t has angles $(0, 0, \pi)$ at $\hat{p}$, then using $\log(\sin(x)) = \log(x) + O_{x \to 0}(x^2)$:

$$\begin{aligned}
&\lim_{\epsilon \to 0^+} \frac{\partial \mathrm{vol}(t + \epsilon \hat{w}_t)}{\partial \hat{w}_t} \\
&\quad = -w_1 \log \sin(\epsilon w_1) - w_2 \log \sin(\epsilon w_2) + (w_1 + w_2) \log \sin(\pi - \epsilon(w_1 + w_2)) \\
&\quad = -w_1 \log(\epsilon w_1) - w_2 \log(\epsilon w_2) + (w_1 + w_2) \log(\epsilon(w_1 + w_2)) + O_{\epsilon \to 0}(\epsilon^2) \\
&\quad = -w_1 \log(w_1) - w_2 \log(w_2) + (w_1 + w_2) \log(w_1 + w_2) + O_{\epsilon \to 0}(\epsilon^2) \\
&\quad > -\infty
\end{aligned}$$

Since for all tetrahedra with non zero angles or angles of the form $(0, 0, \pi)$, the derivative of the volume is bounded, the existence of a tetrahedra with exactly one angle set to zero contradicts the maximality of the volume at that point. Indeed, when getting away from this point, there exists a small neighborhood where the derivative of the volume can be arbitrarily high.

□

We introduce in the next section an algorithm that performs localized combinatorial modifications on a triangulation equipped with an angle structure, in order to get rid of flat tetrahedra.

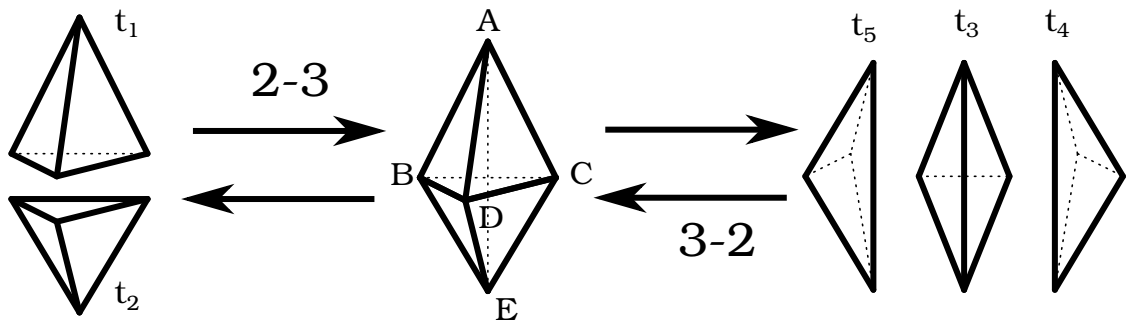

Figure 6.3 – Pachner moves 2-3 and 3-2 with vertices corresponding to the notations of the lemmas of this section.

6.4 Localized combinatorial modifications of triangulations

According to Lemma 6.3.1, the volume maximization either leads to a solution to the gluing equations, or to flat tetrahedra. In this section, we discuss a method to get rid of flat tetrahedra by combinatorial modifications of the triangulation, while attempting to maintain the value of the volume functional. This would lead to a triangulation admitting an angle structure with larger volume than the previous one, allowing to resume the maximization. In order to maintain the value of the volume functional, we introduce *geometric Pachner moves*.

6.4.1 Geometric Pachner moves

We perform Pachner moves on the triangulation that preserves the partial geometric data computed. More precisely, we define:

Definition 6.4.1 (Geometric Pachner move)**.** A *geometric Pachner move* in a triangulation T with angle structure is a Pachner move in T such that the resulting triangulation admits an angle structure with identical dihedral angles for the tetrahedra not involved in the move.

To check if a geometric Pachner move can be done, it must be valid combinatorially, and it should be possible to assign dihedral angles to the new tetrahedra without altering the rest of the angle structure. The combinatorial conditions are simple [72]: for the 2-3 moves (resp. 3-2 move) in Figure 6.3, the tetrahedra sharing the common triangle BDC (resp. common edge AE) must be distinct. The conditions on the angle structures are given by the following lemma:

Lemma 6.4.1. *Given a triangulation with angle structure T, if the combinatorial conditions given above are satisfied:*

- *a 3-2 move is always geometric;*
- *a 2-3 move is geometric if and only if the sum of the two dihedral angles around each edge of the common face is smaller than π.*

Furthermore the new angles can be computed using formulas.

The idea to prove the lemma is to study the system of equations given by the assumption that the angle structure is not altered outside the move, and we break the lemma into three: Lemma 6.4.2 concerns the 3-2 move, Lemma 6.4.3 concerns the 2-3, and Lemma 6.4.5 concerns the values of the angles.

With the notations of Figure 6.3, let $t_1 = ABCD$ and $t_2 = BCDE$ be two distinct tetrahedra glued along their common face, and $t_3 = ABCE$, $t_4 = ACDE$ and $t_5 = ADBE$ three distinct tetrahedra glued around their common edge. Assuming there is an underlying angle structure, let us denote $t(e)$ the value of the dihedral angle around the edge e in the tetrahedron t. Passing from (t_1, t_2) to (t_3, t_4, t_5), *i.e.* doing a 3-2 move, or the opposite without altering the rest of the angle structure leads to the following equations:

$$t_1(BC)+t_2(BC) = t_3(BC),\ t_1(CD)+t_2(CD) = t_4(CD),\ t_1(DB)+t_2(DB) = t_5(DB) \quad (6.1)$$

$$t_1(AB) = t_3(AB)+t_5(AB),\ t_1(AC) = t_3(AC)+t_4(AC),\ t_1(AD) = t_4(AD)+t_5(AD) \quad (6.2)$$

$$t_2(EB) = t_3(EB)+t_5(EB),\ t_2(EC) = t_3(EC)+t_4(EC),\ t_2(ED) = t_4(ED)+t_5(ED) \quad (6.3)$$

The constants, the angles that are fixed in the angle structure, and the unknowns, the angles we want to compute, depends on which move is studied. By equality of the dihedral angles, $t(UV) = t(XY)$ for $UVXY$ vertices of t. This equality is enforced by the framework of the angle structures: for the constraints system, $t(UV)$ and $t(XY)$ both represent the same variables.

For the following two lemma, refer to Figure 6.3 for an illustration.

6.4.1.1 The 3-2 move

Lemma 6.4.2. *Let T be a triangulation with angle structure, let $t_3 = ABCE$, $t_4 = ACDE$ and $t_5 = ADBE$ be three distinct tetrahedra glued around an edge. A 3-2 geometric Pachner move can always be performed at AE.*

proof.

The 3-2 move is combinatorially valid as the resulting tetrahedra and their gluings are well defined. Let us have $t_1 = ABCD$ and $t_2 = BCDE$.

The system composed of Equations 6.1, 6.2 and 6.3 is linear with 6 unknowns: the dihedral angles of t_1 and t_2. We need to check if this system admits a solution where the angles are in $(0, \pi)$. Note that as $t_3(AE)$, $t_4(AE)$, and $t_5(AE)$ are the angles around the edge AE, their sum is 2π.

$$\begin{aligned} t_1(AB) &= t_3(AB) + t_5(AB) \\ &= 2\pi - (t_3(AE) + t_3(AC) + t_5(AE) + t_5(AD)) \\ &< 2\pi - (t_3(AE) + t_5(AE)) && (= t_4(AE)) \\ &< \pi \end{aligned}$$

$$t_1(AB) = t_3(AB) + t_5(AB) > 0$$

Thus, if the system admits a solution, the dihedral angles of t_1 and t_2 are in $(0, \pi)$ by symmetry.

Now let us check if all the equations can be satisfied. From Equation 6.2 and 6.3:

$$t_1(AC)+t_2(EC) = t_3(AC)+t_4(AC)+t_3(EC)+t_4(EC) = 2\pi-(t_3(AE)+t_4(AE)) = t_5(AE)$$

Thus the equations of Equation 6.1 are consequences of the other two. The system is linear with 6 independent equations and 6 unknowns, it admits a solution.

Finally we have:

$$\begin{aligned} t_1(AB) + t_1(AC) + t_1(AD) &= t_3(AB) + t_5(AB) + t_3(AC) + t_4(AC) + t_4(AD) + t_5(AD) \\ &= 3\pi - (t_3(AE) + t_4(AE) + t_5(AE)) \\ &= \pi \end{aligned}$$

Thus the dihedral angles of t_1 sum to π, the same goes for t_2 by symmetry. And the move is always valid as long as we started with an angle structure.

□

6.4.1.2 The 2-3 move

Lemma 6.4.3. *Let T be a triangulation with angle structure, let $t_1 = ABCD$ and $t_2 = BCDE$ be two distinct tetrahedra glued along a face. A 2-3 geometric Pachner move can be performed at BCD if and only if $\forall e \in \{BC, CD, DB\},\ t_1(e) + t_2(e) < \pi$.*

proof.

The 2-3 move is combinatorially valid as the resulting tetrahedra and their gluings are well defined. Let us have $t_3 = ABCE$, $t_4 = ACDE$ and $t_5 = ADBE$.

From Equations 6.1 we have that if $\exists e \in \{BC, CD, DB\},\ t_1(e) + t_2(e) \geq \pi$ then one of the resulting tetrahedra will have a dihedral angle larger than π, preventing the validity of the move. Let us assume it is not the case.

The system composed of Equations 6.1, 6.2 and 6.3 is linear with 9 unknowns: the dihedral angles of t_3, t_4 and t_5. From Equations 6.1, the values of $t_3(AE)$, $t_4(AE)$, and $t_5(AE)$ are fixed and we have:

$$\begin{aligned} &t_3(AE) + t_4(AE) + t_5(AE) \\ &\qquad = t_1(BC) + t_2(BC) + t_1(CD) + t_2(CD) + t_1(DB) + t_2(DB) = 2\pi \end{aligned}$$

Thus the constraint around the edge AE is satisfied.

Summing the equations of Equation 6.2 on the one hand, and the equations of Equation 6.3 on the other hand both gives:

$$\pi = t_3(AB) + t_5(AB) + t_3(AC) + t_4(AC) + t_4(AD) + t_5(AD)$$

We also have that the sum of the dihedral angles of t_3 is π (and by symmetry it is true for t_4 and t_5):

$$\begin{aligned} t_3(AB) + t_3(AC) + t_3(AE) &= t_1(BC) + t_2(BC) + t_1(AB) + t_1(AC) - t_5(AB) - t_4(AC) \\ &= t_1(BC) + t_1(AB) + t_1(AC) + t_2(BC) - t_2(ED) \\ &= \pi \end{aligned}$$

Now, let us note that fixing any unknown fixes the values of the others, thus the system has exactly one degree of freedom: if $(t_3(AB), t_3(AC), t_4(AC), t_4(AD), t_5(AD), t_5(AB))$ is a

solution to the system, then for any $\lambda \in \mathbb{R}$, $(t_3(AB)+\lambda, t_3(AC)-\lambda, t_4(AC)+\lambda, t_4(AD)-\lambda, t_5(AD)+\lambda, t_5(AB)-\lambda)$ is also a solution. This is discussed in Remark 6.4.1. We denote by Λ_+ the set of dihedral angle for which λ is added, and by Λ_- its complement.

The last step of the proof is to show that there exists a choice of λ such that all the dihedral angles are positive, given that the dihedral angles of the tetrahedra sum to π is enough to have them in $(0, \pi)$.

By Lemma 6.4.4, there is always a choice of dihedral angle such that fixing it to 0 ensures that the elements of Λ_+ are positive and those of Λ_- are non negative (or Λ_- and Λ_+ respectively, depending on whether the selected angle is in Λ_+ or Λ_-). If the elements of Λ_+ are positive, then picking a sufficiently small negative λ to modify the dihedral angles will maintain the elements of Λ_+ positive, and will turn positive those of Λ_-, in the other case, in the same way a small positive λ will ensure the positivity of all the angles.

Thus there exists an angle structure corresponding to and coherent with the result of the Pachner move.

□

Lemma 6.4.4. *Let T be a triangulation with angle structure, let $t_1 = ABCD$ and $t_2 = BCDE$ be two distinct tetrahedra glued along a face such that $\forall e \in \{BC, CD, DB\}$, $t_1(e) + t_2(e) < \pi$. Let us have $t_3 = ABCE$, $t_4 = ACDE$ and $t_5 = ADBE$. Then there is always a choice of dihedral angle x in $\{t_3(AB), t_3(AC), t_4(AC), t_4(AD), t_5(AB), t_5(AD)\}$ such that fixing $x = 0$ leads to the elements of $\Lambda_+ = (t_3(AB), t_4(AC), t_5(AD))$ being positive and those of $\Lambda_- = (t_3(AC), t_4(AD), t_5(AB))$ being non negative (or Λ_- and Λ_+ respectively).*

proof.

Let us assume the Lemma is false. From this we build a set of contradictory constraints on the angles of t_1 and t_2.

— If $t_3(AC)$ is set to 0, then

$$t_3(AB) = \pi - t_3(AE) > 0,$$
$$t_5(EB) = t_2(EB) > 0$$
$$t_4(ED) = t_1(AC) > 0.$$

Furthermore

$$t_4(AD) = \pi - (t_4(AC) + t_4(AE)) = t_1(AD) - t_2(EB)$$

and

$$t_5(AB) = t_2(ED) - t_1(AC).$$

Note that the elements of Λ_+ are positive and the elements of Λ_- are non-negative if $t_4(AD)$ and $t_5(AB)$ are non-negative. Let us assume it is not the case and, for instance, that $t_1(AD) - t_2(EB) < 0$.

— If $t_4(AD)$ is set to 0, like previously the elements of Λ_+ are positive, and

$$t_3(AC) = t_2(EB) - t_1(AD) > 0$$

$$t_5(AB) = t_1(AB) - t_2(EC).$$

If the lemma is false, then $t_1(AB) - t_2(EC) < 0$.

— If $t_5(AB)$ is set to 0, like previously the elements of Λ_+ are positive, and

$$t_3(AC) = t_1(AC) - t_2(ED)$$

$$t_4(AD) = t_2(EC) - t_1(AB) < 0.$$

If the lemma is false, then $t_1(AC) - t_2(ED) < 0$.
Taking the constraints together, we have

$$t_1(AB) + t_1(AC) + t_1(AD) < t_2(EB) + t_2(EC) + t_2(ED),$$

which is absurd as these two sums are equal to π. The assumption that $t_1(AD) - t_2(EB) < 0$ must be false, and by symmetry $t_2(ED) - t_1(AC) < 0$ will be false too.

This is absurd and the Lemma is true.

□

Remark 6.4.1 – In Lemma 6.4.3, several angle structures are possible after the 2-3 move as it can be seen in the poof of Lemma 6.4.4. Conversely, several angle structures lead to the same result for the 3-2 move. This is because angle structures are blind to shearing singularities. If such a singularity exists, a 3-2 move can still be performed while maintaining the whole angle structure, but it will decrease the hyperbolic volume of the structure. It is due to the fact that the singularity, which maximized the volume, is fixed in the process.

6.4.1.3 Computing the angles

Lemma 6.4.5. *Let T be a triangulation with angle structure, if a geometric Pachner move can be performed, then the new angle structure can be computed in a constant number of arithmetical operations.*

proof.

3-2 move. From the proof of Lemma 6.4.2, the new angles can be obtained by solving a system of equations with six linear equations.

2-3 move. First, we remind that by Equation 5.1, it is possible to convert angles to edge parameters *et vice versa*. We still consider the notations of Figure 6.3, but we consider the situation in the upper halfspace with B sent to 0, E sent to 1, and D sent to ∞ (Figure 6.4). The position of C depends on the edge parameter of BD in $BCDE$, and the position of A depends on the edge parameter of BD in $ABCD$. Then the edge parameter of BD in $ABDE$ is just the product of the two edge parameter. This construction is valid by Lemma 6.4.3, as the sum of the arguments of both shape parameters is smaller than π. We can use the same procedure to find an edge parameter for $ABCE$ and $ACDE$.

Note that this construction leaves no shearing singularities around AE.

□

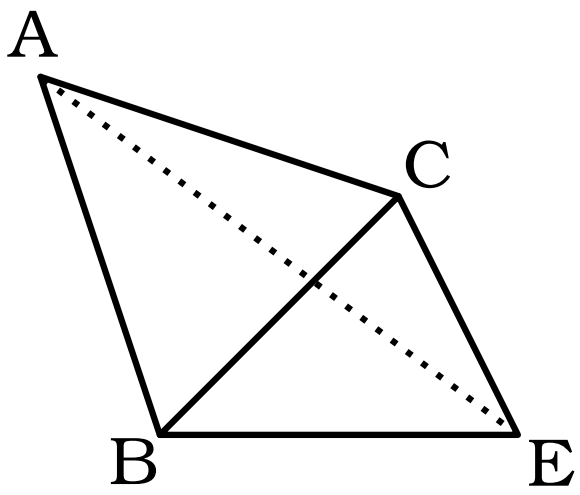

Figure 6.4 – Representation of the proof of Lemma 6.4.5, seen from the point D. The 2-3 move will delete the line BC in favor of AE.

6.4.2 Getting rid of flat tetrahedra

Let T be a triangulation with an angle structure admitting a flat tetrahedron t, and (e, e') the associated edges with dihedral angle π. By Lemma 6.4.1, it is not possible to get rid of a tetrahedron with a geometric 2-3 move. Indeed, if an edge of t has a dihedral angle equal to π, the second tetrahedron concerned by the 2-3 move must have a dihedral angle equal to 0, and consequently a 2-3 move will produce a flat tetrahedron.

In order to get rid of t, our strategy is to turn either e or e' into an edge of degree three, *i.e.* to put it at the center of three tetrahedra on which a 3-2 move can be performed (central edge of Figure 6.3, right). Note that edges of degree 2 prevent the existence of an angle structure as they force the two tetrahedra sharing the edge to be flat. As a consequence, we assume these configurations are removed, which can be done by `SnapPy`'s simplification for instance, see Section 6.5. Consequently, all edges have degree at least 3, and our strategy focuses on *reducing* the incidence degree of angle π edges.

To reduce the degree of an edge e, the strategy is to perform 2-3 moves on the tetrahedra containing e, such that each move reduces the degree of the edge by one. Either for topological (tetrahedron glued to itself) or geometrical reasons, these moves will not always be possible, and the order in which they are done matters. This is described in Figure 6.5.

Remark 6.4.2 – Doing a 2-3 move does not always reduce the degree of the edge, *e.g.*, when a tetrahedron is represented several times around an edge. However, doing a move that does not decrease the degree of the edge may delete the multiple occurrences of a tetrahedron around the edge and allow to continue with the simplification.

Remark 6.4.3 – When a 2-3 move is performed around e, the value of the dihedral angle of the new tetrahedron around e is equal to the sum of the previous two dihedral angles around e. Since the sum of the dihedral angles of a tetrahedron is equal to π, this means successfully reducing the degree of e may unlock previously forbidden moves.

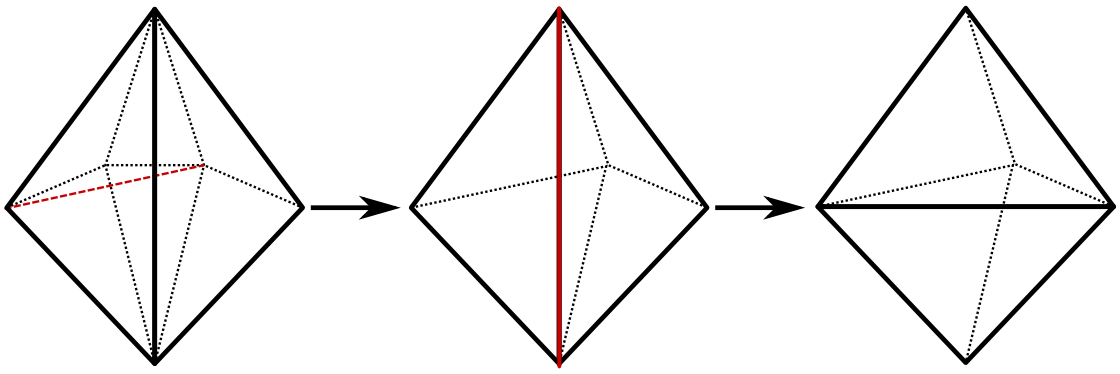

Figure 6.5 – A sequence of moves getting rid of a flat tetrahedron. The bold vertical edge is contained in 4 tetrahedra, three of which are represented behind the edge. The fourth tetrahedron is implicit, situated at the front, and flat. First, create the red edge of the first drawing with a 2-3 move. Then delete the red edge of the second drawing with a 3-2 move.

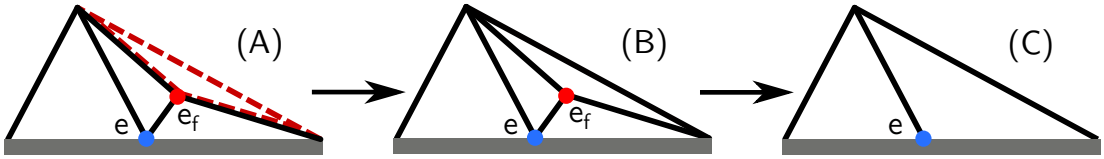

Figure 6.6 – Sequences of moves to reduce the degree of an edge when no 2-3 move is available, seen from above (triangles represent sections of tetrahedra, edge section of triangles and dots section of edges). In all drawings, the gray rectangle represents the flat tetrahedron, e (light blue dot) is the edge of the flat tetrahedron of which we want to reduce the degree. Assuming no 2-3 move is available, we pick another edge e_f (red dot), if a 3-2 move can be performed on e_f, we are in case (B) and the 3-2 move reduces the degree of e (case (C)). Otherwise, we are in case (A) we need to create the red dashed tetrahedron by decreasing the degree of e_f, this can be done by calling recursively our procedure on e_f.

Recursive moves. If no geometric Pachner move is possible on an edge e, we attempt to reduce the degree of a nearby edge e_f, *i.e.*, an edge for which there exists a tetrahedron containing e and e_f; see Figure 6.6 where e_f is represented by the red dot, as it is seen from above. More precisely, let f be a triangle containing e such that the associated 2-3 move is forbidden for geometric reasons, then by Lemma 6.4.1 there is an edge e_f of f for which the associated dihedral angle is at least π.

In consequence, reducing the degree of e_f to three without modifying the tetrahedra containing f and then performing a 3-2 move at e_f will reduce the degree of e by one; see Figure 6.6.

Note that in case a geometric Pachner move is not possible on any pair of tetrahedra containing e_f either, we can call the procedure recursively in a neighborhood of e_f, using the argument above to pass from e to e_f.

Remark 6.4.4 – The choice of e_f in f is unique: it is not possible to have two dihedral angles larger than π; selecting a move to reduce the degree of e boils down to selecting a triangle containing e.

Procedure summary. The procedure to get rid of a flat tetrahedron is a tree-like *backtracking search*, each branch corresponding to a choice of 2-3 or 3-2 move to perform. The moves used

are geometric to preserve the volume maximization advancement. A flat tetrahedron can only be deleted with a 3-2 move: the first step is to *reduce the degree* of one of its edges to three. To reduce the degree of an edge, the solution is to perform 2-3 moves on two tetrahedra containing this edge. If a 2-3 move is not possible for geometric reasons, we are in the situation of Figure 6.6, and the procedure to *reduce the degree* can be called *recursively* on a neighboring edge. Performing a 3-2 move on this latter edge resulting in a decrease of the degree of the initial one. The procedure ends when the initial edge has degree three and the flat tetrahedron can be removed or when no move can be applied.

6.4.3 Implementation details

The implementation faces several practical challenges.

Breaking infinite loops. As such, the algorithm may loop infinitely on some instance, as 2-3 and 3-2 moves may reverse themselves. To counteract this phenomenon and avoid redundant modifications, a solution is to store at each modification the *isomorphism signature* of the triangulation [17], characterizing uniquely the isomorphism type of the triangulation. This allows us to recognize already processed triangulations and break branches of the backtracking algorithms. Note however that this is costly compared to the Pachner moves, and it makes the procedure no longer local.

Selecting the edge e. When attempting to remove a flat tetrahedron, one needs to choose between the two π-angled edges e and e' to reduce. In our implementation, we consider both edges, and select the one that has the larger smallest angle in its link. This performs better than a random choice in our experiments.

Pruning the backtrack search. Some triangulations may have edges of large degree (more than 10), which produces wide search trees. Additionally, the recursive calls to the degree reduction procedure may induce trees of large depth. Experimentally, the better strategy consists of exploring exhaustively the first levels of the tree. We set the width of exploration to 8 and explore the first 2 levels of the search tree.

Sequencing of Pachner moves. Different sequencings of Pachner moves lead to different triangulations. In practice, we favor 2-3 moves over recursive ones, which performs best. Additionally, among the 2-3 moves performed to get rid of a flat tetrahedron containing edge e of angle π, we prioritize moves that eliminate tetrahedra for which e has a small dihedral angle. Among the recursive ones, we used the same method as the one choosing between e and e', indeed choosing a recursive move boils down to choosing an edge to minimize its degree.

6.5 Experiments

In this section, we study the experimental performance of our approach to find a triangulation with a CHS, and compare its behavior with the software `SnapPy` [22]. `SnapPy` is the state-of-the-art software to study the geometric properties of knots and 3-manifolds, and is widely used in the low-dimensional topology community. Following this analysis, we propose and study a hybrid method with practical interest.

`SnapPy`. `SnapPy`'s method is based on an implementation from Weeks, its uses a random re-triangulation followed by a simplification. The first step is constituted of $4n$ random 2-3 moves,

where n is the number of tetrahedra in the input triangulation. The simplification performs non-deterministic modifications to decrease the number of tetrahedra in the triangulation. Notably it removes some configurations that prevent angle structures from existing. The verification of the existence of a CHS is based on a Newton's method to solve the gluing equations [88].

Remark 6.5.1 – The number of $4n$ random 2-3 moves is arbitrary and the program could behave better with more ou less moves, depending on the cases. On some examples, the program seems to stay stuck on some bad configurations, lowering the number of moves could favor this behavior. However, this problem could be also a consequence of the simplification strategy. Either way, we use `SnapPy` as it is.

Data set. We apply our algorithms to the census of prime hyperbolic knots with up to 19 crossings. This census has been constituted by the efforts of many researchers in the field, and recently completed with the exhaustive enumeration of all knots with crossing number smaller than 20 † [16].

For each knot, given by a knot diagram, we compute a triangulation of the knot complement using `Regina` [17], and simplify it with `SnapPy`. We then keep the triangulations admitting an angle structure but not a CHS, and hence requiring re-triangulation. All the others, without angle structure or admitting a CHS, were discarded. They constitute the *Failure on first try* data of Table 6.1.

The knots are grouped by crossing numbers (from 14 to 19), and on whether they are alternating or not. In Section 6.5.2, our experiments are run on the first 2500 knots of each of the 12 groups having an angle structure but no CHS, and in Section 6.5.3 we use the first 10.000 knots of the same data sets.

6.5.1 Our program and current state of the code

Our implementation is done in `Python`, to be able to interface with `Regina` and `SnapPy` (and not `SnaPpea`). The idea behind using `Python` was also to enable shorter development times. The basic tools to handle triangulations where rewritten to have more control on the behavior of the simulation and we rely on external libraries only for the isomorphism signatures, some linear programming to find a point to begin the optimization, and to perform the optimization (we use the `SLSQP` [49] optimization method from SciPy [86]).

However this choice of language leads to costly computation times, decision was taken to not render public this version of the code and switch to `C++`, using another library to manipulate the triangulations.

The version of the program presented in Section 6.5.3 ‡, which outperforms the state of the art in terms of performance, is a simpler `C` version directly implemented in `SnapPy`'s kernel. We are in discussion with the developers to integrate this code in the library `SnapPy`.

6.5.2 Success rate and combinatorial performance

In terms of Pachner moves. Figure 6.7 (left) represents the rate of knots on which our algorithm succeeds to find a triangulation with a CHS, for all the 12 groups of knots. It represents the success rate as a function of the number of Pachner moves, the higher success rate groups are the alternating knots. With Figure 6.7 (right), which represents this success rate for optimization

†. The census is available at https://regina-normal.github.io/data.html
‡. Available at https://github.com/orouille/SnapPy

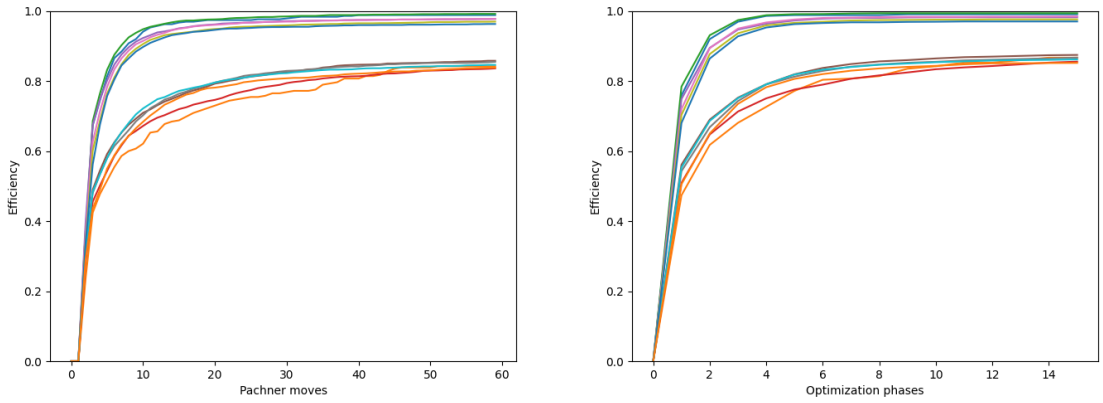

Figure 6.7 – On the sample of triangulations, success rate in finding a CHS for different crossing numbers and alternabilities. The limit rate of success for alternating knots is 0.98, the limit rate for non-alternating knots is 0.87. Left: success rate against the number of Pachner moves. Right: success rate against the number of optimization phases.

	# of optim phases						# of moves				
	1	2	3	4	5		2	3	4	10	30
Efficiency alter	0.73	0.89	0.95	0.97	0.97		0.36	0.63	0.72	0.92	0.97
Efficiency non-alter	0.53	0.67	0.74	0.78	0.81		0.30	0.47	0.52	0.70	0.81

Figure 6.8 – Average of success rates for the alternating and non-alternating groups of knots of Figure 6.7.

phases, we see that few Pachner moves are done on average between the phases, hinting that the convex optimization will likely be the time bottleneck.

While there is a significant difference between the efficiency on alternating and non-alternating knots, all the curves have the same behavior: the first few Pachner moves are very effective. An important point is that, compared to the number of moves done by `SnapPy`, at least four times the number of tetrahedra and then roughly the same number for the simplification times the number of re-triangulation, our method uses a much lower number of Pachner moves on average (see Figure 6.7, left). This is of *combinatorial interest*, as doing a small number of moves can mitigate the impact of the procedure on the properties of the triangulation, such as keeping a small treewidth for instance.

After the first few steps, the growth of the success rate slows down drastically. An interpretation of this phenomenon is that the tetrahedra created by the 2-3 moves tend to to be more flat than the original ones. This leads to an increase in the number of required re-triangulations and issues with floating point arithmetic.

In terms of *re-triangulation*. In order to compare the behaviors of our method and of the state of the art: we want to know if the two methods struggle on the same triangulations. Both methods using sequences of re-triangulations, we use the length of these sequences as metrics.

We compare in Figure 6.9 the average number of randomized re-triangulations required by `SnapPy` to find a triangulation with a CHS, and the (deterministic) number of re-triangulations

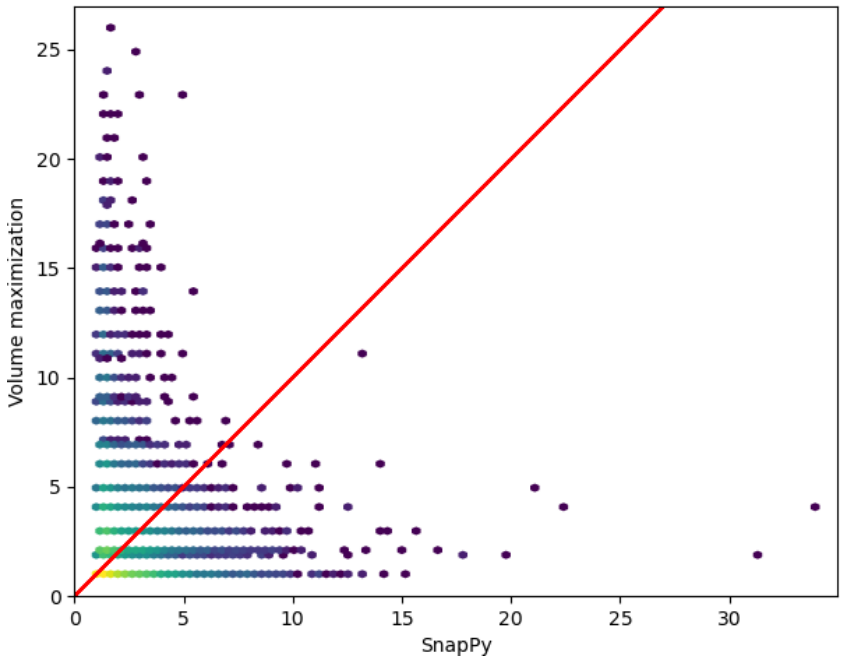

Figure 6.9 – Number of re-triangulations required by our method over the number of re-triangulations required by `SnapPy` on the 12 groups of knots, gathered in bins (the color indicates the log of the number of points inside). Since our method is deterministic, the points have discrete ordinates. The diagonal $x = y$ appears in red.

of our method. The majority of the CHS are found within few re-triangulations on average: both methods manage to find 78% of them within two steps.

However, it appears that for the manifolds requiring a large number of re-triangulations with either method, the other one will perform well on it: the performance of the methods are substantially orthogonal for the difficult cases. This phenomenon highlights the fact that the methods are *complementary*.

Limitations. It is to be noted that our method suffers from several phenomena: there are manifolds on which our method fails, the reasons to this being convergence problems because of the floating point arithmetic, the creation of flatter tetrahedra or the volume modification mentioned in Remark 6.4.1. Furthermore some triangulations have several very high degree edges and looking for the correct sequence of geometric Pachner moves can be costly. In terms of time performance, the constraint convex optimization is an important bottleneck, as well as the computation and book-keeping of a large number of isomorphism signatures.

However, in light of the previous results, we design a hybrid algorithm, mixing `SnapPy`'s pipeline together with the heuristics based on localized geometric Pachner moves introduced in this chapter, in order to outperform both methods in terms of experimental timings.

6.5.3 Hybrid algorithm and time performance

As is, `SnapPy` does not produce angle structures as defined in Section 6.2, as it constructs *negative tetrahedra*, i.e., tetrahedra whose shape has a negative imaginary part. Our hybrid method

consists of calling SnapPy to randomize and simplify the triangulation, and, in case the triangulation admits only few negative tetrahedra (less than four in our experiments), call the resolution of flat tetrahedra with geometric Pachner moves on these negative tetrahedra, as introduced in Section 6.4. Loop until a CHS is found.

Our implementation is done in C directly in SnapPy's kernel and consists of a simplified version of Section 6.4's method. For each negative tetrahedron, we try to reduce the degree of one of its edges down to 3 in turn using only geometric 2-3 moves, we try all the edges, and we do not use recursive moves or heuristics to perform the geometric moves.

The results of this method are summarized in Figure 6.10 (Figure 6.11 is given to help read Figure 6.10), where the time to compute the CHS are compared for the new hybrid method and the usual SnapPy pipeline, on the first 10.000 triangulations of the datasets of Section 6.5. The hybrid method using localized geometric Pachner moves shows, at worst, similar time performance compared to SnapPy, and performs significantly better overall. On average, the hybrid method is 20% faster, however, it is to be noted that, on most cases, few re-triangulations are required in which case the hybrid method and SnapPy show naturally similar time performance. More interestingly, on cases requiring many more re-triangulations in the SnapPy pipeline, the hybrid methods performs much better than SnapPy, with running times up to 18 times faster.

As indicator of the global behavior of both algorithms, we indicate the linear regression of the data points (black dashed line, slope $= 0.4$) in Figure 6.10, to illustrate that the dense region is not concentrated on the $x = y$ diagonal. Furthermore, this line suggests that if we are not in the dense region where almost all CHS are found instantly, then the gain is not 20%, but 60%.

6.6 Conclusion

The problematic of this work is the computation of complete hyperbolic structures on triangulated 3-manifolds. This can be done on computers by solving Thurston's gluing equations. The state-of-the-art method, implemented by SnapPy, consists in trying to simplify the triangulation before using Newton's method to solve the equations. If this does not succeed, then the only strategy is to find another triangulation of the manifold and to start over. This work well in most cases, but can require a large number of re-triangulations in some cases. The key difficulty is to find a triangulation where the equations admits a solution

We have introduced a new method based on results form Casson and Rivin stating that maximizing the hyperbolic volume yields CHS. When it is not possible to find a solution to the equations on a triangulation, we use the result of the volume maximization to propose another one.

Our algorithm is complementary to SnapPy, and in particular performs much better on almost all cases we have studied where SnapPy struggled to find a solution to the CHS problem. While our current implementation of the whole method is not competitive due to being implemented in Python, we introduced a hybrid method that improves the state-of-the-art in most cases, specifically in difficult ones, without sacrificing SnapPy's efficiency when it performs well.

Our method proposes an improvement in term of computation time over the state-of-the-art, this is very important when running large scale experiments or when the manifolds studied are large. But our method has another interest: since it tries to avoid performing a large number of re-triangulations, we tend to preserve the triangulation whenever possible.

The method and its implementation can be improved: when used alone, it can simply fail, being able to continue with the information we gained would be a great plus. Also, we plan on

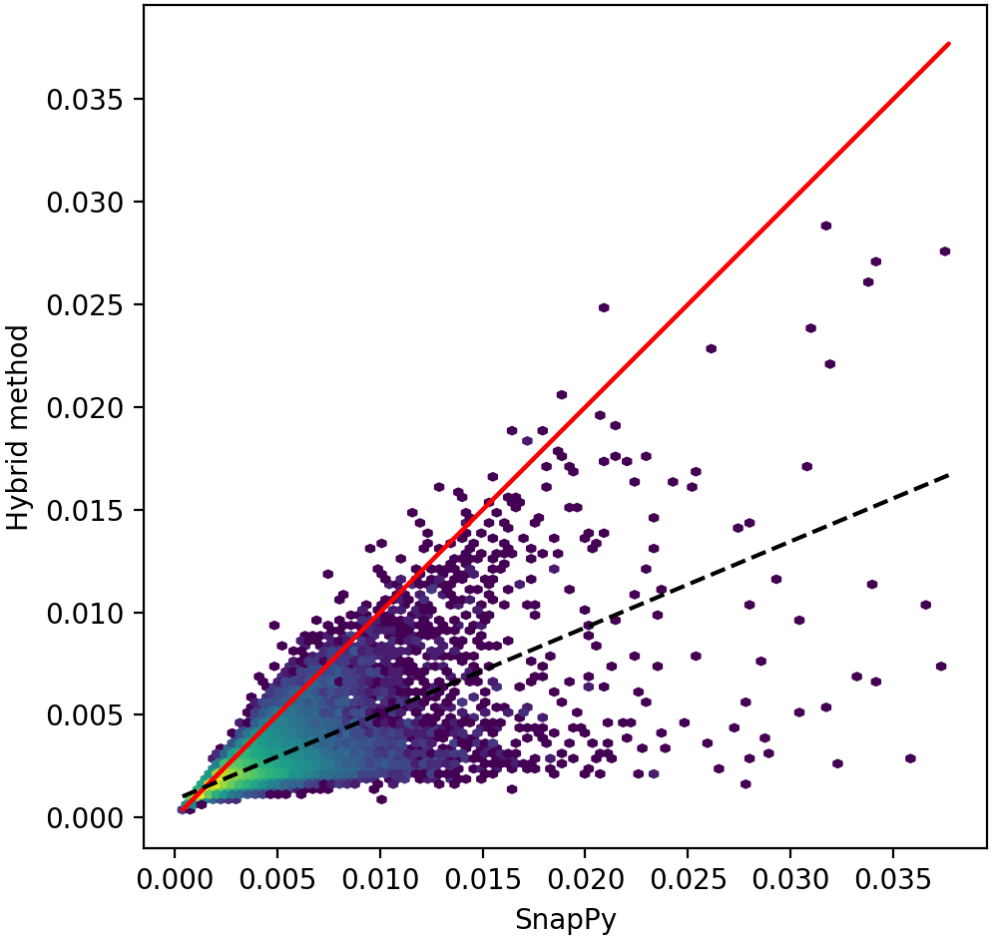

Figure 6.10 – Time comparison of the hybrid method and `SnapPy` in seconds for the 10.000 first triangulations of each crossing number of the data set of the previous section, gathered in bins (the color indicates the log of the number of points inside). Line $x = y$ is plain and red, a linear regression through the data set is dashed and black. For readability, four outlayers favoring the hybrid method are omitted.

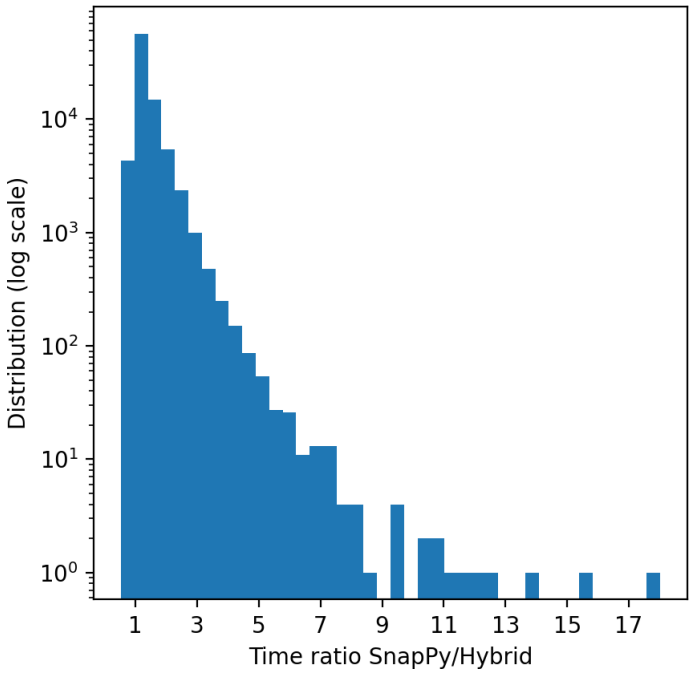

Figure 6.11 – Distribution, in logarithmic scale, of the time required by `SnapPy` over the time required by the hybrid method.

transferring the full method in `C++`, to check its actual performances when `Python` is not used, this will rise questions about the convex programming and arithmetic precision.

The method opens the door for new questions concerning its behavior. A group of questions arises when looking at the volume maximization like a flow: What is the impact of the volume maximization on the triangulation? Which tetrahedra shrink first? Are there combinatorial configurations blocking our method? These questions are close to the study of the *combinatorial Ricci flow* [89], which is dual to our approach, meets similar problems and has known some development in the recent years. Closely linked to the flow, there are questions on the path we take on path in the Pachner graph: these are quite popular in computational topology and geometry, with the problem to know what is happening at blocking nodes for instance. More generally, our graph is less connected than the topological one, how connected is it?

There are other questions concerning our results: given the fact that the dataset we used is actually sorted by the volume, does the hyperbolic volume have an impact on the success rate of the methods? How does the approach perform on very large knots that are not on the census? Are the triangulations we output suitable for Weeks' program that computes canonical triangulations from complete hyperbolic structures [87]?

There are also questions about `SnapPy`'s method we can look at with ours: `SnapPy` retriangulation is a large number of 2-3 moves performed at random, why does it miss so much on some specific examples? What makes triangulations difficult to handle for `SnapPy` and easy for us, *et vise versa*?

In conclusion, while this work has a concrete and direct use in 3-manifolds study, it raises many interesting questions in mathematics, combinatorics, data science, and algorithmics.

Bibliography

[1] Colin Conrad Adams. *The knot book: an elementary introduction to the mathematical theory of knots*. W.H. Freeman, 1994.

[2] James W Alexander. Topological invariants of knots and links. *Transactions of the American Mathematical Society*, 30(2):275–306, 1928.

[3] Javier Arsuaga, Mariel Vazquez, Paul McGuirk, Sonia Trigueros, De Witt Sumners, and Joaquim Roca. Dna knots reveal a chiral organization of dna in phage capsids. *Proceedings of the National Academy of Sciences*, 102(26):9165–9169, 2005. doi:10.1073/pnas.0409323102.

[4] Michael F Atiyah. Topological quantum field theory. *Publications Mathématiques de l'IHÉS*, 68:175–186, 1988.

[5] Dror Bar-Natan, Scott Morrison, and et al. The Knot Atlas, 2015. URL: http://katlas.org.

[6] Bruno Barras, Samuel Boutin, Cristina Cornes, Judicaël Courant, Jean-Christophe Filliatre, Eduardo Gimenez, Hugo Herbelin, Gerard Huet, Cesar Munoz, Chetan Murthy, et al. *The Coq proof assistant reference manual: Version 6.1*. Inria, 1997.

[7] Alexander Barvinok. Computing the ehrhart polynomial of a convex lattice polytope. *Discrete and Computational Geometry*, 1994. URL: https://doi.org/10.1145/1236463.1236468.

[8] Alexander Barvinok. Computing the ehrhart quasi-polynomial of a rational simplex, 2005. URL: https://arxiv.org/abs/math/0504444, arXiv:math/0504444.

[9] Riccardo Benedetti and Carlo Petronio. *Lectures on hyperbolic geometry*. Springer Science & Business Media, 1992.

[10] Laurent Bessières, Gérard Besson, Michel Boileau, Sylvain Maillot, and Joan Porti. *Geometrisation of 3-manifolds*, volume 13. European Mathematical Society, 2010.

[11] Winfried Bruns, Bogdam Ichim, Tim Römer, Richard Sieg, and Christof Söger. Normaliz. algorithms for rational cones and affine monoids. http://normaliz.uos.de, accessed 2022.

[12] Benjamin A Burton. Structures of small closed non-orientable 3-manifold triangulations. *J. Knot Theory Ramifications*, 16(5):545–574, 2007.

[13] Benjamin A Burton. The pachner graph and the simplification of 3-sphere triangulations. In *Proceedings of the twenty-seventh annual symposium on Computational geometry*, pages 153–162, 2011.

[14] Benjamin A Burton. Computational topology with regina: algorithms, heuristics and implementations. *Geometry and topology down under*, 597:195–224, 2013.

[15] Benjamin A Burton. A new approach to crushing 3-manifold triangulations. *Discrete & Computational Geometry*, 52(1):116–139, 2014.

[16] Benjamin A. Burton. The Next 350 Million Knots. In Sergio Cabello and Danny Z. Chen, editors, *36th International Symposium on Computational Geometry (SoCG 2020)*, volume 164 of *Leibniz International Proceedings in Informatics (LIPIcs)*, pages 25:1–25:17, Dagstuhl, Germany, 2020. Schloss Dagstuhl–Leibniz-Zentrum für Informatik. URL: https://drops.dagstuhl.de/opus/volltexte/2020/12183, doi:10.4230/LIPIcs.SoCG.2020.25.

[17] Benjamin A. Burton, Ryan Budney, William Pettersson, et al. Regina: Software for low-dimensional topology. http://regina-normal.github.io/, 1999–2021.

[18] Benjamin A. Burton, Clément Maria, and Jonathan Spreer. Algorithms and complexity for Turaev-Viro invariants. *J. Appl. Comput. Topol.*, 2(1-2):33–53, 2018. doi:10.1007/s41468-018-0016-2.

[19] Qingtao Chen and Tian Yang. Volume conjectures for the Reshetikhin–Turaev and the Turaev–Viro invariants. *Quantum Topology*, 9(3):419–460, 2018. doi:10.4171/QT/111.

[20] John H Conway. An enumeration of knots and links, and some of their algebraic properties. In *Computational problems in abstract algebra*, pages 329–358. Elsevier, 1970.

[21] Alexander Coward and Marc Lackenby. An upper bound on Reidemeister moves. *American Journal of Mathematics*, 136(4):1023–1066, 2014. URL: http://www.jstor.org/stable/24477273.

[22] Marc Culler, Nathan M. Dunfield, and Jeffrey R. Weeks. SnapPy, a computer program for studying the geometry and topology of 3-manifolds. https://snappy.math.uic.edu/, 1991–2021.

[23] Blake Dadd and Aochen Duan. Constructing infinitely many geometric triangulations of the figure eight knot complement. *Proceedings of the American Mathematical Society*, 144(10):4545–4555, 2016.

[24] Alex Davies, Petar Veličković, Lars Buesing, Sam Blackwell, Daniel Zheng, Nenad Tomašev, Richard Tanburn, Peter Battaglia, Charles Blundell, András Juhász, Marc Lackenby, Geordie Williamson, Demis Hassabis, and Pushmeet Kohli. Advancing mathematics by guiding human intuition with ai. *Nature*, 600:70–74, 12 2021. doi:10.1038/s41586-021-04086-x.

[25] Renaud Detcherry and Efstratia Kalfagianni. Gromov norm and Turaev-Viro invariants of 3-manifolds, 2017. arXiv:1705.09964.

[26] Renaud Detcherry, Efstratia Kalfagianni, and Tian Yang. Turaev–Viro invariants, colored jones polynomials, and volume. *Quantum Topology*, 9:775–813, 2018.

[27] Manfredo Perdigao Do Carmo and J Flaherty Francis. *Riemannian geometry*, volume 6. Springer, 1992.

[28] Clifford H Dowker and Morwen B Thistlethwaite. Classification of knot projections. *Topology and its Applications*, 16(1):19–31, 1983.

[29] Eugène Ehrhart. Sur les polyèdres rationnels homothétiques á n dimensions. *Comptes rendus de l'Académie des Sciences*, 254:616–618, 1962.

[30] Ioannis Z. Emiris and Vissarion Fisikopoulos. Efficient random-walk methods for approximating polytope volume. In *Proceedings of the Thirtieth Annual Symposium on Computational Geometry*, SOCG'14, page 318–327, New York, NY, USA, 2014. Association for Computing Machinery. doi:10.1145/2582112.2582133.

[31] Claus Ernst and DW Sumners. The growth of the number of prime knots. In *Mathematical proceedings of the cambridge philosophical society*, volume 102, pages 303–315. Cambridge University Press, 1987.

[32] Vissarion Fisikopoulos and Apostolos Chalkis. Volesti. https://github.com/vissarion/volume_approximation, accessed 2022.

[33] Laurent Fousse, Guillaume Hanrot, Vincent Lefèvre, Patrick Pélissier, and Paul Zimmermann. Mpfr: A multiple-precision binary floating-point library with correct rounding. *ACM Trans. Math. Softw.*, 33(2):13–es, June 2007. doi:10.1145/1236463.1236468.

[34] Michael H. Freedman, Alexei Kitaev, Michael J. Larsen, and Zhenghan Wang. Topological quantum computation, 2001. URL: https://arxiv.org/abs/quant-ph/0101025, doi:10.48550/ARXIV.QUANT-PH/0101025.

[35] David Futer and François Guéritaud. From angled triangulations to hyperbolic structures, 2010. doi:http://dx.doi.org/10.1090/conm/541/10683.

[36] Mikhail Gromov. Volume and bounded cohomology. *Publ. Math., Inst. Hautes Étud. Sci.*, 56:5–99, 1982.

[37] Wolfgang Haken. Theorie der Normalflächen: Ein Isotopiekriterium für den Kreisknoten. *Acta Mathematica*, 105(3-4):245 – 375, 1961. doi:10.1007/BF02559591.

[38] Joel Hass, Jeffrey C. Lagarias, and Nicholas Pippenger. The computational complexity of knot and link problems. *J. ACM*, 46(2):185–211, 1999. URL: http://dx.doi.org/10.1145/301970.301971, doi:10.1145/301970.301971.

[39] Allen Hatcher. *Algebraic topology*. Cambridge University Press, 2005. URL: https://pi.math.cornell.edu/~hatcher/AT/ATpage.html.

[40] Craig D. Hodgson and Jeffrey R. Weeks. Symmetries, isometries and length spectra of closed hyperbolic three-manifolds. *Experimental Mathematics*, 3(4):261 – 274, 1994. URL: https://doi.org/, doi:em/1048515809.

[41] Jim Hoste, Morwen Thistlethwaite, and Jeff Weeks. The first 1,701,936 knots. *Math. Intelligencer*, 20(4):33–48, 1998.

[42] William Jaco and J. Hyam Rubinstein. 0-Efficient Triangulations of 3-Manifolds. *Journal of Differential Geometry*, 65(1):61 – 168, 2003. doi:10.4310/jdg/1090503053.

[43] William Jaco and Peter B Shalen. Seifert fibered spaces in 3-manifolds. In *Geometric topology*, pages 91–99. Elsevier, 1979.

[44] Vaughan FR Jones. A polynomial invariant for knots via von neumann algebras. In *Fields Medallists' Lectures*, pages 448–458. World Scientific, 1997.

[45] Rinat M. Kashaev. The hyperbolic volume of knots from the quantum dilogarithm. *Letters in Mathematical Physics*, 39(3):269–275, Feb 1997. doi:10.1023/A:1007364912784.

[46] Robion Kirby and Paul Melvin. Local surgery formulas for quantum invariants and the Arf invariant. *Geom. Topol. Monogr.*, pages (7):213–233, 2004. URL: http://dx.doi.org/10.2140/gtm.2004.7.213.

[47] Hellmuth Kneser. Geschlossene flächen in dreidimensionalen mannigfaltigkeiten. *Jahresbericht der Deutschen Mathematiker-Vereinigung*, 38:248–259, 1929.

[48] Hellmuth Kneser. Geschlossene flächen in dreidimensionalen mannigfaltigkeiten. *Jahresbericht der Deutschen Mathematiker-Vereinigung*, 38:248–259, 1929. URL: http://eudml.org/doc/145838.

[49] D. Kraft. *A Software Package for Sequential Quadratic Programming*. Deutsche Forschungs- und Versuchsanstalt für Luft- und Raumfahrt Köln: Forschungsbericht. Wiss. Berichtswesen d. DFVLR, 1988.

[50] Greg Kuperberg. Algorithmic homeomorphism of 3-manifolds as a corollary of geometrization. *Pacific Journal of Mathematics*, 301(1):189–241, 2019.

[51] Marc Lackenby. Word hyperbolic dehn surgery. *Inventiones mathematicae*, pages 243–282, 2000. doi:https://doi.org/10.1007/s002220000047.

[52] Marc Lackenby. A polynomial upper bound on reidemeister moves. *Annals of Mathematics*, pages 491–564, 2015.

[53] Charles Newton Little. On knots, with a census for order 10. *Transactions of the Connecticut Academy of Arts and Sciences*, 7(3):27–43, 1885.

[54] Charles Newton Little. Alternate +/-knots of order eleven. *Transactions of the Royal Society of Edinburgh*, 36(9):253–255, 1890.

[55] Charles Newton Little. Non-alternate +/-knots. *Transactions of the Royal Society of Edinburgh*, 39(30):771–778, 1890.

[56] Clément Maria and Owen Rouillé. Computation of Large Asymptotics of 3-Manifold Quantum Invariants. In *ALENEX 2021 - SIAM Symposium on Algorithm Engineering and Experiments*, Alexandria / Virtual, United States, January 2021. URL: https://hal.archives-ouvertes.fr/hal-03133238, doi:10.1137/1.9781611976472.15.

[57] Clément Maria and Owen Rouillé. Computing complete hyperbolic structures on cusped 3-manifolds. *European Symposium on Algorithms*, abs/2112.06360, 2022. URL: https://arxiv.org/abs/2112.06360.

[58] Clément Maria and Jonathan Spreer. Admissible colourings of 3-manifold triangulations for Turaev-Viro type invariants. In Piotr Sankowski and Christos D. Zaroliagis, editors, *24th Annual European Symposium on Algorithms, ESA 2016, August 22-24, 2016, Aarhus, Denmark*, volume 57 of *LIPIcs*, pages 64:1–64:16. Schloss Dagstuhl - Leibniz-Zentrum für Informatik, 2016. doi:10.4230/LIPIcs.ESA.2016.64.

[59] Clément Maria and Jonathan Spreer. A polynomial-time algorithm to compute Turaev-Viro invariants tv(4,q) of 3-manifolds with bounded first Betti number. *Found. Comput. Math.*, 20(5):1013–1034, 2020. doi:10.1007/s10208-019-09438-8.

[60] Bruno Martelli. An introduction to geometric topology. *arXiv preprint arXiv:1610.02592*, 2016.

[61] Sergei Matveev. *Algorithmic Topology and Classification of 3-Manifolds*. Number 9 in Algorithms and Computation in Mathematics. Springer, Berlin, 2003.

[62] Sergei Matveev et al. Manifold recognizer. http://www.matlas.math.csu.ru/?page=recognizer, accessed August 2012.

[63] Cameron McA and John Luecke. Knots are determined by their complements. *Journal of the American Mathematical Society*, pages 371–415, 1989.

[64] J. Milnor. A unique decomposition theorem for 3-manifolds. *American Journal of Mathematics*, 84(1):1–7, 1962. URL: http://www.jstor.org/stable/2372800.

[65] Edwin E. Moise. Affine structures in 3-manifolds: V. the triangulation theorem and hauptvermutung. *Annals of Mathematics*, 56(1):96–114, 1952. URL: http://www.jstor.org/stable/1969769.

[66] George D. Mostow. *Strong Rigidity of Locally Symmetric Spaces*. Princeton University Press, 1973. URL: https://doi.org/10.1515/9781400881833, doi:doi:10.1515/9781400881833.

[67] Leonardo de Moura, Soonho Kong, Jeremy Avigad, Floris van Doorn, and Jakob von Raumer. The lean theorem prover (system description). In *International Conference on Automated Deduction*, pages 378–388. Springer, 2015.

[68] Hitoshi Murakami and Jun Murakami. The colored Jones polynomials and the simplicial volume of a knot. *Acta Math.*, 186(1):85–104, 2001. doi:10.1007/BF02392716.

[69] Hitoshi Murakami and Yoshiyuki Yokota. *Volume Conjecture for Knots*. Springer, 2018. doi:https://doi.org/10.1007/978-981-13-1150-5.

[70] Barbara Nimershiem. Geometric triangulations of a family of hyperbolic 3-braids, 2021. arXiv:2108.09349.

[71] Tomotada Ohtsuki and Toshie Takata. On the quantum su(2) invariant at q=exp(4 pi i/n) and the twisted reidemeister torsion for some closed 3-manifolds. *Communications in Mathematical Physics*, 370(1):151–204, August 2019. doi:10.1007/s00220-019-03489-2.

[72] Udo Pachner. P.l. homeomorphic manifolds are equivalent by elementary shellings. *European Journal of Combinatorics*, 12(2):129–145, 1991. URL: https://www.sciencedirect.com/science/article/pii/S0195669813800807, doi:https://doi.org/10.1016/S0195-6698(13)80080-7.

[73] Lionel Pournin. The flip-graph of the 4-dimensional cube is connected. *Discrete & Computational Geometry*, 49(3):511–530, 2013.

[74] Gopal Prasad. Strong rigidity of q-rank 1 lattices. *Inventiones mathematicae*, 21(4):255–286, 1973.

[75] Jessica S Purcell. *Hyperbolic knot theory*, volume 209. American Mathematical Soc., 2020.

[76] Igor Rivin. Euclidean structures on simplicial surfaces and hyperbolic volume. *Annals of Mathematics*, 139:553–580, 1994.

[77] J. Hyam Rubinstein, Henry Segerman, and Stephan Tillmann. Traversing three-manifold triangulations and spines, 2018. URL: https://arxiv.org/abs/1812.02806, doi:10.48550/ARXIV.1812.02806.

[78] Peter Guthrie Tait. On knots i. *Transactions of the Royal Society of Edinburgh*, 28(39):145–190, 1876.

[79] Peter Guthrie Tait. On knots ii. *Transactions of the Royal Society of Edinburgh*, 32(40):327–342, 1883.

[80] Peter Guthrie Tait. On knots iii. *Transactions of the Royal Society of Edinburgh*, 32(41):493–506, 1884.

[81] William Thomson. II. on vortex atoms. *The London, Edinburgh, and Dublin Philosophical Magazine and Journal of Science*, 34(227):15–24, 1867.

[82] W. P. Thurston. *The geometry and topology of 3-manifolds*, volume 1. Princeton University Press, Princeton, N.J., 1980. Electronic version 1.1 - March 2002. URL: http://library.msri.org/books/gt3m/.

[83] William P Thurston. Three dimensional manifolds, kleinian groups and hyperbolic geometry. *Bulletin (New Series) of the american mathematical society*, 6(3):357–381, 1982.

[84] Vladimir G. Turaev and Oleg Y. Viro. State sum invariants of 3-manifolds and quantum $6j$-symbols. *Topology*, 31(4):865–902, 1992.

[85] Andrei V Malyutin. On the Question of Genericity of Hyperbolic Knots. *International Mathematics Research Notices*, 2020(21):7792–7828, 09 2018. arXiv:https://academic.oup.com/imrn/article-pdf/2020/21/7792/34303153/rny220.pdf, doi:10.1093/imrn/rny220.

[86] Pauli Virtanen, Ralf Gommers, Travis E. Oliphant, Matt Haberland, Tyler Reddy, David Cournapeau, Evgeni Burovski, Pearu Peterson, Warren Weckesser, Jonathan Bright, Stéfan J. van der Walt, Matthew Brett, Joshua Wilson, K. Jarrod Millman, Nikolay Mayorov, Andrew R. J. Nelson, Eric Jones, Robert Kern, Eric Larson, C J Carey, İlhan Polat, Yu Feng, Eric W. Moore, Jake VanderPlas, Denis Laxalde, Josef Perktold, Robert Cimrman, Ian Henriksen, E. A. Quintero, Charles R. Harris, Anne M. Archibald, Antônio H. Ribeiro, Fabian Pedregosa, Paul van Mulbregt, and SciPy 1.0 Contributors. SciPy 1.0: Fundamental Algorithms for Scientific Computing in Python. *Nature Methods*, 17:261–272, 2020. doi:10.1038/s41592-019-0686-2.

[87] Jeffrey R. Weeks. Convex hulls and isometries of cusped hyperbolic 3-manifolds. *Topology and its Applications*, 52(2):127–149, 1993. URL: https://www.sciencedirect.com/science/article/pii/0166864193900329, doi:https://doi.org/10.1016/0166-8641(93)90032-9.

[88] Jeffrey R. Weeks. Computation of hyperbolic structures in knot theory. *Handbook of Knot Theory*, 10 2003. doi:10.1016/B978-044451452-3/50011-3.

[89] Xu Xu. Combinatorial ricci flow on cusped 3-manifolds. *arXiv preprint arXiv:2009.05477*, 2020.

Appendix

APPENDIX A

Additional data about the Turaev-Viro sequences

This section provides additional experiments for Section 4.7.

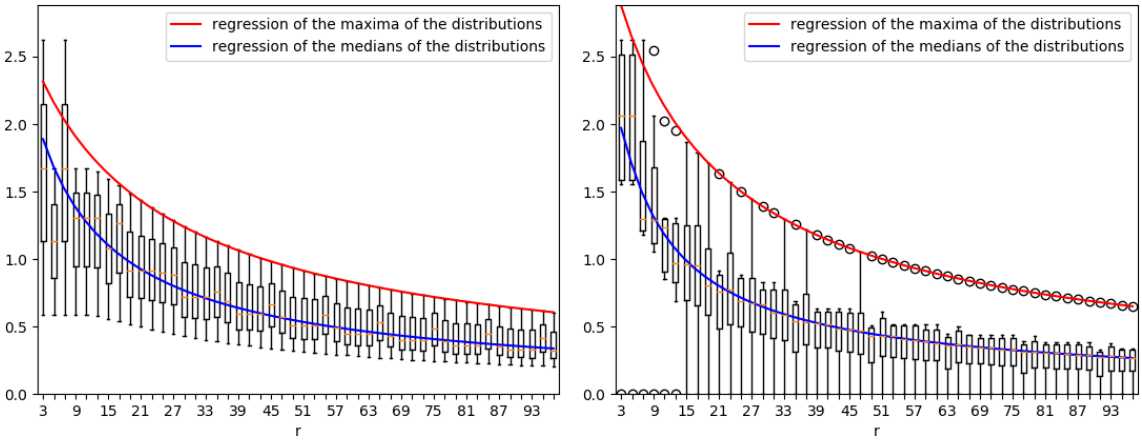

(a) $n = 1$ (b) $n = 2$

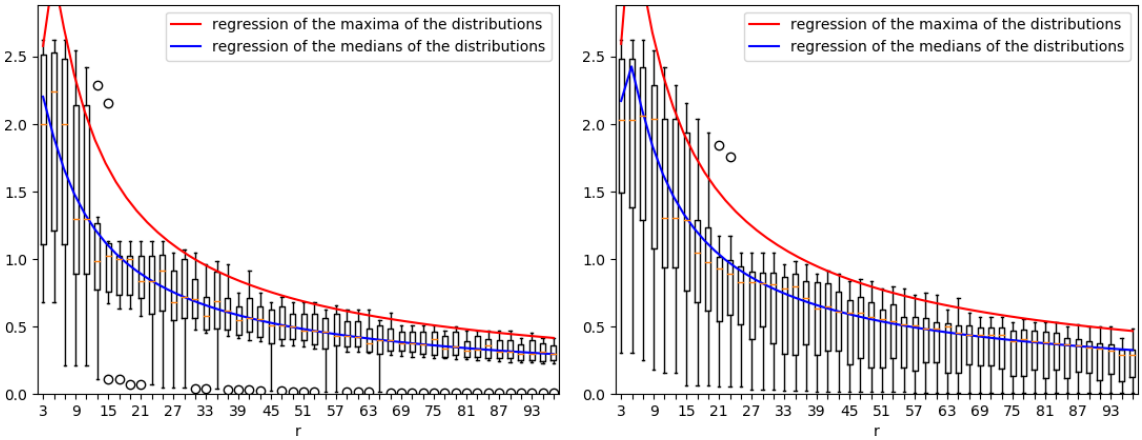

(c) $n = 3$ (d) $n = 4$

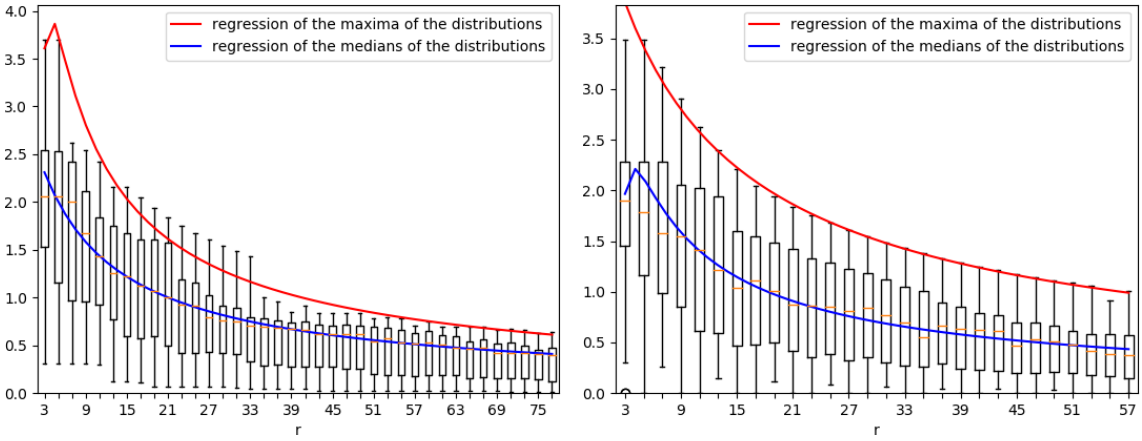

(e) $n = 5$ (f) $n = 6$

Figure A.1 – Distribution of $(S_r(M))_r$ for all manifolds with minimal triangulation of size from one (a) to six (f). Are shown the regressions of the maxima and the medians of the distributions according to Model 1.

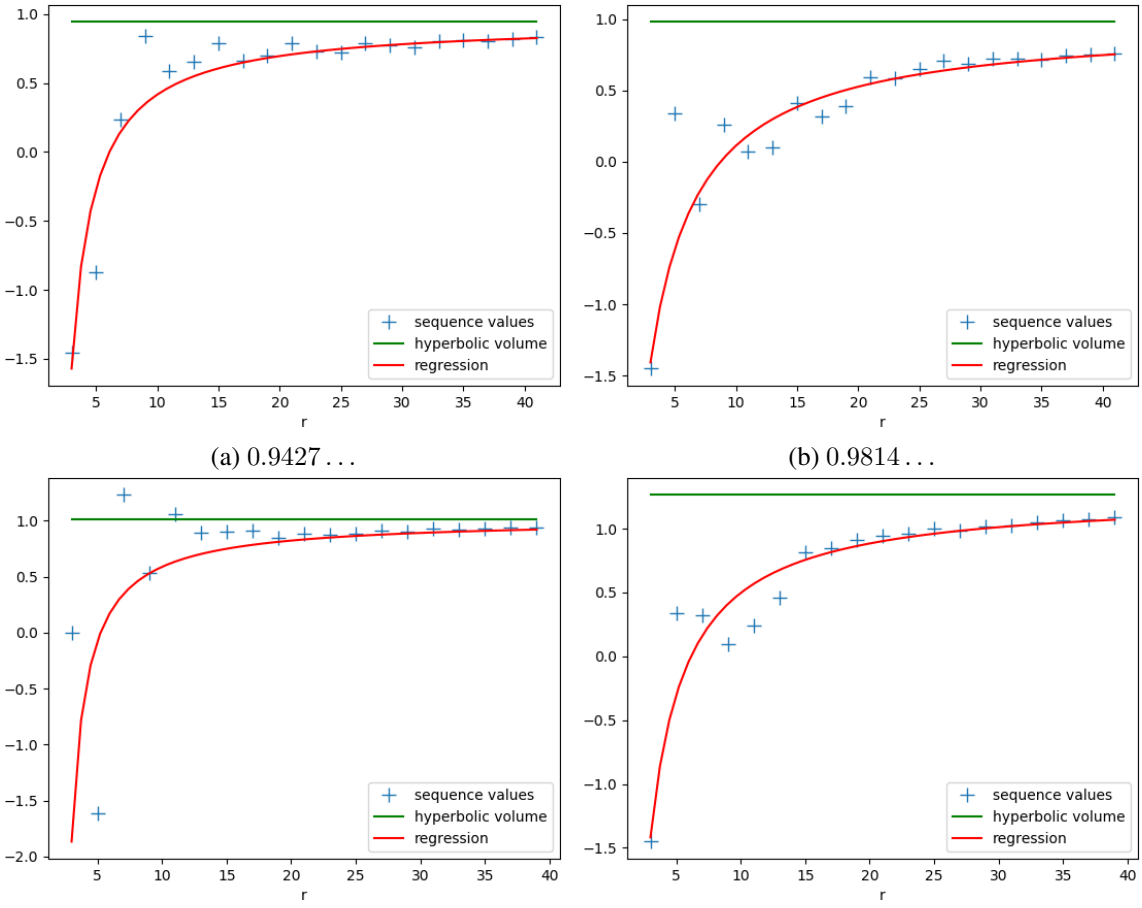

(a) 0.9427 . . . (b) 0.9814 . . .

(c) 1.0149 . . . (d) 1.2637 . . .

Figure A.2 – Graph of the sequences of Conjecture 4.9 for all closed hyperbolic 3-manifolds admitting a nine tetrahedra triangulation. The regression with Model 2 is shown in red and the hyperbolic volumes are shown in green. The captions correspond to the hyperbolic volumes of the manifolds.

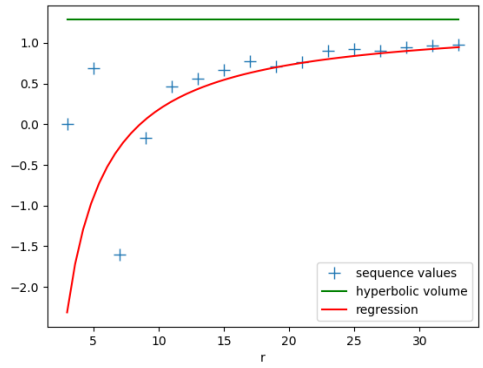

(a) 1.2844 . . .

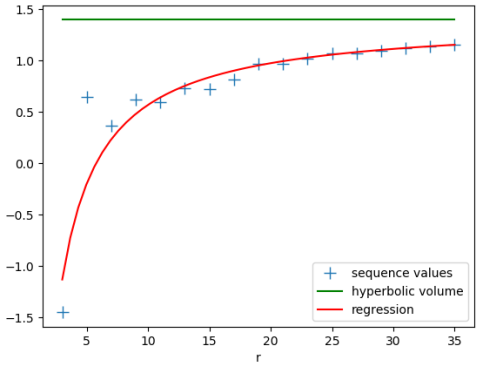

(b) 1.3985 . . .

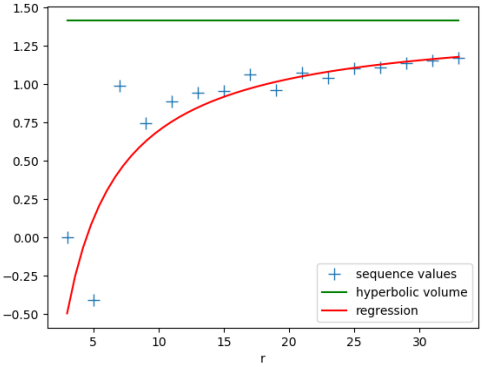

(c) 1.4140 . . . , $\mathbb{Z}_6$

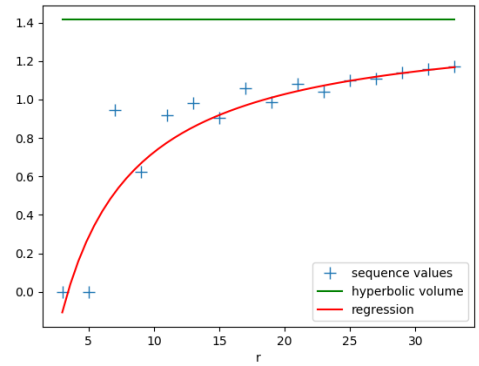

(d) 1.4140 . . . , $\mathbb{Z}_{10}$

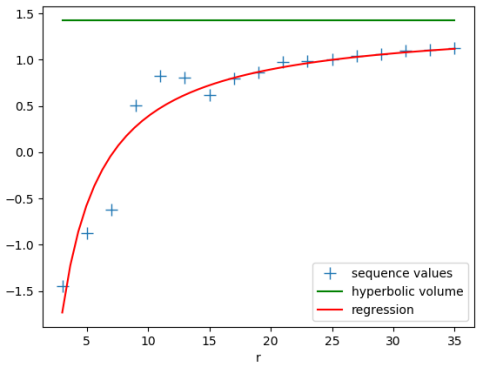

(e) 1.4236 . . .

Figure A.3 – Graph of the sequences of Conjecture 4.9 for different closed hyperbolic 3-manifolds admitting a ten tetrahedra triangulation. The regression with Model 2 is shown in red and the hyperbolic volumes are shown in green. The captions correspond to the hyperbolic volumes of the manifolds, and occasionally followed by the first homology group, and by the length of the shortest closed geodesic to clarify the ambiguities.

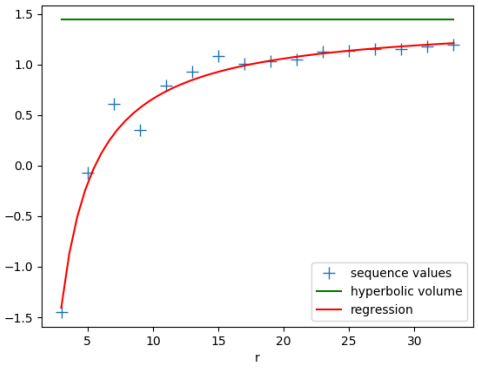

(a) 1.4406 . . .

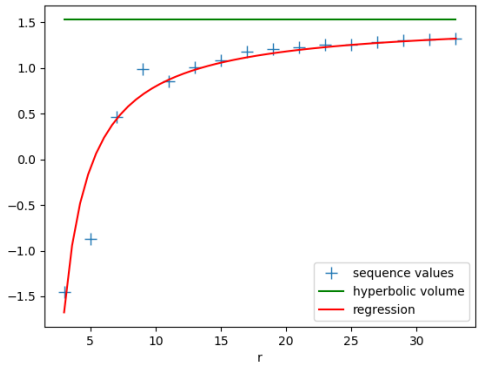

(b) 1.5294 . . .

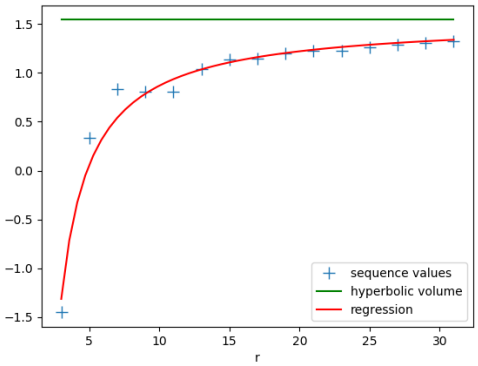

(c) 1.5435 . . . , $\mathbb{Z}_{35}$

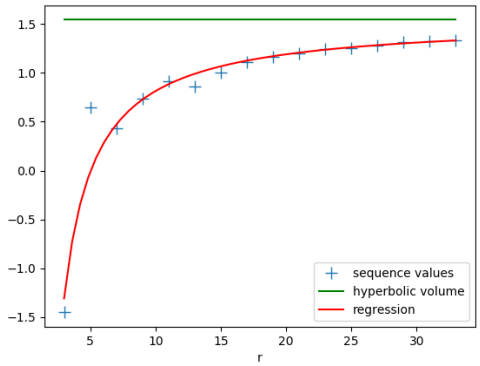

(d) 1.5435 . . . , $\mathbb{Z}_{21}$

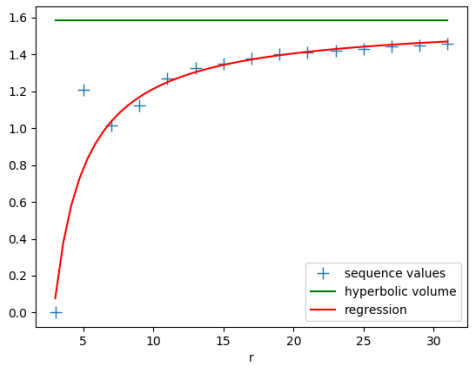

(e) 1.5831 . . . , $\mathbb{Z}_{40}$

Figure A.4 – Graph of the sequences of Conjecture 4.9 for different closed hyperbolic 3-manifolds admitting a ten tetrahedra triangulation. The regression with Model 2 is shown in red and the hyperbolic volumes are shown in green. The captions correspond to the hyperbolic volumes of the manifolds, and occasionally followed by the first homology group, and by the length of the shortest closed geodesic to clarify the ambiguities.

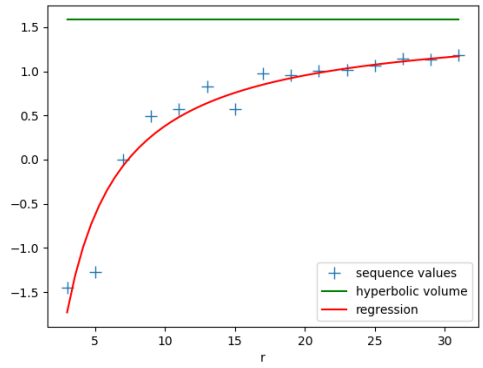

(a) $1.5831\ldots,\ \mathbb{Z}_{21}$

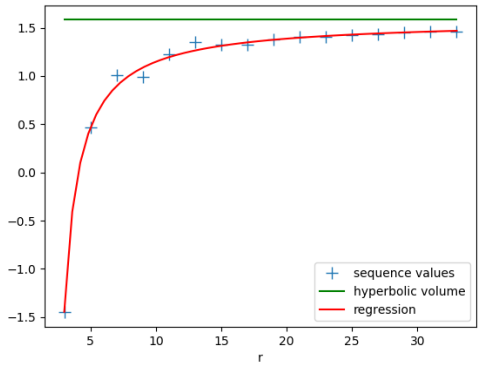

(b) $1.5831\ldots,\ \mathbb{Z}_3+\mathbb{Z}_9$

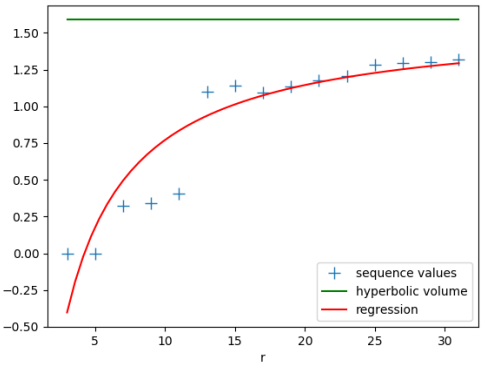

(c) $1.5886\ldots,\ \mathbb{Z}_{30},\ 0.3046$

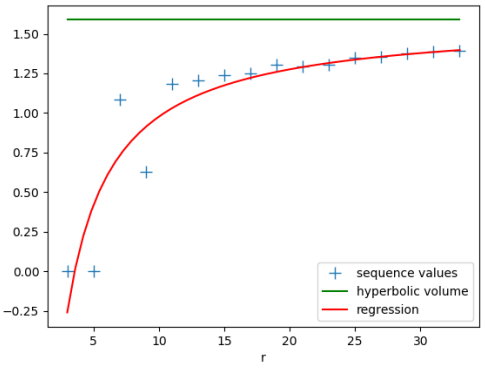

(d) $1.5886\ldots,\ \mathbb{Z}_{30},\ 0.5345$

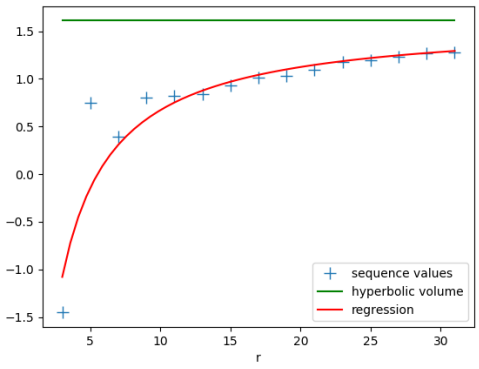

(e) $1.6104\ldots$

Figure A.5 – Graph of the sequences of Conjecture 4.9 for different closed hyperbolic 3-manifolds admitting a ten tetrahedra triangulation. The regression with Model 2 is shown in red and the hyperbolic volumes are shown in green. The captions correspond to the hyperbolic volumes of the manifolds, and occasionally followed by the first homology group, and by the length of the shortest closed geodesic to clarify the ambiguities.

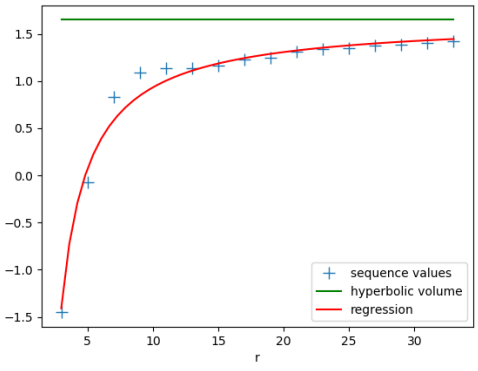

(a) $1.6496\ldots$, $\mathbb{Z}_7$

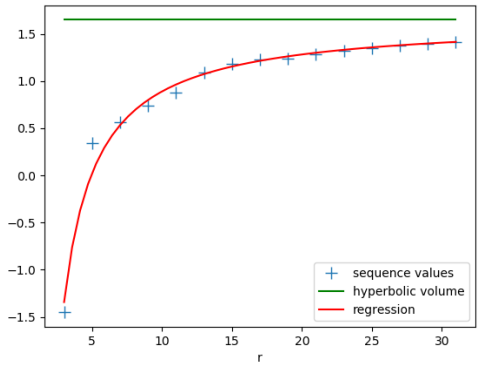

(b) $1.6496\ldots$, $\mathbb{Z}_{15}$

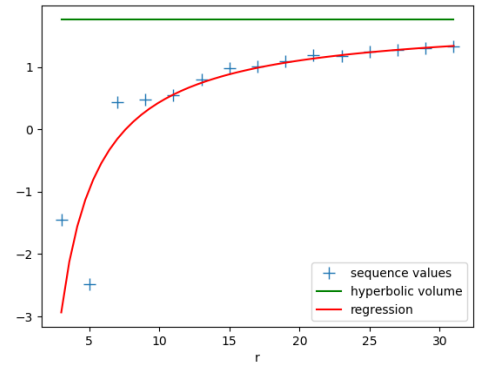

(c) $1.7571\ldots$

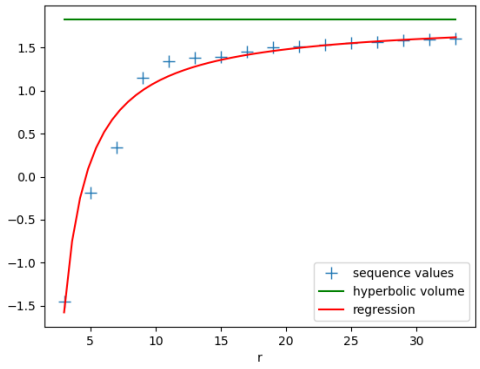

(d) $1.8243\ldots$

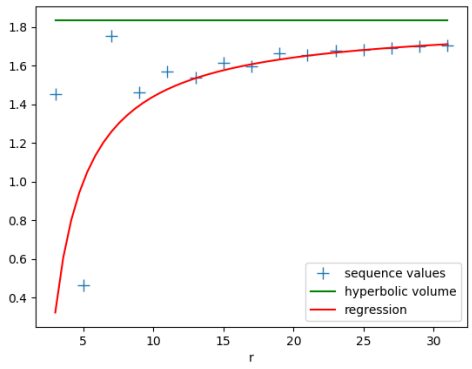

(e) $1.8319\ldots$

Figure A.6 – Graph of the sequences of Conjecture 4.9 for different closed hyperbolic 3-manifolds admitting a ten tetrahedra triangulation. The regression with Model 2 is shown in red and the hyperbolic volumes are shown in green. The captions correspond to the hyperbolic volumes of the manifolds, and occasionally followed by the first homology group, and by the length of the shortest closed geodesic to clarify the ambiguities.

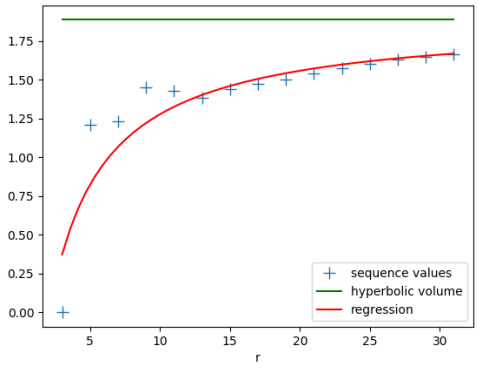

(a) $1.8854\ldots$, $\mathbb{Z}_{40}$

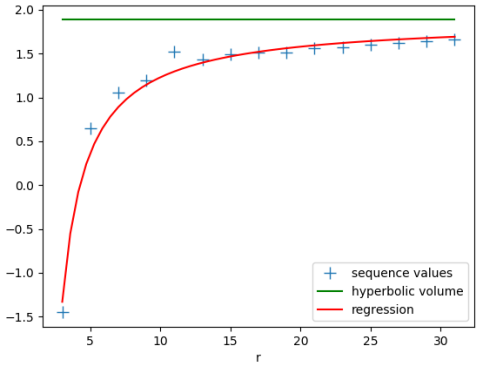

(b) $1.8854\ldots$, $\mathbb{Z}_7 + \mathbb{Z}_7$

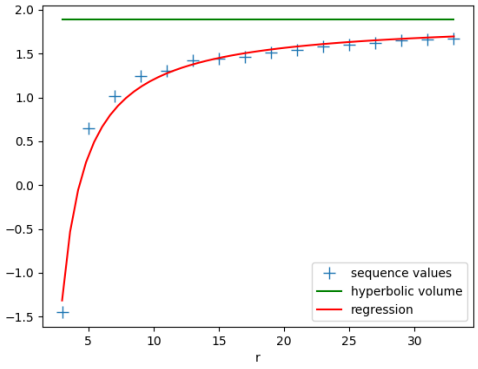

(c) $1.8854\ldots$, $\mathbb{Z}_{39}$

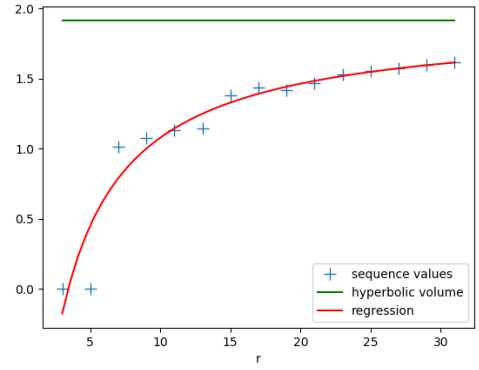

(d) $1.9108\ldots$

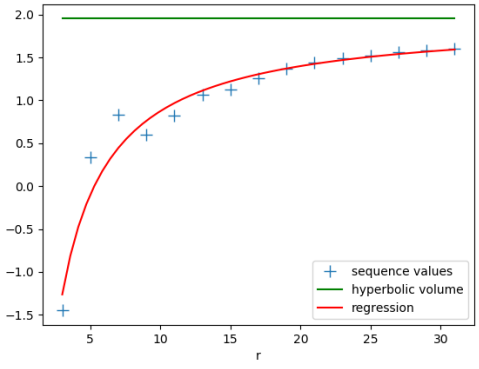

(e) $1.9537\ldots$

Figure A.7 – Graph of the sequences of Conjecture 4.9 for different closed hyperbolic 3-manifolds admitting a ten tetrahedra triangulation. The regression with Model 2 is shown in red and the hyperbolic volumes are shown in green. The captions correspond to the hyperbolic volumes of the manifolds, and occasionally followed by the first homology group, and by the length of the shortest closed geodesic to clarify the ambiguities.